State estimation for non-linear transmission models of Tuberculosis

by

Duayne Strydom

Submitted in partial fulfillment of the requirements for the degree
Master of Engineering (Electronic Engineering)

in the

Department of Electrical, Electronic and Computer Engineering
Faculty of Engineering, Built Environment and Information Technology

UNIVERSITY OF PRETORIA

November 2020

SUMMARY

STATE ESTIMATION FOR NON-LINEAR TRANSMISSION MODELS OF TUBERCULOSIS

by

Duayne Strydom

Supervisor(s):	Prof. I. K. Craig, Dr. J. D. le Roux
Department:	Electrical, Electronic and Computer Engineering
University:	University of Pretoria
Degree:	Master of Engineering (Electronic Engineering)
Keywords:	extended Kalman filter, hybrid extended Kalman filter, modelling, non-linear observability, state and parameter estimation, Tuberculosis quanta estimation

Given the high prevalence of Tuberculosis (TB) and the mortality rate associated with the disease, numerous models, such as the Gammaitoni and Nucci (GN) model, were developed to model the risk of transmission. These models typically rely on a quanta generation rate as a measurement of infectivity. However this state cannot be measured directly.

Since the quanta generation rate cannot be measured directly, the unique contribution of this work is the development of state estimators to estimate the quanta generation rate from available measurements. Towards this end, the GN model is adapted into an augmented single-room GN model, and a simplified two-room GN model. A sensitivity analysis is performed on both models to determine the effects of deviation of parameters and the effect thereof on the uncertainty of the quanta state. An algebraic identifiability analysis is performed on the models to determine whether the parameters are identifiable and distinguishable from one another.

An observability analysis shows that both models are observable, i.e. it is theoretically possible to estimate the number of quanta (the quanta state) and the quanta generation rate given available

measurements. An additional measurement (rate of change of the measurable variable) is added to increase the observability of the models. Kalman filters are used to estimate the quanta state.

First, a continuous-time extended Kalman filter (CEKF) is used for both adapted models using a simulation and measurement time of 60s. Reasonable quanta state estimates are achieved in both cases. A more realistic scenario, with a measurement rate of 1 day, is used next. For these estimates, a hybrid extended Kalman filter (HEKF) is used. Performance of the filter degrades for the quanta state estimates of the HEKFs. The effects of filter tuning and a greater deviation in initial estimates are also investigated and compared.

The CEKFs, the adapted models, and real-time measurements could potentially be used in a control system feedback loop to reduce the transmission of TB in confined spaces such as hospitals.

LIST OF ABBREVIATIONS

TB	Tuberculosis
M. tb	*Mycobacterium tuberculosis*
GN	Gammaitoni and Nucci
KF	Kalman filter
EKF	Extended Kalman filter
CEKF	Continuous-time extended Kalman filter
HEKF	Hybrid extended Kalman fitler
UKF	Unscented Kalman filter
EnKF	Ensemble Kalman filter
MHE	Moving horizon estimator
WR	Wells-Riley
SR	Single-room
TR	Two-room
DR	Dose-response

TABLE OF CONTENTS

CHAPTER 1 INTRODUCTION

1.1 PROBLEM STATEMENT

1.1.1 Context of the problem

Tuberculosis (TB) is a bacterial disease caused by *Mycobacterium tuberculosis* (*M. tb*) [1]. In most cases the disease infects the lungs (pulmonary TB). TB is most commonly spread when droplet nuclei, containing *Mycobacterium tuberculosis* bacilli, are expelled from persons with active pulmonary TB and inhaled by susceptible individuals. Estimates show that a quarter of the world's population is latently infected with TB. Latently infected persons are infected with the disease but are not symptomatic. Approximately 5-10% of these persons will become actively infected, with an estimated 10 million world-wide cases of TB in 2018 [1, 2, 3, 4]. TB is one of the top 10 causes of death globally.

Given the high prevalence of TB and the mortality rate associated with the disease, numerous models were developed over the years to model risk of transmission, especially for confined spaces. The Wells-Riley (WR) model is commonly used to model such risk [5, 6, 7]. Another popular model is the Gammaitoni and Nucci (GN) model [8]. It was shown that the WR and GN models are fundamentally the same, but that unlike the WR model, the GN model allows for the use of nonsteady-state conditions of airborne infectious particles [9]. Additionally, the GN model is in state-space format, which makes it suitable for the design of a state estimator that can estimate unknown states [10]. Other notable models include the Mass Action and Riley, Murphy and Riley model [9, 11].

An important parameter in TB transmission models is the quanta state. Quanta is defined by [5] as the number of droplet nuclei that would infect 63.2% of exposed individuals to that number of droplet

nuclei. It quantifies the infectiousness of the airborne agent. In other words, the infectiousness of the disease and the number of the infectious agent in the room can be expressed by the number of quanta [9]. For the remainder of this work, the number of quanta is referred to as the quanta state. The difference of each individual's immunological response to the disease and the characteristics of the pathogen make it impossible to measure quanta directly. Although quanta is a theoretical unit of measure, it allows one to mathematically compare different scenarios of risk of transmission and how control mechanisms may affect the risk of transmission [12, 13].

There is considerable variability in infectiousness between patients with respiratory diseases [6]. The quanta generation rate is defined as the rate at which quanta is produced by infective people [8]. Quanta generation rate estimates per infectious individual range from 1 - 10 quanta $\cdot$ h^{-1} for the rhinovirus and 15-128 quanta $\cdot$ h^{-1} for influenza [14]. In the case of TB, [15] give 1 - 50 quanta $\cdot$ h^{-1} as a suitable range for the quanta generation rate, whereas others indicate a range of 1.25 - 60 quanta $\cdot$ h^{-1} [16, 17]. In the case of an intubation-related outbreak, the estimate can go as high as 30840 quanta $\cdot$ h^{-1} [8, 9, 17]. If this quanta generation rate in a TB transmission model is can be estimated, rather than back-calculated, which is the common approach, it will provide a better indication of the risk of transmission.

The quanta generation rate parameter is often back-calculated, and not estimated as in this work. Back-calculating this parameter can yield significantly different results, depending on whether a steady-state of a dynamic model is used. For example, the WR model can be manipulated to back-calculate a quanta generation rate. The spread of influenza in a Boeing 737 was back-calculated with both a steady-state and a dynamic WR model in [14]. Quanta generation rates of 15 and 77 quanta $\cdot$ h^{-1} were back-calculated using the steady-state WR model for air exchange rates of 0.1 and 0.5/h respectively, whereas quanta generation rates of 79 and 128 quanta $\cdot$ h^{-1} were calculated using the dynamic WR model from the same data. Similar results were also obtained by [16] and [17].

Because of the variability of the quanta state and the ranges of the estimates, the uncertainty of this parameter is large. The problem of using backwards calculation is that much of the internal dynamics are lost and only the end result is taken into account. Backwards calculating the quanta generation rate can lead to an incorrect estimate thereof and most often does not account for non-steady-state cases such as varying ventilation rates or varying number of infectors.

For experiments conducted at the AIR facility in eMalahleni, South Africa, a quanta generation rate of 2.5 quanta $\cdot$ h^{-1} was calculated using a Nelder-Mead search algorithm [4]. Although this method is more accurate than back-calculation, it is not suited for a control system feedback loop or for real-time estimates.

1.1.2 Research gap

The standard GN model contains uncertainty lumped into one parameter and any deviation of the other model parameters will result in a compensation in the said parameter, causing an incorrect estimate of the estimated parameter. If the parameter can be estimated more accurately, given noisy measurements and in real time, the models along with the estimators can be used in a control system to more efficiently reduce the risk of transmission.

1.2 RESEARCH OBJECTIVE

The aim of this work is to estimate the quanta generation rate for risk of transmission as applied to a multi-room model, and to reduce the uncertainty that is present when estimating this parameter.

1.3 APPROACH

Two models are investigated, a single-room and multi-room model. The two models will be brought into a form that is more suited to the estimation requirements by estimating the parameter containing most of the uncertainty. The sensitivity to deviation of the parameters will also be investigated to determine the effect of the uncertainty in each of the parameters.

The models are analysed using control systems theory to determine whether estimation is possible and state estimators are then designed to estimate the model states. Different estimators are used and compared to determine the viability given different measurement intervals.

The effect of estimator tuning parameters and different initial estimates are also compared. Data from the AIR (Airborne Infections Research) facility and from literature are used to simulate the models and test the estimators.

1.4 RESEARCH CONTRIBUTION

This research describes a method to estimate in real-time the number of quanta, i.e., the infectiousness of TB in a room or ward and provides a foundation on which to implement autonomous control of the reduction in the transmission of TB through single- and multi-room environments.

1.5 RESEARCH OUTPUTS

This research led to the following publications:

- D. Strydom, R. R. Küsel, and I. K. Craig, "When is it appropriate to model transmission of tuberculosis using a dose response model?" *IFAC-PapersOnLine*, vol. 50, no. 2, pp. 31-36, 2017
- D. Strydom, I. K. Craig, and J. D. le Roux, "State Estimation for Non-linear State-space Transmission Models of Tuberculosis", *Risk Analysis, Submitted*

1.6 OVERVIEW OF STUDY

Since the quanta generation rate cannot be measured directly, the unique contribution of this work is the development of state estimators to estimate the quanta generation rate from available measurements. Towards this end, the GN model is adapted into an augmented single-room GN model, and a simplified two-room GN model.

Both models are shown to be observable, i.e. it is theoretically possible to estimate the quanta state given available measurements. Kalman filters are used to estimate the quanta state. First, a continuous-time extended Kalman filter (CEKF) is used for both adapted models using a simulation and measurement time of 60s. Accurate quanta state estimates are achieved in both cases for initial quanta generation rates of 150 quanta $\cdot d^{-1}$. The NRMSE of the augmented single-room model is 29.4 times smaller than the standard single-room model and the simplified two-room model is 420.3 times smaller than the standard two-room model. Comparatively, the initial quanta generation rates of the standard models would have to be guessed to within 2.5 quanta $\cdot d^{-1}$ to achieve better estimates. A more realistic scenario, with a measurement rate of 1 day, is used next. For these estimates, a hybrid

extended Kalman filter (HEKF) is used. Poor quanta state estimates are achieved. The HEKFs, the adapted models, and real-time measurements could potentially be used in a control system feedback loop to reduce the transmission of TB in confined spaces such as hospitals.

The models in this work are simulated to mimic the readings from the multi-room AIR (Airborne Infections Research) facility in eMalahleni, South Africa that studies the risk of transmission of TB [4, 18, 19]. The CEKFs and HEKFs are then used to see if one can estimate the states and quanta generation rates of the simulated models.

Different risk of transmission models from literature are presented in Chapter 2 together with model modifications that allow for improved parameter estimation. Sensitivity and identifiability analyses are performed in Chapter 3. Observability analyses are performed in Chapter 4 to determine whether the quanta parameter can be theoretically estimated. Chapter 5 shows the development of continuous-time, hybrid non-linear state estimators, and the simulation results obtained. Chapters 6 and 7 discuss the results and conclude the findings respectively.

CHAPTER 2 TUBERCULOSIS AND RISK OF TRANSMISSION MODELS

2.1 CHAPTER OVERVIEW

This chapter describes continuous-time nonlinear state-space risk of transmission models that simulate the infection of uninfected (susceptible) individuals by infectious individuals. Two models are presented that model the risk of transmission in single- and two-room cases. The models are then modified to better allow estimation of the model states. Simulation data for the models are presented, which were used to simulate the risk of transmission at a multi-room AIR (Airborne Infections Research) facility in eMalahleni, South Africa.

2.2 AIR EXPERIMENT

The multi-room environment considered is an AIR (Airborne Infections Research) facility in eMalahleni, South Africa [4, 18, 19]. The standard GN model only works if the infectious individuals and susceptible individuals are in the same room [4]. Therefore, a modified two-room GN model is used in this work [4], where the infectious individuals and susceptible individuals are separated and placed in adjacent rooms. This two-room GN model is used to simulate the spread of the disease in the AIR facility [4, 18]. The two-room GN model also incorporates an incubation period which is not accounted for in the GN model [4].

Simulation data are used to estimate the quanta parameters for risk of transmission of TB models as applied to a single and multi-room environment from published papers of experiments conducted at the AIR facility in eMalahleni, South Africa [4, 18, 19]. As in the AIR experiment, sentinel guinea

pigs are often used to measure the risk of transmission of TB [4, 20]. The AIR facility has three 2-bed inpatient wards that are connected by airtight ventilation systems to two identical rooms containing sentinel guinea pigs [4, 18]. The air is vented from the wards into the animal rooms. The air in the wards is assumed to be well mixed with the help of paddle fans to circulate the air in the room. A basic layout of the facility is shown in Figure 2.1.

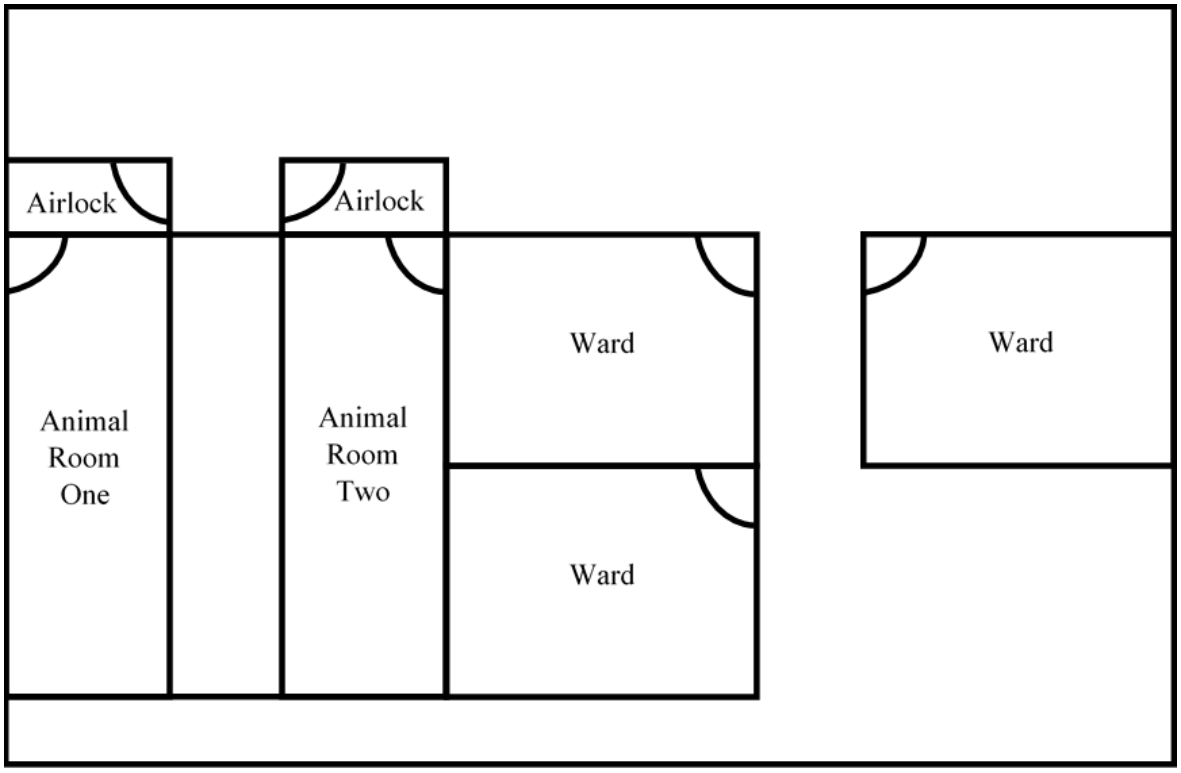

Figure 2.1. Basic layout of AIR facility in eMalahleni, South Africa [4].

If the ward air was not well mixed, zonal models incorporation the proximity to the source of the infection would have to be considered [21, 22, 23].

2.3 STATE-SPACE REPRESENTATION

State-space representations can be used to describe numerous processes including processes in chemistry, biology, physics and engineering [10]. If a mathematical model can be derived for a process, the model can be used to control the process and give information about the process.

State-space models can represent linear and nonlinear systems, and although most real world processes are nonlinear, linear estimation and control is much more accessible and better understood [10].

The use of state-space representations not only allows the modelling of nonlinear systems, but also systems with nonzero initial conditions. Another advantage of using state-space includes modelling systems with multiple inputs and outputs [24].

A state-space model consists of a set of first order differential equations of the states and an algebraic equation describing the output as a function of the states. A general non-linear state-space model can be written as:

$$\begin{aligned} \dot{x} &= f(x) + g(x)u \\ y &= h(x), \end{aligned} \tag{2.1}$$

where x is the state vector, $\dot{x}$ is the derivative of the state vector with respect to time, y is the output vector, u is the input vector, f is the system function, g is the input function in terms of x, and h is the output function.

A linear state-space model can be written as:

$$\begin{aligned} \dot{x} &= Ax + Bu \\ y &= Zx + Du, \end{aligned} \tag{2.2}$$

where A is the system matrix, B is the input matrix, Z is the output matrix and D is the feedforward matrix.

2.4 MODEL DESCRIPTIONS

Two distinct risk of transmission model scenarios are presented: a single-room and a two-room case. In each case a standard and a modified model is presented. Table 2.1 summarises the states and parameters of the single-room models in Section 2.4.1, and Table 2.2 summarises the states and parameters of the two-room models in Section 2.4.2.

2.4.1 Single-room GN models

2.4.1.1 Standard single-room GN model

For the GN model (obtained from literature), it is assumed that the susceptible guinea pigs and the infected individuals are in the same room, the guinea pigs do not become infectious (they do not

contribute to new infections of susceptible guinea pigs), and that the three wards are combined into a single space.

The GN transmission model is shown in (2.3) [8]:

$$\begin{aligned} \dot{S} &= -\left(\tfrac{p}{V}\right) CS \\ \dot{C} &= \phi I_w - \tfrac{F}{V} C, \end{aligned} \tag{2.3}$$

where S is the number of susceptible animals and C is the number of quanta in the room. As per the model definition in [8], variables S and C are considered as continuous and real. The pulmonary ventilation rate p, the room volume V, and the quanta generation rate per infectious individual ϕ, are constants. The number of infectious individuals in a room, i.e., the number of sick patients, is known a-priori and is represented by I_w. The flow rate of air F is measured by means of a SCADA system.

The number of infected animals is measured through the diagnosis of TB. Therefore, the number of susceptible animals S is equal to the difference between the initial number of susceptible animals in the room and the number of infected animals.

Tuberculin skin tests (TST) are used at the AIR facility to measure whether an animal is infected [18]. This is a common test which is easy to administer and evaluate [25] to diagnose TB in both patients and guinea pigs [26]. If the TST results in induration of >5 mm the animal or patient is assumed to be infected with TB. The specificity of the test for humans is reported as between 59% and 97%, and the sensitivity as 77% [27, 28]. The range of specificity is as a result of uncharacterized variance in the health of patients tested. Since the AIR facility made use of highly susceptible sentinel guinea pigs, there is little uncertainty whether guinea pigs will be infected if exposed to infectious particles. Guinea pigs have been successfully used in numerous TB studies [6, 29, 30, 31, 32]. In addition, since TSTs are conducted by medically trained personnel at the AIR facility, there is low uncertainty in the diagnosis whether a guinea pig is infected or not [25].

Rewriting the model in (2.3) in state-space format with $S = x_1$ and $C = x_2$ gives:

$$\begin{aligned} \dot{x_1} &= -\beta x_1 x_2 + w_{x_1} \\ \dot{x_2} &= \phi I_w - \tfrac{F}{V} x_2 + w_{x_2}. \end{aligned} \tag{2.4}$$

where $\beta = p/V$ is the pulmonary ventilation rate over room volume, ϕ is the quanta generation rate. Since the sentinel guinea pigs are highly susceptible to TB, the process noise is defined as additive zero-mean Gaussian noise such that $w_{x_1} \sim \left(0, (\zeta)^2\right)$, where ζ is 5% of the initial rate of change of x_1,and x_{1_0} is the initial condition of x_1. As discussed in Section 1.1.1, the quanta generation rate generally ranges between 24 quanta$\cdot$ d^{-1} to 60 quanta$\cdot$ d^{-1} A significant portion of the model uncertainty is contained within this parameter. Therefore, the process noise for rate of change for x_2 is modelled as additive zero-mean Gaussian noise such that $w_{x_2} \sim \left(0, \left(0.05\frac{dx_2}{dt}|_{t=0}\right)^2\right)$, i.e., the standard deviation is 5% of the initial rate of change in x_2.

The state x_1 is assumed measured as:

$$y = x_1 + v_{x_1}, \tag{2.5}$$

where v_{x_1} is zero-mean additive Gaussian measurement noise. The TST is very reliable specifically for guinea pigs and therefore the measurement noise is defined as $v_{x_1} \sim \left(0, (0.02x_{1_0})^2\right)$.

Table 2.1. Single-room GN model parameters.

Parameter	Unit	Description
S or x_1	animals	number of susceptible animals
C or x_2	quanta	number of quanta in the room
p	m$^3 \cdot$ d^{-1}	pulmonary ventilation rate
V	m^3	room volume
ϕ or x_3	quanta $\cdot$ d$^{-1}\cdot$ ind.$^{-1}$	quanta generation rate per infectious individual
F	m$^3\cdot$ d^{-1}	ventilation flow rate
I_w	individuals	number of infectious individuals

2.4.1.2 Augmented single-room GN model

The model states in (2.4) cannot be accurately estimated if there is a parameter mismatch between the estimation and simulation models. Therefore, an updated model shown in (2.6) is suggested that makes use of one additional quanta generation rate state:

$$\begin{aligned} \dot{x_1} &= -\beta x_1 x_2 + w_{x_1} \\ \dot{x_2} &= x_3 I_w - \tfrac{F}{V} x_2 + w_{x_2} \\ \dot{x_3} &= w_{x_3}, \end{aligned} \tag{2.6}$$

where x_1 and x_2 are as in (2.4), x_3 represents the quanta generation rate. The process noise is defined as additive zero-mean Gaussian noise such that $w_{x_1} \sim \left(0, (\zeta)^2\right)$, $w_{x_2} \sim \left(0, \left(0.01 \frac{dx_2}{dt}|_{t=0}\right)^2\right)$, and $w_{x_3} \sim \left(0, 48^2\right)$. ζ is calculated as for (2.4). The quanta state x_3 is added to allow an estimator to estimate the quanta generation rate parameter. Since the large uncertainty for the quanta generation rate x_3 is captured by w_{x_3}, the uncertainty represented by w_{x_2} is reduced as compared to (2.4).

Similar to (2.5), the state x_1 is assumed measured as:

$$y = h(x) + v_{x_1} = x_1 + v_{x_1}. \tag{2.7}$$

Similar to (2.5), the measurement noise is defined as $v_{x_1} \sim \left(0, (0.02x_{1_0})^2\right)$.

It is important to include the additional state x_3. If x_3 is disregarded and if x_1 is measured at a typical sampling rate of 24 hours (1 day), the number of quanta in the room will reach a steady-state value faster than an estimator can estimate. This can be seen from converting the equation for $\dot{x_2}$ in (2.4) to the Laplace domain:

$$X_2 = \frac{\frac{\phi I_w V}{F}}{\frac{V}{F}s + 1}. \tag{2.8}$$

The shortest time constant of this first-order system is $\frac{V}{F} = 513$ seconds (the parameter values are $V = 112.84$ m^3 as given in Table 2.3, and the maximum value of $F = 0.22$ m$^3 \cdot {}^{-1}$ as shown in Figure 2.3). The settling time for such a system in response to a step input is $\frac{4V}{F} = 2052$ seconds or just over 30 minutes [24]. This is much faster than what an estimator can estimate if x_1 is measured once every 24 hours. The inclusion of the additional state x_3 makes it possible for an estimator to correctly estimate the value of x_2.

The number of quanta in the room x_2, reaches a steady-state value of $x_2 = \frac{\phi I_w V}{F}$, determined by setting $\dot{x_2}$ in (2.4) equal to zero. Thus, if the generation rate ϕ is increased, so does the quanta x_2 present in the room. Inversely, if the ventilation rate F is increased, the quanta in the room x_2 decreases. Therefore, if the ventilation rate F and number of infected individuals I_w are measured and V is known, the number of quanta in the room x_2 can be determined by estimating the quanta generation rate parameter ϕ.

2.4.2 Two-room GN models

2.4.2.1 Standard two-room GN model

For the two-room GN model (which was also obtained from literature) [4], the room in which the susceptible animals are in is called the animal room (animal room one from Figure 2.1) and the room in which the infectious individuals are in is called the ward. The wards in Figure 2.1 were combined into a single space since the air containing TB bacilli vented from each ward was combined before being vented to the animal rooms. In this model the individuals who were exposed to the disease and are not yet infected are labelled exposed individuals. The two-room GN model is described as:

$$\begin{aligned}
\dot{x_1} &= -\frac{p}{V_1}x_5x_1 + w_{x_1} \\
\dot{x_2} &= \frac{p}{V_1}x_5x_1 - \alpha x_2 + w_{x_2} \\
\dot{x_3} &= \alpha x_2 + w_{x_3} \\
\dot{x_4} &= \phi_w I_w - \frac{F_w}{V_w}x_4 + w_{x_4} \\
\dot{x_5} &= \frac{F_{in}}{V_w}x_4 - \frac{F_{out}}{V_1}x_5 + w_{x_5},
\end{aligned} \tag{2.9}$$

where x_1 is the number of susceptible animals in the animal room, x_2 is the number of exposed animals, x_3 is the number of infected animals, x_4 is the number of quanta in the ward, x_5 is the number of quanta in the animal room, p is the pulmonary ventilation rate of the susceptible animals, V_1 is the volume of the animal room, a is the incubation period of the disease, ϕ_w is the quanta generation rate per infectious individual, I_w is the number of infectious individuals in the ward, F_w is the air extraction ventilation rate of the ward, V_w is the volume of the ward, F_{in} is the ventilation rate of the air flowing into the animal room from the ward, and F_{out} is the ventilation rate of the air extracted from the animal room.

The process noise $w_{x_i} \sim (0, \sigma^2_{w_i})$ is modelled as additive zero-mean Gaussian noise. In accordance with the discussion of model uncertainty in (2.4), the process noise distributions for (2.9) are as follows, $w_{x_1} \sim \left(0, (\zeta)^2\right)$, $w_{x_{2,3}} \sim \left(0, \left(0.05\frac{dx_{2,3}}{dt}|_{t=0}\right)^2\right)$ and $w_{x_{4,5}} \sim \left(0, \left(0.05\frac{dx_{4,5}}{dt}|_{t=0}\right)^2\right)$.

The measurement is:

$$y = h(x) + v = \begin{bmatrix} x_1 + v_{x_1} \\ x_3 + v_{x_3} \end{bmatrix}. \tag{2.10}$$

Similar to (2.5) and (2.7), the measurement noise is defined as $v_{x_1} \sim \left(0, (0.02x_{1_0})^2\right)$ and $v_{x_3} \sim \left(0, \left(\frac{dx_3}{dt}|_{t=0}\right)^2\right)$.

Table 2.2. Two-room GN model parameters.

Parameter	Unit	Description
x_1	animals	number of susceptible animals
x_2	animals	number of exposed animals
x_3	animals	number of infected animals
x_4	quanta	number of quanta in ward
x_5	quanta	number of quanta in animal room
p	$\mathrm{m}^3 \cdot \mathrm{d}^{-1}$	pulmonary ventilation rate
V_w	m^3	ward volume
V_1	m^3	animal room volume
ϕ_w	quanta $\cdot\, \mathrm{d}^{-1} \cdot$	quanta generation rate per infectious individual
F_w	$\mathrm{m}^3 \cdot \mathrm{d}^{-1}$	ward flow rate
F_{in}	$\mathrm{m}^3 \cdot \mathrm{d}^{-1}$	animal room intake flow rate
F_{out}	$\mathrm{m}^3 \cdot \mathrm{d}^{-1}$	animal room outlet flow rate
I_w	individuals	number of infectious individuals
α	d^{-1}	incubation period delay rate

2.4.2.2 Simplified GN two-room model

The two-room GN model has the same estimation problem as the single-room GN model. Because the quanta in the ward x_4 tends to a steady-state value, the state will simply return to that steady-state value when estimated. If the two-room GN model is modified by removing the incubation period α and adding the quanta generation rate per infectious individual ϕ_w as an additional state, and it is assumed the number of susceptible animals x_1 is measurable, one can estimate the generation rate ϕ_w and the number of quanta in the two rooms x_4 and x_5. The new model simplified from (2.9) is then

given by:

$$\begin{aligned}\dot{x_1} &= -\frac{p}{V_1}x_5x_1 + w_{x_1}\\ \dot{x_4} &= x_6I_w - \frac{F_w}{V_w}x_4 + w_{x_4}\\ \dot{x_5} &= \frac{F_{in}}{V_w}x_4 - \frac{F_{out}}{V_1}x_5 + w_{x_5}\\ \dot{x_6} &= w_{x_6}.\end{aligned} \tag{2.11}$$

The process noise $w_{x_i} \sim (0, \sigma^2_{w_i})$ is modelled as additive zero-mean Gaussian noise, and the distributions are $w_{x_1} \sim \left(0, (\zeta)^2\right)$, $w_{x_4} \sim \left(0, (0.01x_{4_0})^2\right)$, $w_{x_5} \sim \left(0, \left(0.05\frac{dx_5}{dt}|_{t=0}\right)^2\right)$ and $w_{x_6} \sim \left(0, 48^2\right)$.

The measurement is now given as:

$$y = h(x) + v_{x_1} = x_1 + v_{x_1}. \tag{2.12}$$

Similar to (2.5), (2.7) and (2.10), the measurement noise is defined as $v_{x_1} \sim \left(0, (0.02x_{1_0})^2\right)$.

It is important to note that the modified models are fundamentally the same. For the single-room GN model, if $\dot{x_3} = 0$, then the modified model is the same as the standard model. The same can be said for the two-room models with the additions that the measurement of the two-room model is no longer the infected animals but the susceptible animals and that the incubation period is not taken into account. These alterations to the models allow for better estimation using filters.

2.4.3 Additional models considered

A dose-response (DR) model is discussed in Appendix A for which a sensitivity and identifiablity analysis is performed. Because no measurements of the infectious dose are available, there is no benefit in using the DR model [6, 19], and is not discussed further in this research.

Another model that can be considered in future research is one that uses exhaled air in the form of carbon dioxide (CO_2) levels as a measurement instead of ventilation rate [33]. If the sensors are well placed, this could eliminate the assumption of well mixed air. The model however cannot distinguish between exhaled air from an infectious or susceptible source.

In cases where the infected individuals become infectious, Susceptible-Exposed-Infectious-Recovered (SEIR) models can be used to model the risk of transmission [15]. These models also make use of a

removed state, which describes the removal of infectious individuals from the model at a certain rate, either due to being removed from the same space as the susceptible individuals or other means which prohibit the spread of infection.

2.5 MODEL PARAMETERS AND SIMULATION DATA

Tables 2.3 to 2.6 show the initial model parameters taken from literature for the single- and two-room models. model state values, the parameter values and the noise distribution for the four different models discussed in Section 2.4.1. The data for the model states, and parameters were obtained from an experiment that was conducted at the AIR (Airborne Infections Research) facility in eMalahleni, South Africa [4] in which sentinel guinea pigs were used to measure the risk of transmission. The data for the models were sampled at a sampling rate of 60 s. The quanta generation rate x_2 was backwards calculated from experimental data using a Nelder-Mead search algorithm [4, 19].

ζ is calculated for a more severe case of TB, i.e. an office building outbreak as shown in Table 5.12 in Section 5.5. For this calculation, the ventilation rates are taken as the mean ventilation rate for the room, I_w is taken as the maximum number of infectious individuals and the other model parameters are shown in Tables 2.3 to 2.6. Solving for the steady state of the quanta in the ward for these values and substituting into $dx_1/dt|_{t=0}$, one can calculate ζ for the single room model as:

$$\zeta = 0.05 \cdot \frac{pI_w \phi x_{1_0}}{F}, \tag{2.13}$$

where use is made of $x_2(\infty) = \frac{\phi I_w V}{F}$.

ζ for the two room model can be calculated as:

$$\zeta = 0.05 \cdot \frac{pI_w \phi V_1 F_{in} x_0}{F_w F_{out}}, \tag{2.14}$$

where use is made of $x_4(\infty) = \frac{\phi I_w V_w}{F_w}$ and $x_5(\infty) = \frac{\phi I_w V_1 F_{in}}{F_w F_{out}}$.

The infectious individual excitation data (number of infectious individuals in the ward I_w) is shown in Figure 2.2. Figure 2.3 shows the ventilation rate out of the ward F_w. The ventilation rate into and out of the animal rooms (F_{in} and F_{out}) are shown in Figure 2.4 [4].

Table 2.3. Initial state values, parameter values, and noise distribution for the standard single-room GN model in (2.4) and (2.5):

Model states	**Initial Value**
x_1	90 animals
x_2	0 quanta
Parameters	**Value**
ϕ	60 quanta $\cdot d^{-1}$
p	0.23 $\mathrm{m}^3 \cdot \mathrm{h}^{-1}$
V	112.84 m^3
Process and measurement noise	**Distribution**
w_{x_1}	$\left(0, (0.3312)^2\right)$
w_{x_2}	$\left(0, (22.603)^2\right)$
v_{x_1}	$\left(0, (1.8)^2\right)$

Table 2.4. Initial state values, parameter values, and noise distribution for the augmented single-room GN model in (2.6) and (2.7):

Model states	**Initial Value**
x_1	90 animals
x_2	0 quanta
x_3	60 quanta $\cdot \mathrm{d}^{-1}$
Parameters	**Value**
p	0.23 $\mathrm{m}^3 \cdot \mathrm{h}^{-1}$
V	112.84 m^3
Process and measurement noise	**Distribution**
w_{x_1}	$\left(0, (0.3312)^2\right)$
w_{x_2}	$\left(0, (22.603)^2\right)$
w_{x_3}	$\left(0, (48)^2\right)$
v_{x_1}	$\left(0, (1.8)^2\right)$

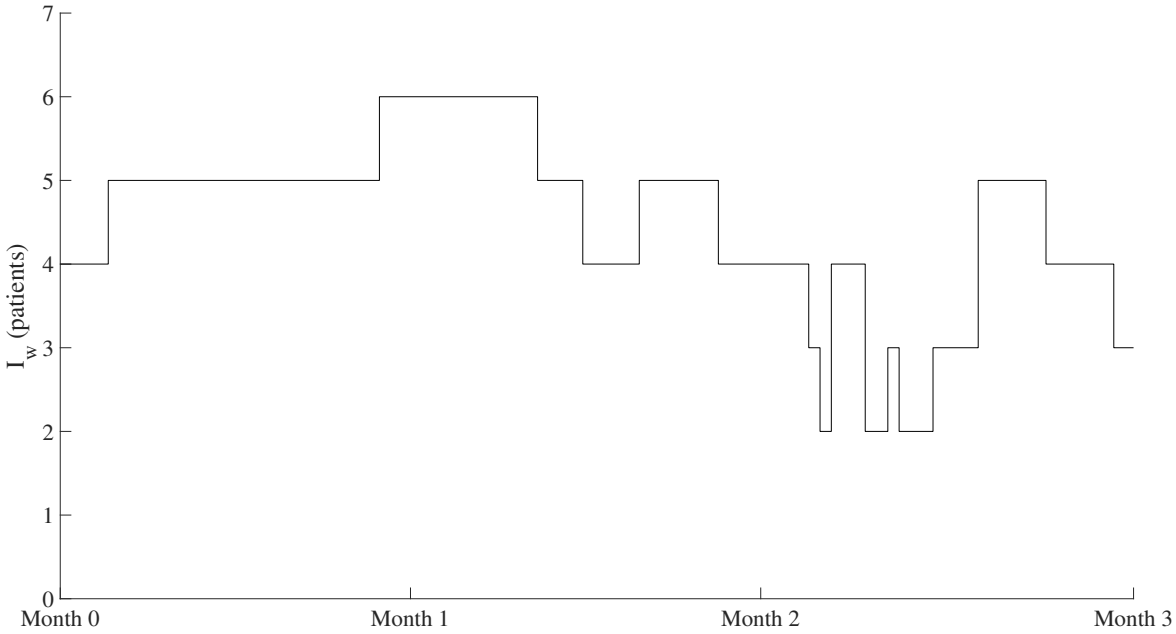

Figure 2.2. Measured number infectious individuals in the ward [4].

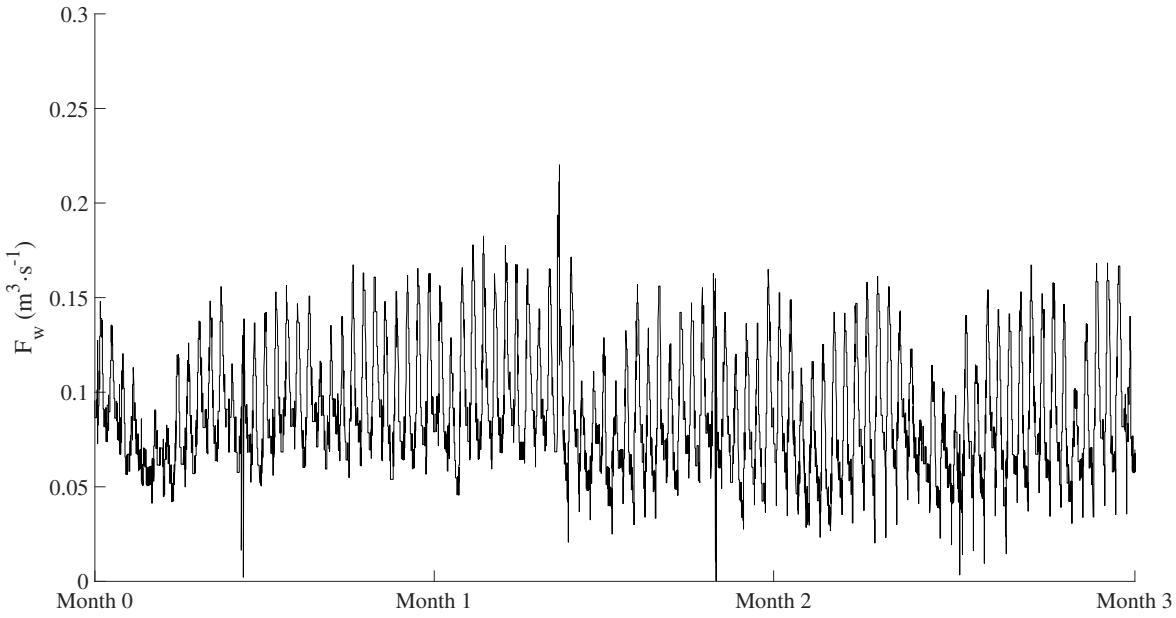

Figure 2.3. Air flow out of the ward, measured in $m^3 \cdot s^{-1}$ [4]. The flow rate was measured in $m^3 \cdot s^{-1}$ but time scaled to $m^3 \cdot d^{-1}$ in the simulations.

Table 2.5. Initial state values, parameter values, and noise distribution for the standard two-room GN model in (2.9) and (2.10):

Model states	**Initial Value**
x_1	90 animals
x_2	0 animals
x_3	0 animals
x_4	0 quanta
x_5	0 quanta
Parameters	**Value**
ϕ	60 quanta $\cdot$ d^{-1}
p	0.23 m$^3\cdot$ h^{-1}
V_w	112.84 m^3
V_1	3.4965 m^3
α	0.03 d^{-1}
Process and measurement noise	**Distribution**
w_{x_1}	$\left(0,(0.6912)^2\right)$
w_{x_2}	$\left(0,(0.0112)^2\right)$
w_{x_3}	$\left(0,(0.0014)^2\right)$
w_{x_4}	$\left(0,(23.603)^2\right)$
w_{x_5}	$\left(0,(0.6918)^2\right)$
v_{x_1}	$\left(0,(1.8)^2\right)$
v_{x_3}	$\left(0,(0.007)^2\right)$

Table 2.6. Initial state values, parameter values, and noise distribution for the simplified two-room GN model in (2.11) and (2.12):

Model states	**Initial Value**
x_1	90 animals
x_4	0 quanta
x_5	0 quanta
x_5	60 quanta $\cdot$ d^{-1}
Parameters	**Value**
p	0.23 m$^3\cdot$ h^{-1}
V_w	112.84 m^3
V_1	3.4965 m^3
Process and measurement noise	**Distribution**
w_{x_1}	$\left(0,(0.6912)^2\right)$
w_{x_4}	$\left(0,(23.603)^2\right)$
w_{x_5}	$\left(0,(0.6918)^2\right)$
w_{x_6}	$\left(0,(48)^2\right)$
v_{x_1}	$\left(0,(1.8)^2\right)$

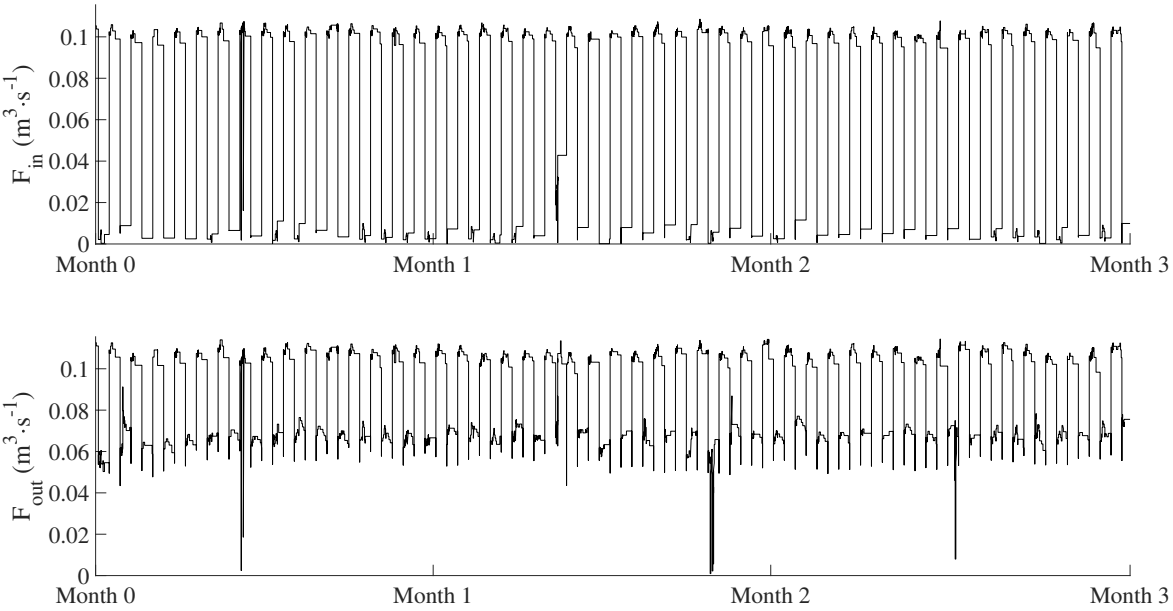

Figure 2.4. Air flow out of and into the animal room, measured in $m^3 \cdot s^{-1}$ [4]. The flow rate was measured in $m^3 \cdot s^{-1}$ but time scaled to $m^3 \cdot d^{-1}$ in the simulations.

CHAPTER 3 SENSITIVITY AND IDENTIFIABILITY

3.1 CHAPTER OVERVIEW

In this chapter sensitivity analyses were performed on the models in Section 2.4 to determine the sensitivity to deviation in each of the model parameters. An identifiability analysis was performed on the models in order to determine whether the model parameters are distinguishable given available measurements.

3.2 SENSITIVITY ANALYSIS

In order to determine the sensitivity of the number of susceptible individuals to deviations of the model parameters, the simulation parameters were deviated by increasing and decreasing the initial values by 10% from the values in Tables 2.3 and 2.5 [4, 19]. The results are shown in Figures 3.1 to 3.7, and the sensitivities for the modified GN models, (2.6) and (2.11), are plotted separately.

Figure 3.1 shows a deviation of a single infectious patient I_w in the wards instead of a 10% deviation, seeing that there cannot be a 10% increase in the number of patients. Figure 3.2 shows the effect of a 10% deviation of the quanta generation rates x_3 and x_6 on the the number susceptible guinea pigs x_1. The sensitivity to a deviation of the pulmonary ventilation rate p on the the number susceptible guinea pigs x_1 is shown in Figure 3.3. The effect of a 10% deviation of the ward extraction ventilation rate F or F_w on the the number susceptible guinea pigs x_1 is shown in Figure 3.4. A 10% deviation of the ventilation rate into and out of the animal room F_{in} and F_{out} on the the number susceptible guinea pigs x_1 is shown in Figures 3.5 and 3.6, respectively. Figure 3.7 shows the effect of a larger deviation of

30% in the ranges of the quanta generation rates on the the number susceptible guinea pigs x_1. The larger deviation for the quanta generation rates was investigated because of the uncertainty that lies in this parameter.

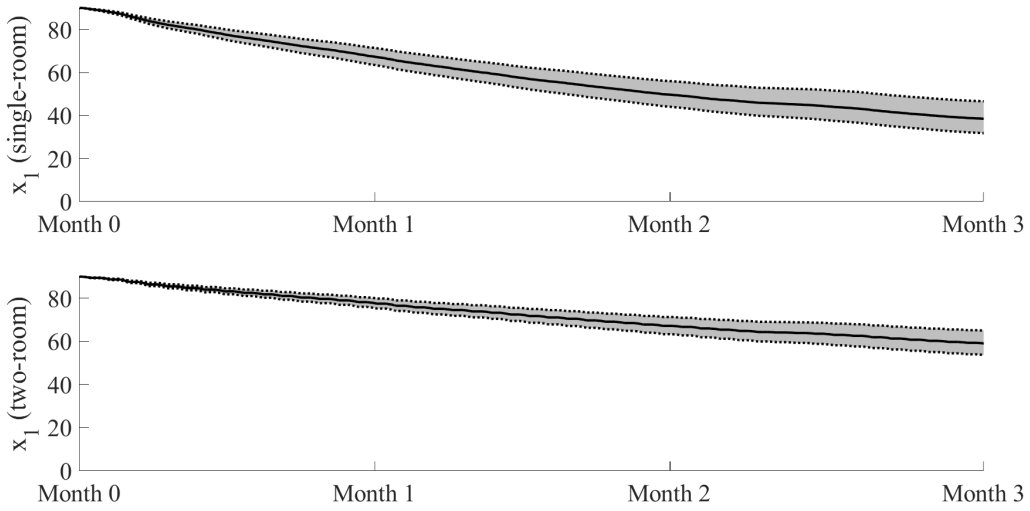

Figure 3.1. Sensitivity of number of susceptible guinea pigs to deviation of the number of infectors for the augmented single-room and simplified two-room GN models. The deviations at the end of the simulations are 21.098% and 10.040%.

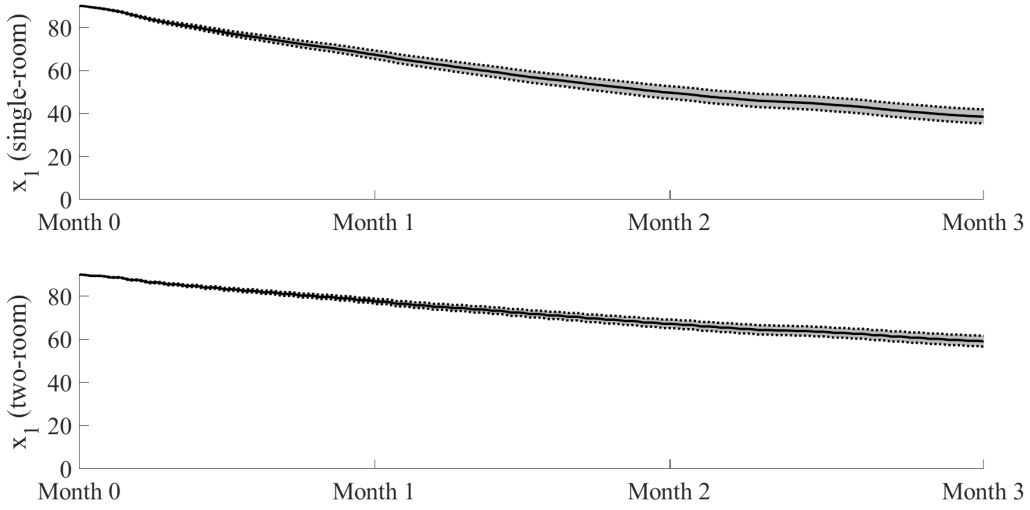

Figure 3.2. Sensitivity of number of susceptible guinea pigs to deviation of the quanta generation rates for the augmented single-room and simplified two-room GN models. The deviations at the end of the simulations are 8.866% and 4.305%.

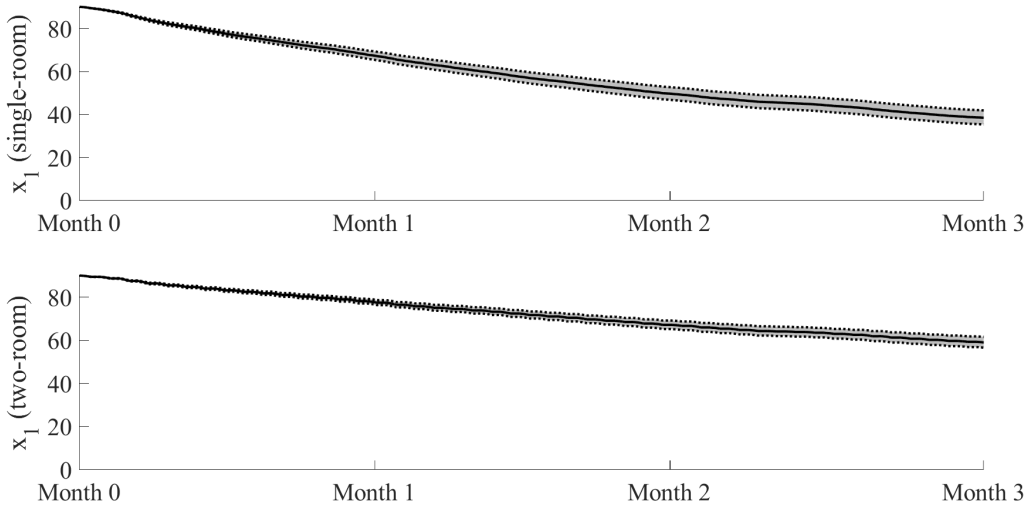

Figure 3.3. Sensitivity of number of susceptible guinea pigs to deviation of the pulmonary ventilation rate for the augmented single-room and simplified two-room GN models. The deviations at the end of the simulations are 8.867% and 4.306%.

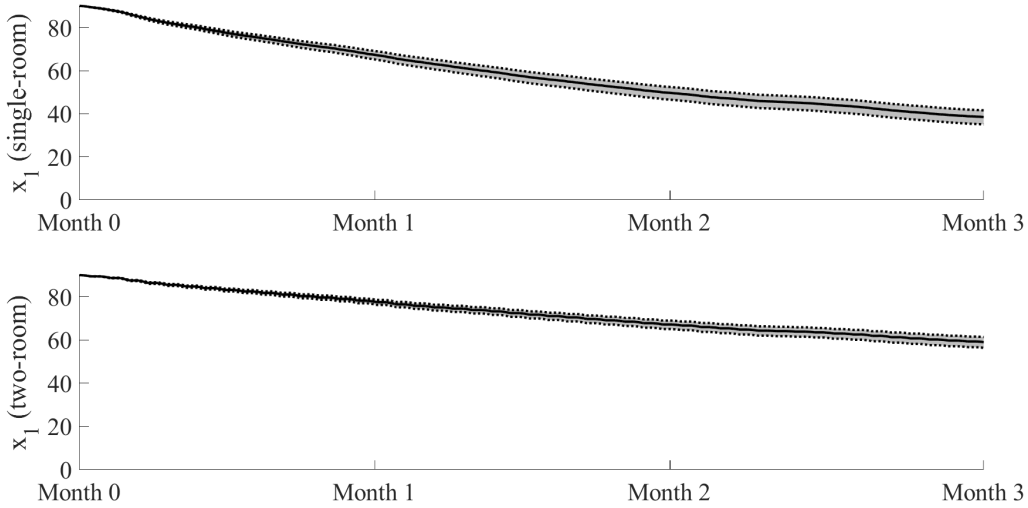

Figure 3.4. Sensitivity of number of susceptible guinea pigs to deviation of the ward ventilation rate for the augmented single-room and simplified two-room GN models. The deviations at the end of the simulations are 7.978% and 3.871%.

The analysis in Figures 3.1 to 3.4 and Figure 3.7 shows that the augmented single-room GN model in (2.6) has deviations of 21.098% for the predicted number of susceptible guinea pigs for a deviation of

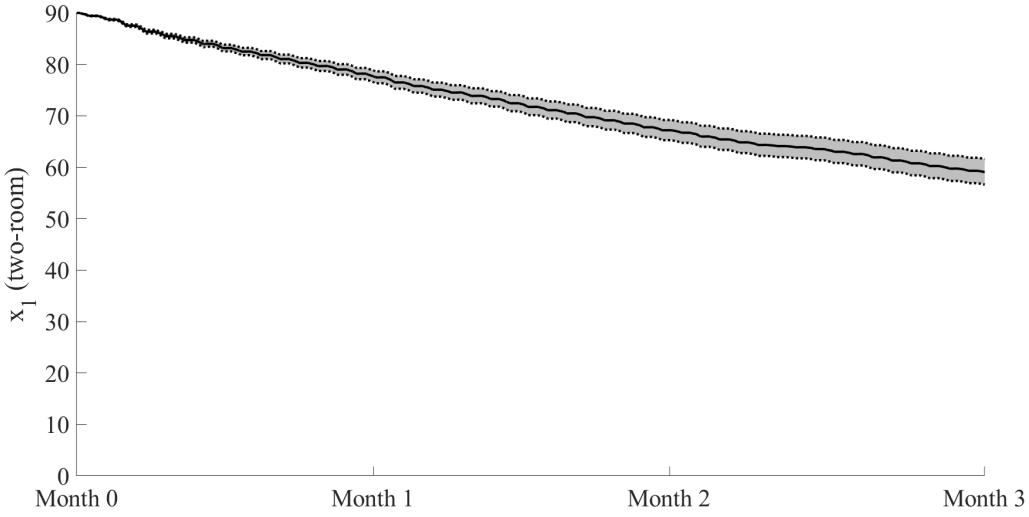

Figure 3.5. Sensitivity of number of susceptible guinea pigs to deviation of the ventilation rate into the animal room for the augmented single-room and simplified two-room GN models. The deviation at the end of the simulation is 4.309%.

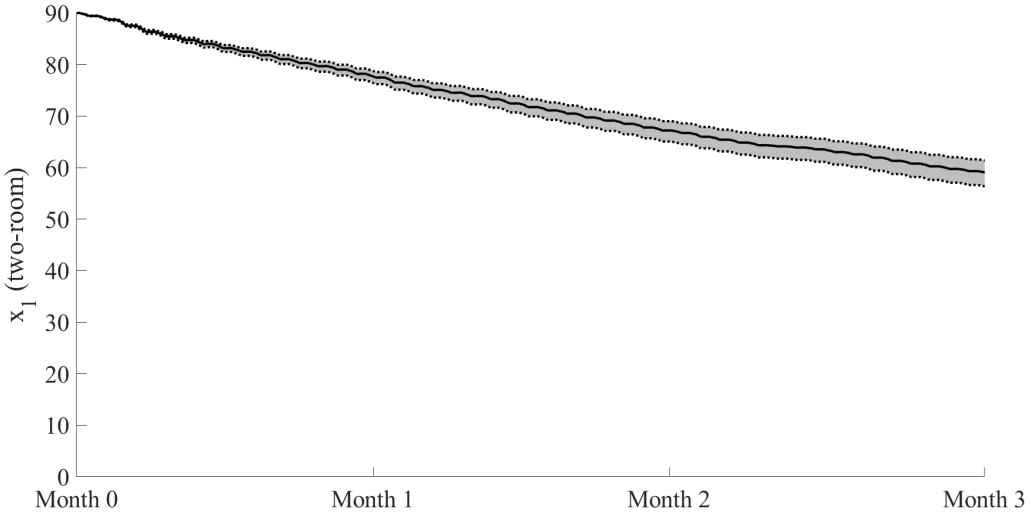

Figure 3.6. Sensitivity of number of susceptible guinea pigs to deviation of the ventilation rate out of the animal room for the augmented single-room and simplified two-room GN models. The deviation at the end of the simulation is 3.922%.

a single infectious individual I_w, 8.866%, 8.867% and 7.978% for the predicted number of susceptible guinea pigs for the x_3, p, and F parameters respectively and a 29.035% deviation was noted in Figure

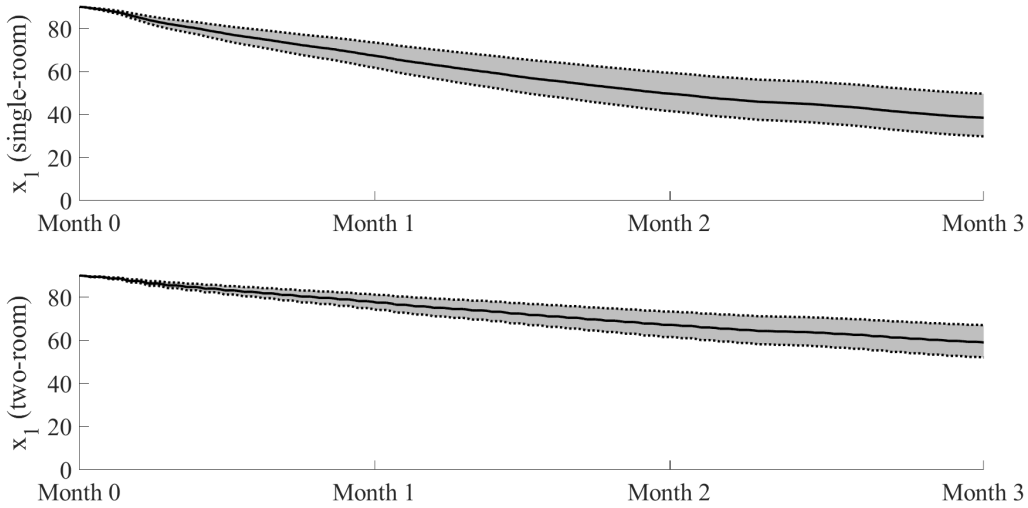

Figure 3.7. Sensitivity of number of susceptible guinea pigs to deviation of the range of the quanta generation rate for the augmented single-room and simplified two-room GN models. The deviations at the end of the simulations are 29.035% and 13.484%.

3.7 for the larger deviation of the quanta parameter x_2.

Figures 3.1 to 3.7 show that the two-room model in (2.11) has deviations of 10.04% for the deviation of a single infector I_w, 4.305%, 4.306%, 3.871%, 4.309% and 3.922% for the predicted number of susceptible guinea pigs for the deviation of the x_3, p, F_w, F_{in} and F_{out} parameters, respectively. A deviation of 13.484% was observed in Figure 3.7 for the larger deviation of the quanta parameter x_6.

The deviation is measured at the end of each simulation. The non-linear relationship of the deviation of each of the model parameters and the predicted number of susceptibles adds to the model uncertainty. Table 3.1 summarises the results obtained for the deviation of the number of susceptibles x_1 at the end of each simulation.

In general, the augmented single-room GN model is more sensitive to parameter variations than the simplified two-room GN model, except for changes in the ventilation rate into and out of the animal room as shown in Figures 3.5 and 3.6, respectively. This is because the deviation that occurs in one parameter for the single-room GN model is divided between two rooms for the two-room model. Only

Table 3.1. Resulting deviation at the end of the simulation for the sensitivity analysis.

Deviated parameter	**Parameter deviation amount**	**Resulting deviation of single-room x_1**	**Resulting deviation of two-room x_1**
I_w	1 individual	21.098%	10.04%
ϕ	10%	8.866%	4.305%
p	10%	8.867%	4.306%
F_w	10%	7.978%	3.871%
F_{in}	10%	-	4.309%
F_{out}	10%	-	3.922%
ϕ	30%	29.035%	13.484%

a fraction of the deviated parameter affects the animal room because only a fraction of air is vented from the ward to the animal room. The sensitivity of the augmented single-room GN model is the same as the standard single-room GN model since the quanta generation rate parameter simply becomes a state instead of a parameter. The sensitivity of the simplified two-room GN model is less than the standard two-room GN model because of the reduced number of uncertain parameters, although some of the internal dynamics are lost.

3.3 IDENTIFIABILITY ANALYSIS

The sensitivity analysis showed little variation between the two models when parameter sweeps are performed. To investigate the difference in the identifiability of the augmented single-room and simplified two-room models, an algebraic identifiability method was used. Algebraic identifiability is a means to determine whether various parameters of an equation can be distinguished from output measurements given known inputs [34]. The algebraic identifiability gives a theoretical indication of what variables and parameters are independently identifiable in the model.

Since only the susceptible animals x_1 is measurable, the solution of x_2 from the single-room GN model in (2.4) is:

$$x_2 = \frac{I_w \phi V}{F} + k_1 e^{-\frac{F}{V}t}, \tag{3.1}$$

where k_1 is a constant.

The infectious particles at time zero are taken as $x_2(0) = x_{20}$ and is substituted into (2.4), which gives:

$$\frac{dx_1}{dt} = -\frac{p}{V}\left(\frac{I_w\phi V}{F} + \left(x_{20} - \frac{I_w\phi V}{F}\right)e^{-\frac{F}{V}t}\right)x_1. \tag{3.2}$$

For simplicity the most common case was considered, where the number of infectious particles are zero for the initial time frame considered. Therefore:

$$\frac{dx_1}{dt} = -\frac{pI_w\phi}{F}\left(1 - e^{-\frac{F}{V}t}\right)x_1. \tag{3.3}$$

To solve this algebraically, let:

$$\theta_1 = -\frac{pI_w\phi}{F}\left(1 - e^{-\frac{F}{V}t}\right), \tag{3.4}$$

and expressing the equation in terms of the measured variable gives:

$$\dot{y} = \theta_1 x_1. \tag{3.5}$$

The rank is calculated in order to determine whether the parameters are identifiable:

$$\begin{aligned}[x_1]\,[\theta_1] &= [\dot{x}_1] \\ rank\,[x_1] &= 1.\end{aligned} \tag{3.6}$$

Since the rank is the same length as the unknown parameter θ, this parameter is algebraically identifiable. From (3.5) it is evident that at least two measurements are necessary to identify the parameters.

The derivation as performed in (3.1) is repeated for the simplified two-room model. The results obtained are shown below in (3.7) and (3.8). The analytic solution of x_4 and x_5 in (2.11) is,

$$\begin{aligned}x_4 &= \frac{I_w\phi V_w}{F_w} + \left(x_{40} - \frac{I_w\phi V_w}{F_w}\right)e^{-\frac{F_w}{V_w}t} \\ x_5 &= \frac{F_{in}}{V_w}\frac{V_1}{F_{out}}\left(\frac{I_w\phi V_w}{F_w} + \left(x_{40} - \frac{I_w\phi V_w}{F_w}\right)e^{-\frac{F_w}{V_w}t}\right) + \left(x_{50} - \frac{F_{in}}{V_w}\frac{V_1}{F_{out}}x_{40}\right)e^{-\frac{F_{out}}{V_1}t}.\end{aligned} \tag{3.7}$$

This can be substituted into $\frac{dx_1}{dt}$ in (2.11) to give,

$$\frac{dx_1}{dt} = -\frac{p}{V_1}\left(\frac{F_{in}}{V_w}\frac{V_1}{F_{out}}\left(\frac{I_w\phi V_w}{F_w}+\left(x_{40}-\frac{I_w\phi V_w}{F_w}\right)e^{-\frac{F_w}{V_w}t}\right)+\left(x_{50}-\frac{F_{in}}{V_w}\frac{V_1}{F_{out}}x_{40}\right)e^{-\frac{F_{out}}{V_1}t}\right)x_1. \quad (3.8)$$

Let $x_{40} = 0$ and $x_{50} = 0$ then:

$$\frac{dx_1}{dt} = -\frac{pF_{in}I_w\phi}{F_{out}F_w}\left(1-e^{-\frac{F_w}{V_w}t}\right)x_1. \quad (3.9)$$

Again let:

$$\theta_2 = -\frac{pF_{in}I_w\phi}{F_{out}F_w}\left(1-e^{-\frac{F_w}{V_w}t}\right). \quad (3.10)$$

As with the equation above, (3.9) is expressed in terms of measured variables:

$$\dot{x_1} = \theta_2 x_1. \quad (3.11)$$

The rank results in the same rank as in (3.6). Using this method of algebraic identifiability, it can be seen that only a single parameter of the model is identifiable from measured data. However, what this also reveals, is that backwards calculation of the parameters would contain any deviations of the other parameters from the actual value.

For example, if the average pulmonary ventilation rate of the guinea pigs was 10% less compared to the value taken from the literature, and the source of infectious particles is backwards calculated, then the source of infectious particles would be estimated to be 10% greater than it actually is.

This implies that it is impossible to distinguish the difference of the deviation of one parameter from its true value of one parameter from that of another.

CHAPTER 4 OBSERVABILITY

4.1 CHAPTER OVERVIEW

In this chapter, observability analyses are performed for each of the models in Section 2.4 to determine whether the states are observable and can therefore be estimated from a theoretical point of view.

4.2 OBSERVABILITY THEORY

4.2.1 Linear Observability

The observability of a system is a measure of how well one can observe the states of a system or, rather, the ability to determine the initial conditions given measured inputs and outputs [10]. A definition for continuous-time observability is given for an LTI SISO system [10]:

A continuous time system is observable if, for any initial state $x(0)$ *and any final time* $t > 0$*, the initial state* $x(0)$ *can be uniquely determined by knowledge of the input* $u(\tau)$ *and output* $y(\tau)$ *for all* $\tau \in [0,t]$.

For the general linear system given in (2.2), the observability matrix is given as:

$$O = \begin{bmatrix} Z \\ ZA \\ \vdots \\ ZA^{n-1} \end{bmatrix}. \tag{4.1}$$

where Z is the output matrix and A is the system matrix.

The system in (2.2) is said to be observable if the rank of the observability matrix of the system is equal to the number of states n [10, 24].

4.2.2 Non-linear Observability

The system in (2.1), with $dim(x) = n$ and $dim(y) = m$, is locally (weakly) observable at x_0 if there exists a neighbourhood X_0 of x_0 such that for every x_1, which is an element of the neighbourhood $X_1 \subset X_0$ of x_0, the indistinguishability of the states x_0 and x_1 implies that $x_0 = x_1$. The two states, x_0 and x_1, are said to be indistinguishable if for every admissible input, u, the output y of (2.1) for the initial state x_0 and for the initial state x_1 is identical [35].

Distribution is the assignment of a subspace to each point x in the vector space $\mathcal{R}$, and codistribution is then the linear forms (including pointwise addition and multiplication) of a distribution.

The observability codistribution of x_0 is given by:

$$d\mathcal{O} = span\{dh_j, dL_f h_j, ..., dL_f^{n-1} h_j\}; j = 1...m, \tag{4.2}$$

where h_j is the j-th measurement function and L_f is the Lie derivative to be defined shortly. (The linear span of a set S of vectors, denoted $span(S)$, is the smallest linear subspace that contains the set. Given a set of smooth vector fields the distribution $D(x)$ is defined as: $D(x) = spanf_1, ..., f_m(x)$ such that the elements of D at any point x are of the form: $\alpha_1(x)f_1(x) + \alpha_2 f_2(x) + ... + \alpha_m(x)f_m(x)$. The dual of a distribution is a codistribution such that the elements of a codistribution are row vectors [36].)

If the system satisfies the so called observability rank condition, i.e. the observability codistribution $d\mathcal{O}$ has dimension n at x_0, then the system is locally observable [35].

$L_f h$ denotes the Lie derivative of h with respect to f, which is calculated using:

$$L_f h = \sum_{i=1}^{n} \frac{\partial h}{\partial x_i} f_i. \tag{4.3}$$

The Lie derivative of dh with respect to f is given as:

$$L_f dh = \left(\frac{\partial dh^T}{\partial x} f \right)^T + dh \frac{\partial f}{\partial x} = dL_f h. \tag{4.4}$$

Once the observability is determined and the system is indeed observable, the states of the model can be theoretically estimated using state estimators [10].

4.3 SINGLE-ROOM GN MODEL OBSERVABILITY

4.3.1 Observability of standard single-room GN model

The standard single-room GN model in (2.4) and (2.5) can be written in the state-space form of (2.1) as:

$$\begin{aligned} \dot{x_1} &= f_1 = -\beta x_1 x_2 \\ \dot{x_2} &= f_2 = \phi I - \tfrac{F}{V} x_2 \\ y &= h = x_1 . \end{aligned} \tag{4.5}$$

The partial derivative of h in (4.5) with respect to x is:

$$dh = \begin{bmatrix} 1 & 0 \end{bmatrix}. \tag{4.6}$$

The Lie derivative of the model in (4.5) is:

$$L_f h = -\beta x_1 x_2, \tag{4.7}$$

and its partial derivative with respect to x is:

$$dL_f h = \begin{bmatrix} -\beta x_2 & -\beta x_1 \end{bmatrix} \tag{4.8}$$

The observability codistribution for (4.5) is:

$$d\mathcal{O} = \begin{bmatrix} dh \\ dL_f h \end{bmatrix} = \begin{bmatrix} 1 & 0 \\ -\beta x_2 & -\beta x_1 \end{bmatrix}. \tag{4.9}$$

The rank of $d\mathcal{O}$ in (4.9) is 2, and is equal to the number of states in (2.4). This means that the model is locally observable at x_0. The determinant of the observability codistribution matrix is:

$$det(d\mathcal{O}) = -\beta x_1 . \tag{4.10}$$

Therefore, the standard single-room model is observable as long as:

$$-\beta x_1 \neq 0. \tag{4.11}$$

4.3.2 Observability of augmented single-room GN model

The augmented single-room GN model given in (2.6) and (2.7) can be written in the state-space form of (2.1). Given the measurement x_1, the observability codistribution can be obtained as follows. The partial derivative of h in (2.7) with respect to x is:

$$dh = \begin{bmatrix} 1 & 0 & 0 \end{bmatrix} \tag{4.12}$$

The Lie derivative of the model in (2.6) is:

$$L_f h = \begin{bmatrix} -\beta x_1 x_2 \end{bmatrix}, \tag{4.13}$$

and its partial derivative with respect to x is:

$$dL_f h = \begin{bmatrix} -\beta x_2 & -\beta x_1 & 0 \end{bmatrix}. \tag{4.14}$$

The repeated Lie derivative of the model in (2.6) is:

$$L_f^2 h = \begin{bmatrix} \beta^2 x_1 x_2^2 - \beta x_1 (I_w x_3 - \frac{F}{V} x_2) \end{bmatrix}, \tag{4.15}$$

and its partial derivative with respect to x is:

$$dL_f^2 h = \begin{bmatrix} \beta^2 x_2^2 - \beta (I_w x_3 - \frac{F}{V} x_2) & 2x_1 x_2 \beta^2 + \frac{F}{V} x_1 \beta & -\beta I_w x_1 \end{bmatrix}. \tag{4.16}$$

The codistribution of the augmented single-room GN model with the added measurement then becomes:

$$d\mathcal{O} = \begin{bmatrix} 1 & 0 & 0 \\ -\beta x_2 & -\beta x_1 & 0 \\ A & B & -\beta I_w x_1 \end{bmatrix}, \tag{4.17}$$

where:

$$A = \beta^2 x_2^2 - \beta(\frac{F}{V}x_2 - I_w x_3)$$
$$B = 2x_1 x_2 \beta^2 + \frac{F}{V}x_1 \beta. \tag{4.18}$$

The rank of $d\mathcal{O}$ in (4.17) is 3 and is equal to the number of states in (2.6). The determinant of the observability codistribution matrix is:

$$det(d\mathcal{O}_{1:3;1:3}) = \beta^2 I_w x_1^2. \tag{4.19}$$

Therefore, the augmented single-room model is locally observable as long as:

$$\beta^2 I_w x_1^2 \neq 0. \tag{4.20}$$

4.4 TWO-ROOM GN MODEL OBSERVABILITY

4.4.1 Observability of standard two-room GN model

Although it is not shown, the rank of $d\mathcal{O}$ for the standard measurement function (2.12) is 4. Since this is less than the number of states in (2.9), the model is unobservable. Using the results obtained from an algebraic identifiability analysis in a previous study and adding another measurement to the model, this rank can be increased [19]. The additional measurement is the rate of change in number of susceptibles $\dot{x_1}$. Therefore, the measurement vector (2.10) for the standard two-room GN model is amended as follows:

$$y = h(x) = \begin{bmatrix} x_1 \\ x_3 \\ \dot{x_1} \end{bmatrix}, \tag{4.21}$$

where $\dot{x_1} = -\frac{p}{V_1}x_5 x_1$.

Eq. (2.9) and (4.21) can be written in the form of (2.1) to give the state-space representation of the standard two-room GN model.

$$\begin{aligned}
\dot{x_1} &= f_1(x) = -\frac{p}{V_1}x_5x_1 \\
\dot{x_2} &= f_2(x) = \frac{p}{V_1}x_5x_1 - \alpha x_2 \\
\dot{x_3} &= f_3(x) = \alpha x_2 \\
\dot{x_4} &= f_4(x) = \phi_w I_w - \frac{F_w}{V_w}x_4 \\
\dot{x_5} &= f_5(x) = \frac{F_{in}}{V_w}x_4 - \frac{F_{out}}{V_1}x_5 \\
y &= h(x) = \begin{bmatrix} x_1 & x_3 & \dot{x_1} \end{bmatrix}
\end{aligned} \tag{4.22}$$

If $\dot{x}_1$ is added as a measurement, the observability codistribution matrix is as in (4.26). The partial derivative of h in (4.21) with respect to x is:

$$dh = \begin{bmatrix} 1 & 0 & 0 & 0 & 0 \\ 0 & 0 & 1 & 0 & 0 \\ -\frac{px_5}{V_1} & 0 & 0 & 0 & -\frac{px_1}{V1} \end{bmatrix} \tag{4.23}$$

The Lie derivative of the model in (4.22) is:

$$L_f h = \begin{bmatrix} -\frac{px_1x_5}{V_1} \\ \alpha x_2 \\ \frac{p^2x_1x_5^2}{V_1^2} + \frac{F_{out}px_1x_5}{V_1^2} - \frac{F_{in}px_1x_4}{V_1V_w} \end{bmatrix}, \tag{4.24}$$

and its partial derivative with respect to x is:

$$dL_f h = \begin{bmatrix} -\frac{px_5}{V_1} & 0 & 0 & 0 & -\frac{px_1}{V_1} \\ 0 & \alpha & 0 & 0 & 0 \\ \frac{p^2x_5^2}{V_1^2} + \frac{F_{out}px_5}{V_1^2} - \frac{F_{in}px_4}{V_1V_w} & 0 & 0 & -\frac{F_{in}px_1}{V_1V_w} & \frac{F_{out}px_1}{V_1^2} + \frac{2p^2x_1x_5}{V_1^2} \end{bmatrix}. \tag{4.25}$$

The resulting observability codistribution matrix is:

$$d\mathcal{O} = \begin{bmatrix} 1 & 0 & 0 & 0 & 0 \\ 0 & 0 & 1 & 0 & 0 \\ -\frac{p}{V_1}x_5 & 0 & 0 & 0 & -\frac{p}{V_1}x_1 \\ -\frac{p}{V_1}x_5 & 0 & 0 & 0 & -\frac{p}{V_1}x_1 \\ 0 & 0 & \alpha & 0 & 0 \\ O_1 & 0 & 0 & O_2 & O_3 \end{bmatrix}, \tag{4.26}$$

where:

$$\begin{aligned} O_1 &= \frac{pF_{out}x_5}{V_1^2} - \frac{pF_{in}x_4}{V_1V_w} + \frac{p^2x_5^2}{V_1^2} \\ O_2 &= -\frac{F_{in}px_1}{V_1V_w} \\ O_3 &= \frac{F_{out}px_1}{V_1^2} + \frac{2p^2x_1x_5}{V_1^2}. \end{aligned} \tag{4.27}$$

The rank of $d\mathcal{O}$ in (4.26) is 5 and is equal to the number of states in (2.9).

The determinant of the full-rank portion (rows 1 to 3, 5 and 6; and columns 1 to 5) of the observability codistribution matrix is:

$$det(d\mathcal{O}_{1:3,5,6;1:5}) = -\frac{F_{in}\alpha p^2x_1^2}{V_1^2V_w}. \tag{4.28}$$

Therefore, the standard two-room model is locally observable as long as:

$$-\frac{F_{in}\alpha p^2x_1^2}{V_1^2V_w} \neq 0. \tag{4.29}$$

4.4.2 Observability of simplified two-room GN model

Similar to (4.21) above, the measurement in (2.12) is amended as follows:

$$y = h(x) = \begin{bmatrix} x_1 \\ -\frac{p}{V_1}x_1 \end{bmatrix}. \tag{4.30}$$

Therefore, if (2.11) and (4.30) are written in the form of (2.1), and dh, $dL_f h$ and $dL^2{}_f h$ are calculated as in (4.31) and (4.33). The partial derivative of h in (4.30) with respect to x is:

$$dh = \begin{bmatrix} 1 & 0 & 0 & 0 \\ -\frac{px_5}{V_1} & 0 & -\frac{px_1}{V_1} & 0 \end{bmatrix} \tag{4.31}$$

The Lie derivative of the model in (4.22) is:

$$L_f h = \begin{bmatrix} -\frac{px_1x_5}{V_1} \\ \frac{p^2x_1x_5^2}{V_1^2} + \frac{F_{out}px_1x_5}{V_1^2} - \frac{F_{in}px_1x_4}{V_1V_w} \end{bmatrix}, \tag{4.32}$$

and its partial derivative with respect to x and the partial derivative of the repeated Lie derivative with respect to x is:

$$\begin{aligned} dL_f h &= \begin{bmatrix} -\frac{px_5}{V_1} & 0 & -\frac{px_1}{V_1} & 0 \\ O_1 & O_2 & O_3 & 0 \end{bmatrix} \\ dL^2{}_f h &= \begin{bmatrix} O_4 & O_5 & O_6 & 0 \\ O_7 & O_8 & O_9 & O_{10}. \end{bmatrix} \end{aligned} \tag{4.33}$$

The resulting observability codistribution matrix is:

$$d\mathcal{O} = \begin{bmatrix} 1 & 0 & 0 & 0 \\ -\frac{p}{V_1}x_5 & 0 & -\frac{p}{V_1}x_1 & 0 \\ -\frac{p}{V_1}x_5 & 0 & -\frac{p}{V_1}x_1 & 0 \\ O_1 & O_2 & O_3 & 0 \\ O_4 & O_5 & O_6 & 0 \\ O_7 & O_8 & O_9 & O_{10} \end{bmatrix}, \tag{4.34}$$

where:

$$
\begin{aligned}
O_1 = O_4 &= \frac{pF_{out}x_5}{V_1^2} - \frac{pF_{in}x_4}{V_1V_w} + \frac{p^2x_5^2}{V_1^2} \\
O_2 = O_5 &= -\frac{F_{in}px_1}{V_1V_w} \\
O_3 = O_6 &= \frac{F_{out}px_1}{V_1^2} + \frac{2p^2x_1x_5}{V_1^2} \\
O_7 &= \frac{F_{in}F_{out}px_4}{V_1^2V_w} - \frac{3F_{out}p^2x_5^2}{V_1^3} - \frac{F_{out}^2px_5}{V_1^3} - \frac{p^3x_5^3}{V_1^3} \\
&\quad + \frac{F_{in}F_wpx_4}{V_1V_w^2} - \frac{F_{in}I_wpx_6}{V_1V_w} + \frac{3F_{in}p^2x_4x_5}{V_1^2V_w} \\
O_8 &= \frac{F_{in}F_{out}px_1}{V_1^2V_w} + \frac{F_{in}F_wpx_1}{V_1V_w^2} + \frac{3F_{in}p^2x_1x_5}{V_1^2V_w} \\
O_9 &= \frac{3F_{in}p^2x_1x_4}{V_1^2V_w} - \frac{F_{out}^2px_1}{V_1^3} - \frac{6F_{out}p^2x_1x_5}{V_1^3} \\
&\quad - \frac{3p^3x_1x_5^2}{V_1^3} \\
O_{10} &= -\frac{F_{in}I_wpx_1}{V_1V_w}.
\end{aligned}
\tag{4.35}
$$

The rank of $d\mathcal{O}$ in (4.34) is 4 and is equal to the number of states in (2.11). Therefore, the simplified two-room model is locally observable as long as the states do not reduce the rank of (4.34) to less than 4.

The determinant of the full-rank portion (rows 1,2, 5 and 6; and columns 1 to 4) of the observability codistribution matrix is:

$$det(d\mathcal{O}_{1,2,5,6;1:4}) = -\frac{F_{in}^2I_wp^3x_1^3}{V_1^3V_w^2}. \tag{4.36}$$

Therefore, the simplified two-room model is locally observable as long as:

$$-\frac{F_{in}^2I_wp^3x_1^3}{V_1^3V_w^2} \neq 0. \tag{4.37}$$

CHAPTER 5 STATE ESTIMATION, SIMULATIONS AND RESULTS

5.1 CHAPTER OVERVIEW

Continuous-time EKFs and hybrid EKFs are used to estimate the states in the models given in Section 2.4 from the available measurements. Simulation setup and results for the continuous-time and hybrid EKFs for the modified and unmodified models are given in this section.

5.2 BACKGROUND TO KALMAN FILTERING

5.2.1 Kalman Filters

A nonlinear system can be approximated by a linear system using Taylor series expansion [10, 24]. The system is expanded around a nominal operating point $\bar{x}$. If the system is linearized around a point such that $\tilde{x} = x - \bar{x}$ is small, the higher powers of the Taylor series expansion will also be small. For the nonlinear system in (5.2), assuming $\tilde{x}$ is small, the system can be approximated as:

$$\begin{aligned} \dot{x} &\approx f(\bar{x},\bar{u},\bar{w}) + \left.\frac{\partial f}{\partial x}\right|_0 (x-\bar{x}) + \left.\frac{\partial f}{\partial u}\right|_0 (u-\bar{u}) + \left.\frac{\partial f}{\partial w}\right|_0 (w-\bar{w}) \\ &= \dot{\bar{x}} + C\tilde{x} + B\tilde{u} + L\tilde{w}, \end{aligned} \tag{5.1}$$

where higher order terms were neglected and $C = \frac{\partial f}{\partial x}|_0$, $B = \frac{\partial f}{\partial u}|_0$, and $L = \frac{\partial f}{\partial w}|_0$.

By subtracting $\dot{\bar{x}}$ from both sides and setting $\bar{w} = 0$ since the mean of the noise is zero, one obtains (5.2):

$$\dot{\tilde{x}} = C\tilde{x} + B\tilde{u} + Lw. \tag{5.2}$$

Processes are often affected by important variables that are not measured, measured and/or unmeasured disturbances, and noisy instruments. State estimators can combine measurements containing noise with process models to estimate the states of such processes.

A dependency on the information of the states of a process is prevalent in model-based control [37]. Deterministic approaches or Bayesian approaches may be used to develop state estimators, with the most commonly used Bayesian estimator being the Kalman filter (KF) [38]. The KF can be used to accurately estimate states of a process where the number of measurements are limited. The KF can also account for uncertainties in the models and the effects of unmeasured disturbances [37]. The KF generates the maximum *a posteriori* estimates in the Bayesian case for a linear dynamic system subjected to additive process and measurement noises with a multivariate Gaussian distribution [39]. If there is a case where the noise in the system is not Gaussian, the KF is still the best linear filter [10].

The KF propagates the mean and the covariance of a system over time. The mean and covariance of each state are then the estimates of the state and the state covariance respectively. Each time a measurement is made, the estimates of the states are updated by the KF. *A priori* and *a posteriori* state estimates are made, where the *a priori* estimate is the state estimate before a measurement is made and the *a posteriori* estimate is the state estimate after a measurement is made. The time-update estimates for the states and the estimates for the covariance of the estimates are derived and used to calculate the KF gain. The time-update estimates are made *a priori*. The KF gain is used to calculate the *a posteriori* estimates after each measurement.

The continuous-time KF for the linear system in (2.2) is given in (5.3):

$$\begin{aligned} K &= PZ^T R^{-1} \\ \dot{\hat{x}} &= A\hat{x} + Bu + K(y - Z\hat{x}) \\ \dot{P} &= -PZ^T R^{-1} ZP + AP + PA^T + Q, \end{aligned} \tag{5.3}$$

where K is the KF gain, P is the estimation-error covariance matrix, R is the measurement noise covariance matrix and Q is the process noise covariance matrix. For the continuous-time KF the propagation and estimation updates are made at the same time, as seen in (5.3).

The estimation-error covariance is effectively an indication of the uncertainty of the estimate. The

diagonal elements P_{11} to P_{nn} of the matrix P shows the covariance of the error between the estimated and actual states of the model and thereby the variance for each of the model states x_1 to x_n, respectively.

5.2.2 Extended Kalman filters

The most commonly used non-linear state estimator is the extended Kalman filter (EKF) [10, 38, 40]. Alternative estimators such as the unscented Kalman filter (UKF) or ensemble Kalman filter (EnKF) have been proposed for nonlinear systems because the EKF is not the optimal nonlinear state estimator. Because of the prevalence and increased interest in constrained controllers, the use of a constrained estimator such as the moving horizon estimator (MHE) has been suggested. The UKF, EnKF and MHE techniques, including techniques designed for non-normal and non-Gaussian process features, have been proposed for chemical processes [37, 40]. Implementing these techniques require knowledge about the process states and the process model. These models often contain model-plant-mismatch in both the parameters and the structure of the model [37, 41].

An EnKF has been used for parameter estimation for the infection rate and fraction of smear positive cases in India. The study uses a deterministic model of TB that models the risk of infection of TB across India and makes use of least squares estimation and an EnKF to determine the infection rate and the number of new cases [42]. Unlike this Indian case study, the work described in this paper estimates the generation rate of quanta for models in confined spaces such as hospitals and workplaces.

5.2.2.1 Continuous-time EKF

Many systems can be approximated as linear systems, and for these an ordinary KF can be used [10]. If a non-linear system can be linearized such that the states represent the deviation from a nominal trajectory of the non-linear system, a linearized KF, known as an EKF, can be used. The EKF estimates the deviation from the nominal state trajectory of a non-linear system. If the nominal state trajectory is unknown, the EKF estimate can be used as the nominal state trajectory. The system is linearized around the estimate, and the estimate is based on the linearized system.

Continuous-time EKFs (CEKF) were designed for the systems in (2.4), (2.6), (2.9) and (2.11). The system equations for the CEKFs are defined as [10]:

$$\begin{aligned} \dot{x} &= f(x,u,w,t) \\ y &= h(x,v,t) \\ w(t) &\sim (0,Q); v \sim (0,R), \end{aligned} \tag{5.4}$$

where $f(x,u,w,t)$ is the continuous-time system, $h(x,v,t)$ is the measurement model, $w(t)$ and $v(t)$ are the zero-mean Gaussian process noise and measurement noise respectively, and Q and R is the process noise covariance matrix and the measurement noise covariance matrix respectively. Matrices Q and R are positive definite and constant.

The continuous-time EKF algorithm consists of two steps, the linearization step and the measurement update step [10]. The linearization step, which uses a Taylor series approximation, is given as:

$$\begin{aligned} \Gamma &= \frac{\partial f}{\partial x}|_{\hat{x}} \\ L &= \frac{\partial f}{\partial w}|_{\hat{x}} \\ H &= \frac{\partial h}{\partial x}|_{\hat{x}} \\ M &= \frac{\partial h}{\partial v}|_{\hat{x}}. \end{aligned} \tag{5.5}$$

The measurement update step is:

$$\begin{aligned} \dot{\hat{x}} &= f(\hat{x},u,w_0,t) + K[y - h(\hat{x},v_0,t)] \\ K &= PH^T R^{-1} \\ \dot{P} &= \Gamma P + P\Gamma^T + LQL^T - PH^T R^{-1} HP, \end{aligned} \tag{5.6}$$

where $\hat{x}$ is the estimate of x, P is the estimation-error covariance of $\hat{x}$, and K is the KF gain [10, 38]. The estimation algorithm can be changed for cases where measurement updates occur at irregular sampling intervals, which itself occurs at multiples of the sampling time to form a hybrid EKF.

The EKF is initialised using:

$$\begin{aligned} \hat{x}_0 &= E[x_0] \\ P_0 &= E[(x_0 - \hat{x}_0)(x_0 - \hat{x}_0)^T], \end{aligned} \tag{5.7}$$

where x_0 is a vector containing the initial states and $\hat{x}_0$ is the initial estimates of x_0.

5.2.2.2 Hybrid EKF

Increasing the simulation step time and the measurement time for the models can result in numerical integration inaccuracies when running simulations [43]. To circumvent this, a hybrid EKF (HEKF) can be used. The HEKF will allow one to simulate the system and update the filter at different time intervals or when measurements are available.

HEKFs are used for continuous-time systems where discrete-time measurements are available. The HEKF uses continuous-time update equations to evaluate the discrete-time values of the model states, x, and the covariance of the estimation error, P, and updates the state estimate using a discrete-time KF.

The HEKF process is similar to the EKF. However, the update step is split into the continuous-time update equations (where the models are simulated in continuous-time) and the discrete measurement update equations (where the filter estimates are updated).

The continuous-time update equations are:

$$\begin{aligned} \dot{\hat{x}} &= f(\hat{x}, u, \omega_0, t) \\ \dot{P} &= \Gamma P + P\Gamma^T + LQL^T, \end{aligned} \tag{5.8}$$

and the discrete measurement update equations are:

$$\begin{aligned} K_k &= P_k^- H_k^T (H_k P_k^- H_k^T + M_k R_k M_k^T)^{-1} \\ x_k^+ &= x_k^- + K_k[y_k - h_k(\hat{x}_k^-, v_0, t_k)] \\ P_k^+ &= (I_D - K_k H_k) P_k^- (I_D - K_k H_k)^T \\ &\quad + K_k M_k R_k M_k^T K_k^T, \end{aligned} \tag{5.9}$$

where k denotes the k-th discrete-time measurement, P_k^- is the covariance of x_k before the measurement update, and P_k^+ is the covariance of x_k after the measurement update. I_D is an identity matrix. x_k^- is the estimate of x before the measurement update is made and x_k^+ is the estimate of x after the measurement update is made.

5.2.3 Setting up the Kalman filter

5.2.3.1 The covariance matrices Q and R

Proper functioning of the KF depends on the correct specification of the process and measurement noise covariance matrices, Q and R. These matrices are indicative of the relative confidence of the filter model and the measurements. Q is then the amount of uncertainty one has in the model and R is the uncertainty in the measurements [37]. The Q and R matrices can, if incorrectly specified, cause the filter to under-perform or cause the estimates to diverge [37].

The R matrix can usually be derived from the measurement device characteristics. Increasing the covariance estimate of R can make the filter more robust to errors in measurements. Selecting a too large R can cause an offset or divergence in the presence of model mismatch [40]. Q is commonly chosen arbitrarily because estimation of the process noise covariance is more complicated [37, 40]. If Q is guessed lower than the actual covariance, then the filter may be too confident in the model and if the covariance is guessed too high the estimates may be noisy and the uncertainty in the estimates would increase [37].

Various methods for estimating the process noise covariance exist including Bayesian methods, maximum likelihood methods, covariance matching, and correlation techniques [38, 40, 44]. These methods can however be computationally excessive or give biased estimates. A least-squares method can be used wherein the Q and R covariances are estimated and calculated using least-squares problem solving [44]. This method does not consider structural and parametric errors [40].

The methods mentioned thus far assume that the noise characteristics are zero mean and have Gaussian distribution [38]. This would only be the case for processes at steady state [37]. Time-varying online computation of Q have more recently been used [37, 38, 40]. Online estimation of the process noise covariance has been made using linearised, Monte Carlo and direct optimisation and extended expectation maximisation approaches. The linearised and Monte Carlo approaches make use of calculated parameter covariances and probability density functions of the parameters, respectively to calculate a time-varying $Q(t)$ [37, 40]. The direct optimisation approach finds the optimal solution to minimise an objective function to solve for $Q(t)$ [38]. The extended expectation maximisation approach

uses linearisation of the model along with smoothed state and covariance estimates to calculate $Q(t)$ [38]. The direct optimisation and extended expectation maximisation methods also compute $R(t)$, P_0 and x_0.

Since the measurement data in this paper are generated using the models in Section 2.4, and measurement and process noise is added to these models in the form of Gaussian noise, the Q and R are known *a priori* and chosen based on this knowledge. Both Q and R for the KFs are chosen as 1.5 times greater than the actual measurement and process noise covariances to ensure the uncertainty of the KFs are greater than that of the simulated models [40].

5.2.3.2 The initial error covariance matrix

Assuming a more severe outbreak, such as an office building outbreak (Table 5.12), the range of each of the states is either known, or can be calculated. According to [40], P_0 can be specified as:

$$\begin{aligned} \hat{x}_0 &= E[x_0] \\ P_0 &= diag((\hat{x}_0 - x_0)^T(\hat{x}_0 - x_0)), \end{aligned} \tag{5.10}$$

where x_0 is assumed to be the minimum value of x, $x_0 = x_{min}$ and $\hat{x}_0$ is the nominal value of x, $\hat{x}_0 = 0.5(x_{max} + x_{min})$.

Table 5.1 shows the ranges of each of the states for each model. The maximum number of quanta in each room is obtained by using the average ventilation rates of F_w, F_{in} and F_{out} and calculating the steady state value of the number of quanta in the room for the maximum number of infectious individuals I_w measured.

Because there is low uncertainty in the measurement of the number of infected guinea pigs, P_0 for x_1 is chosen smaller than the nominal value. $P_{0_{x_1}}$ is chosen using $\hat{x}_0 = 0.1(x_{max} + x_{min})$.

Table 5.1. Range of each state for each model given in Section 2.4.1.

Standard single-room GN model states	**Range**
x_1	$(0, 90)$
x_2	$(0, 35.283)$
Augmented single-room GN model states	**Range**
x_1	$(0, 90)$
x_2	$(0, 35.283)$
x_3	$(0, 300)$
Standard two-room GN model states	**Range**
x_1	$(0, 90)$
x_2	$(0, 90)$
x_3	$(0, 90)$
x_4	$(0, 35.283)$
x_5	$(0, 0.6666)$
Simplified two-room GN model states	**Range**
x_1	$(0, 90)$
x_4	$(0, 35.283)$
x_5	$(0, 0.6666)$
x_6	$(0, 300)$

5.3 SINGLE-ROOM GN MODEL

The model parameters are time-scaled to the sampling time used in the simulations in Sections 5.3.1, 5.3.2 and 5.3.3 and the simulation duration is 3 months.

5.3.1 CEKF for the standard single-room GN model

5.3.1.1 Simulation scenario and setup

Gaussian noise is added to the measured number of susceptibles and each of the states (measurement and process noise) at an interval of 60 s with power equal to R and Q. It is assumed that each infectious individual generates the same number of quanta x_2 and that each of the animals has the same susceptibility. It is also assumed that the infectious individuals I_w remained in the room for the duration of the experiment.

The model parameters are time-scaled to the sampling time used in the simulations and the simulation duration is 3 months. The simulation time step size for the CEKF is the same as the measurement time of 60 s. Table 5.2 shows the measurement noise and process noise covariance matrices and Table 5.3 shows the initial parameters for the CEKF. The initial quanta generation rate ϕ is set as 150 quanta $\cdot$ d $^{-}$1 for the EKF, which results in a parameter mismatch between the simulated model and the EKF model. The simulation data given in Tables 2.3 is used for the simulations.

Table 5.2. CEKF covariance matrix parameters.

R	Q
4.86	$\begin{bmatrix} 0.1838 & 0 \\ 0 & 766.34 \end{bmatrix}$

Table 5.3. CEKF initial parameters for the standard single-room GN model.

Parameter	Estimated Value
$\hat{x}_0$	$\begin{bmatrix} 81 \\ 17.14 \end{bmatrix}$
P_0	$\begin{bmatrix} 81 & 0 \\ 0 & 311.22 \end{bmatrix}$

The initialisation parameters for the CEKF are given in Table 5.3.

The initial number of susceptible animals is taken as $\hat{x}_1 = 81$ animals and the initial quanta in the room as $\hat{x}_2 = 17.14$ quanta. The quanta generation rate is taken as $\phi = 150$ quanta$\cdot$ d$^{-1}\cdot$ ind^{-1}. The

initial estimates in Table 5.3 of the measurable parameters are purposely changed from the actual values in Table 2.3 because the CEKF requires some perturbation to estimate the parameters [10]. The CEKF measurement update matrix K and the estimation-error covariance matrix P are updated as in (5.6).

5.3.1.2 Simulation results

Figures 5.1 and 5.2 show the results of the EKF for the simulated number of susceptible animals and number of quanta in the room states for the standard single-room model. The estimated number of susceptible animals converges almost immediately with the simulated number of susceptible animals. Almost no error can be seen between the estimated and simulated number of susceptible animals.

The estimated number of quanta in the room does not converge. The estimated number of quanta in the room and the simulated number of quanta in the room appear to correlate well, except for a large offset resulting from the parameter mismatch. A zoomed version of the number of quanta in the room is shown in Figure 5.3.

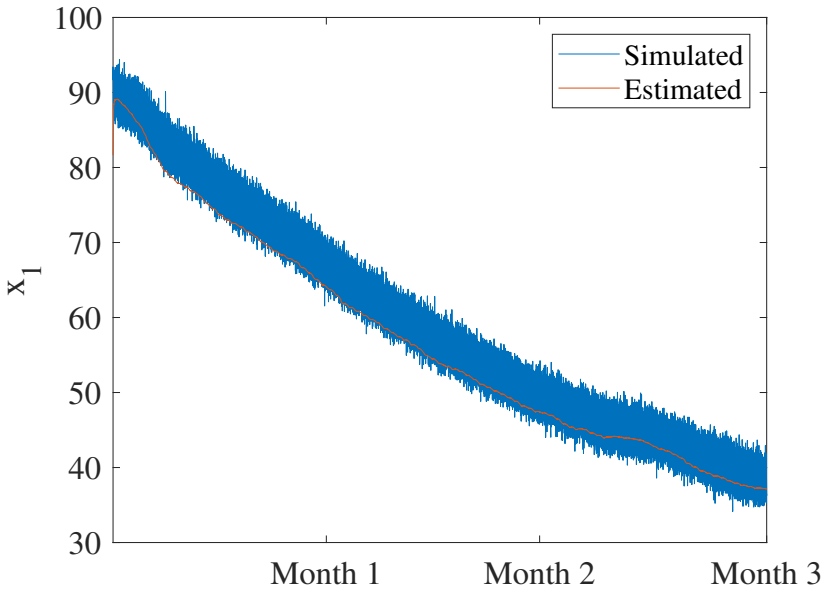

Figure 5.1. Number of susceptible animals of the standard single-room GN model CEKF simulation with a sampling time of 60 s. The simulated number of susceptible animals is shown in blue and the estimated number of susceptible animals is shown in orange.

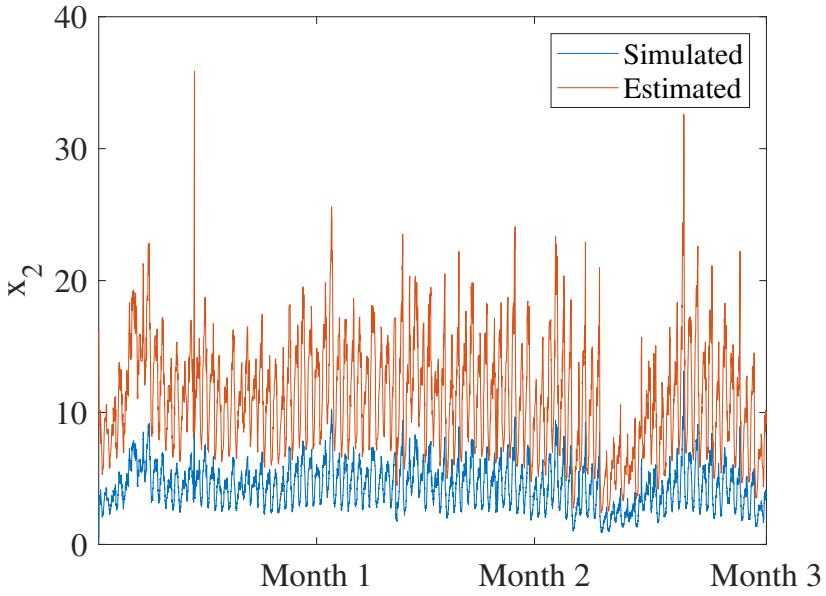

Figure 5.2. Number of quanta in the room of the standard single-room GN model CEKF simulation with a sampling time of 60 s. The simulated number of quanta in the room is shown in blue and the estimated number of quanta in the room is shown in orange.

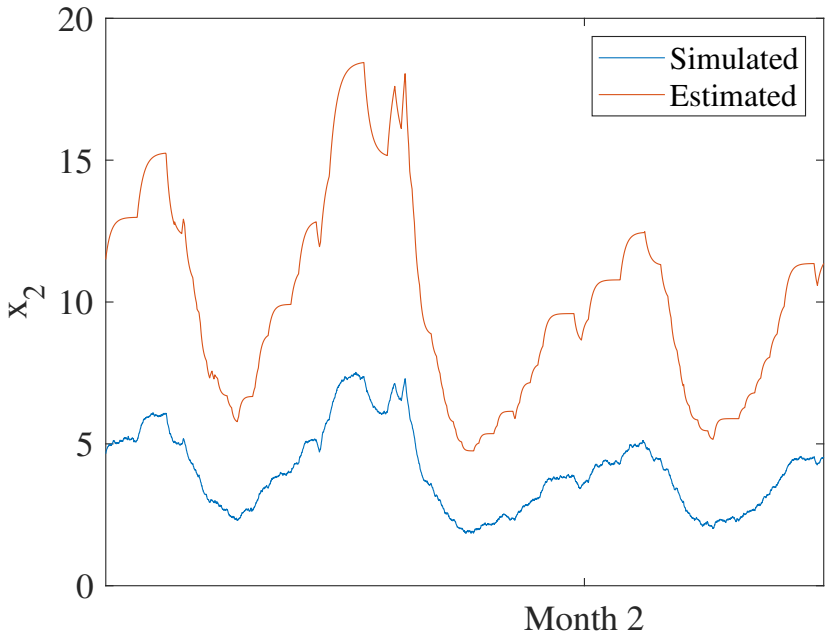

Figure 5.3. Zoomed number of quanta in the room of the standard single-room GN model CEKF simulation with a sampling time of 60 s. The simulated number of quanta in the room is shown in blue and the estimated number of quanta in the room is shown in orange. The period shown is 3 days.

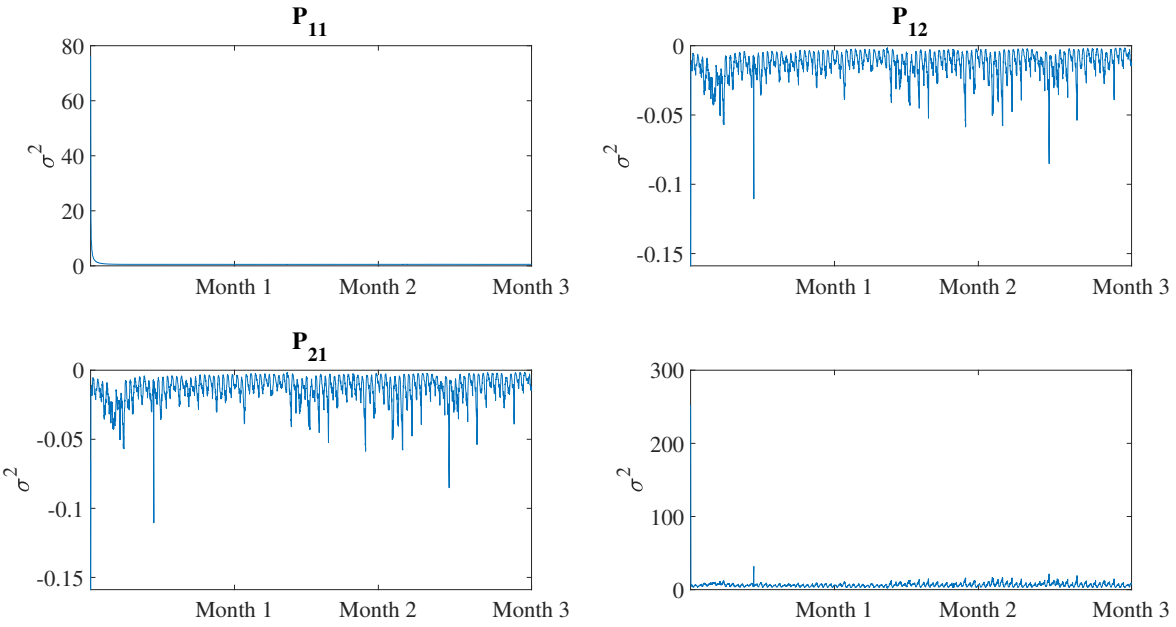

Figure 5.4. Covariance of the estimation-error of the standard single-room GN model CEKF simulation with a sampling time of 60 s.

The diagonal terms of figure 5.4 show the variance of each of the states. Both variances of the states x_1 and x_2 decrease very quickly and remain low for the duration of the simulation.

5.3.2 CEKF for the augmented single-room GN model

5.3.2.1 Simulation scenario and setup

Considering the models given in (2.3) to (2.6), the variable x_1 and parameters p, V, I_w and F can all be measured. The variable x_2 and parameter ϕ can not be measured but can be estimated. Since x_2 is a function of the measured parameters, I_w, V, and F, and the estimated parameter ϕ, one only needs to estimate ϕ to obtain x_2.

The simulation time step size for the CEKF is again the same as the measurement time of 60 s. The measurement and process noise covariance matrices R and Q, were chosen as shown in Table 5.4. The CEKF model is given a 90 quanta $\cdot$ d $^{-}$1 mismatch for the quanta generation rate parameter, ϕ or x_3 in (2.6). The simulation data is the same as for Section 5.3.1.

Table 5.4. CEKF covariance matrix parameters.

R	Q
4.86	$\begin{bmatrix} 0.1838 & 0 & 0 \\ 0 & 766.34 & 0 \\ 0 & 0 & 3456 \end{bmatrix}$

The initialization parameters for the CEKF are given in Table 5.5.

Table 5.5. CEKF initial parameters for the augmented single-room GN model.

Parameter	Estimated Value
$\hat{x}_0$	$\begin{bmatrix} 81 \\ 17.14 \\ 150 \end{bmatrix}$
P_0	$\begin{bmatrix} 81 & 0 & 0 \\ 0 & 311.22 & 0 \\ 0 & 0 & 22500 \end{bmatrix}$

The initial number of susceptible animals is taken as $\hat{x}_1 = 81$ animals and the initial quanta in the room as $\hat{x}_2 = 17.14$ quanta. The quanta generation rate is taken as $\hat{x}_3 = 150$ quanta$\cdot$ d^{-1}. The initial estimates in Table 5.5 of the measurable parameters are purposely changed from the actual values in Table 2.4 because the CEKF requires some perturbation to estimate the parameters [10]. The CEKF measurement update matrix K and the estimation-error covariance matrix P are updated as in (5.6).

5.3.2.2 Simulation results

The number of susceptible animals x_1 decays from 90 to 38 animals in 3 months for a quanta generation rate of $x_3 = 60$ quanta $\cdot$ d^{-1} per infectious individual as shown in Figure 5.5. The CEKF estimate of the number of susceptibles x_1 starts at 81 and converges to the measured number of susceptibles within 0.1542 days. The number of quanta x_2 in the room is simulated in Figure 5.6 and a zoomed version is

shown in Figure 5.7. The estimated number of quanta converges to the simulated number of quanta after 3.9 days.

As seen in Figure 5.8, the estimated quanta generation rate x_3 converges to within 2% of the measured values after just 3.9 days of simulation. This shows that the CEKF can converge to an accurate estimate of the quanta generation rate of the model.

The diagonal terms of figure 5.9 show the variance of each of the states, as with the standard single-room GN model. The variance of the state x_1 decreases very quickly and remains low for the duration of the simulation. The variance for the x_2 state decreases from the initial value but remains large. The variance of the x_3 state reduces by a large amount and steadily increases for the remainder of the simulation.

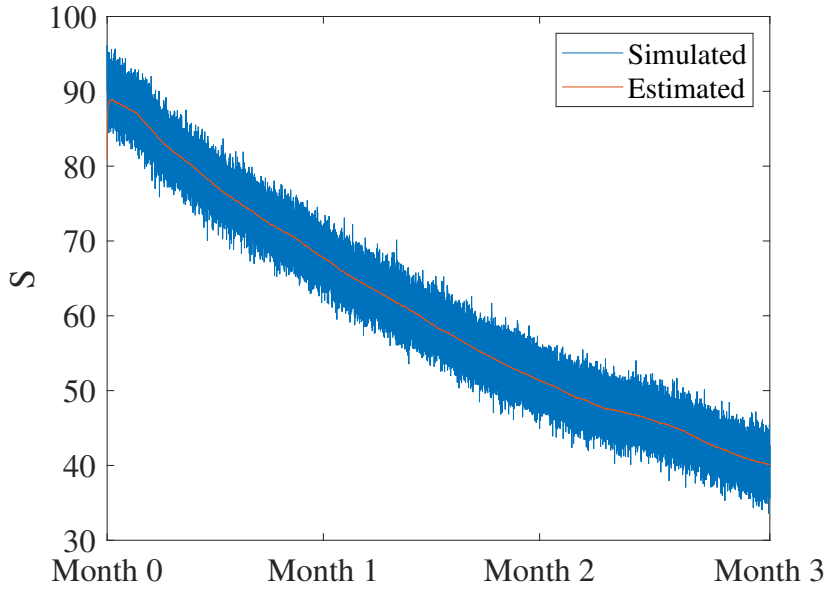

Figure 5.5. Number of susceptible animals of the augmented single-room GN model CEKF simulation with a sampling time of 60 s. The simulated number of susceptible animals is shown in blue and the estimated number of susceptible animals is shown in orange.

Although it is not shown, the CEKF was also simulated for measurement sampling times of both twice per day and once per day in order to view the effects of different sampling times on the estimates. It is important to note that if the sampling time becomes fairly large, some integration error occurs in the simulation. The number of susceptible animals x_1 reduces to 38 animals in the simulation with a measurement sampling time of 60 s and in the worst case only reduces to 44 animals in the simulation

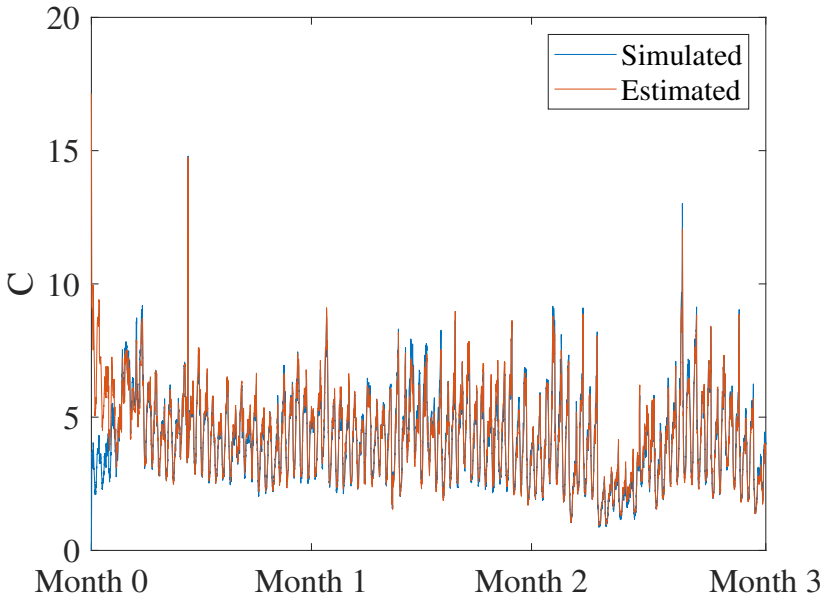

Figure 5.6. Number of quanta in the room of the augmented single-room GN model CEKF simulation with a sampling time of 60 s. The simulated number of quanta in the room is shown in blue and the estimated number of quanta in the room is shown in orange.

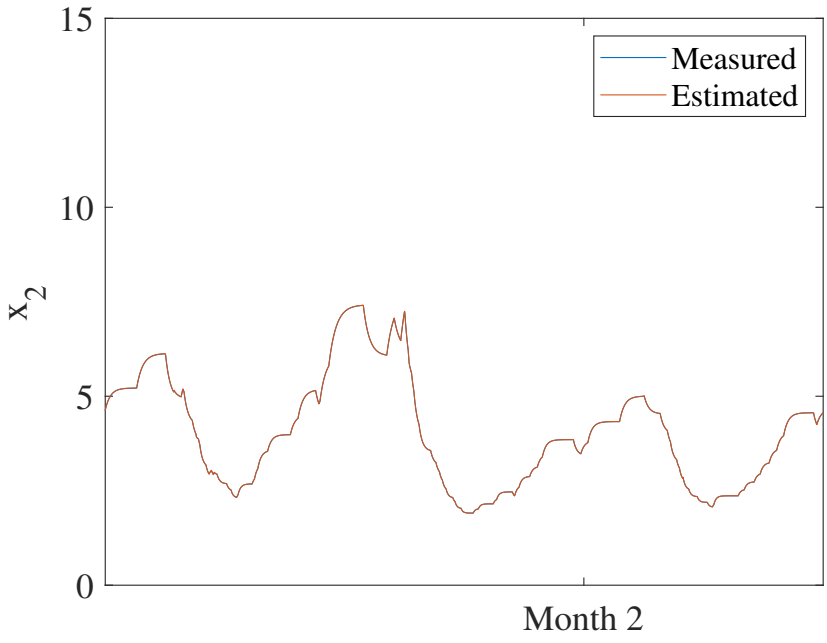

Figure 5.7. Zoomed number of quanta in the room of the augmented single-room GN model CEKF simulation with a sampling time of 60 s. The simulated number of quanta in the room is shown in blue and the estimated number of quanta in the room is shown in orange. The period shown is 3 days.

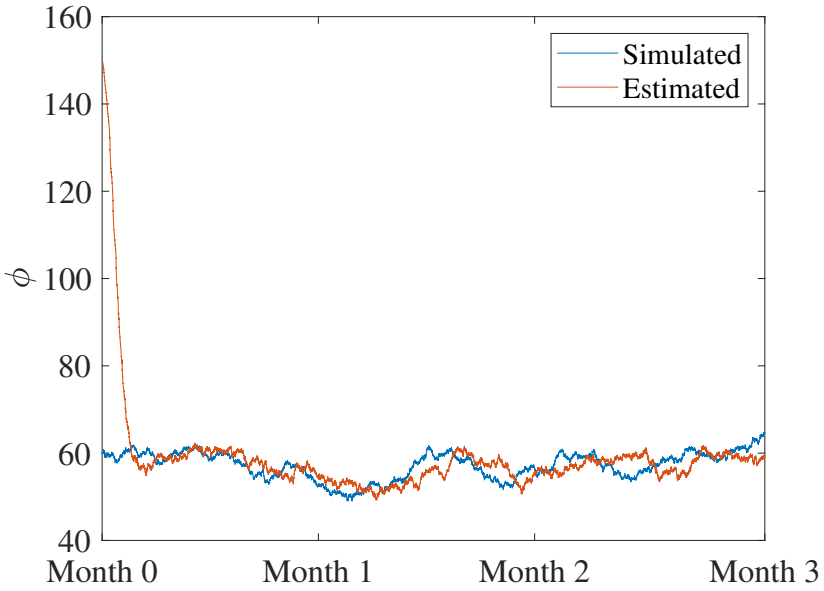

Figure 5.8. Quanta generation rate of the augmented single-room GN model CEKF simulation with a sampling time of 60 s. The blue line indicates the actual quanta generation rate per infectious individual and the orange line represents the estimated quanta generation rate per infectious individual.

with a measurement sampling time of 1 day. The simulation with a measurement sampling time of 1 day also only converged after 2 months. To improve on this situation, an HEKF is used for simulations where the time between measurements of the number of susceptibles is greater than the time between measurements of the other parameters, as is the case in Section 5.3.3.

In order to obtain the best sampling rate (measurement time), one can use a fast Fourier transform of the simulated quanta in the room (or ward) to determine the Nyquist frequency. The Nyquist frequency results in a measurement rate of twice per day and the second harmonic gives a measurement rate of once per day. Sampling at the Nyquist frequency is a minimum requirement for preserving the information contained in the quanta state [45].

The generation rate parameter $x_3 = \phi$ only influences the gain of the state x_2 as seen in (2.8), and is a time-independent constant. Because quanta state x_2 is dependent on the generation rate x_3 (which is constant) and the ventilation rate F (which is measured at a sampling rate of 60 s, much faster than the Nyquist frequency), the estimated number of quanta in the room x_2 can be updated at a rate slower than the Nyquist frequency, seeing as the only uncertain parameter is a constant and that the simulation time is the same as the ventilation sampling rate. Therefore sampling at the second harmonic

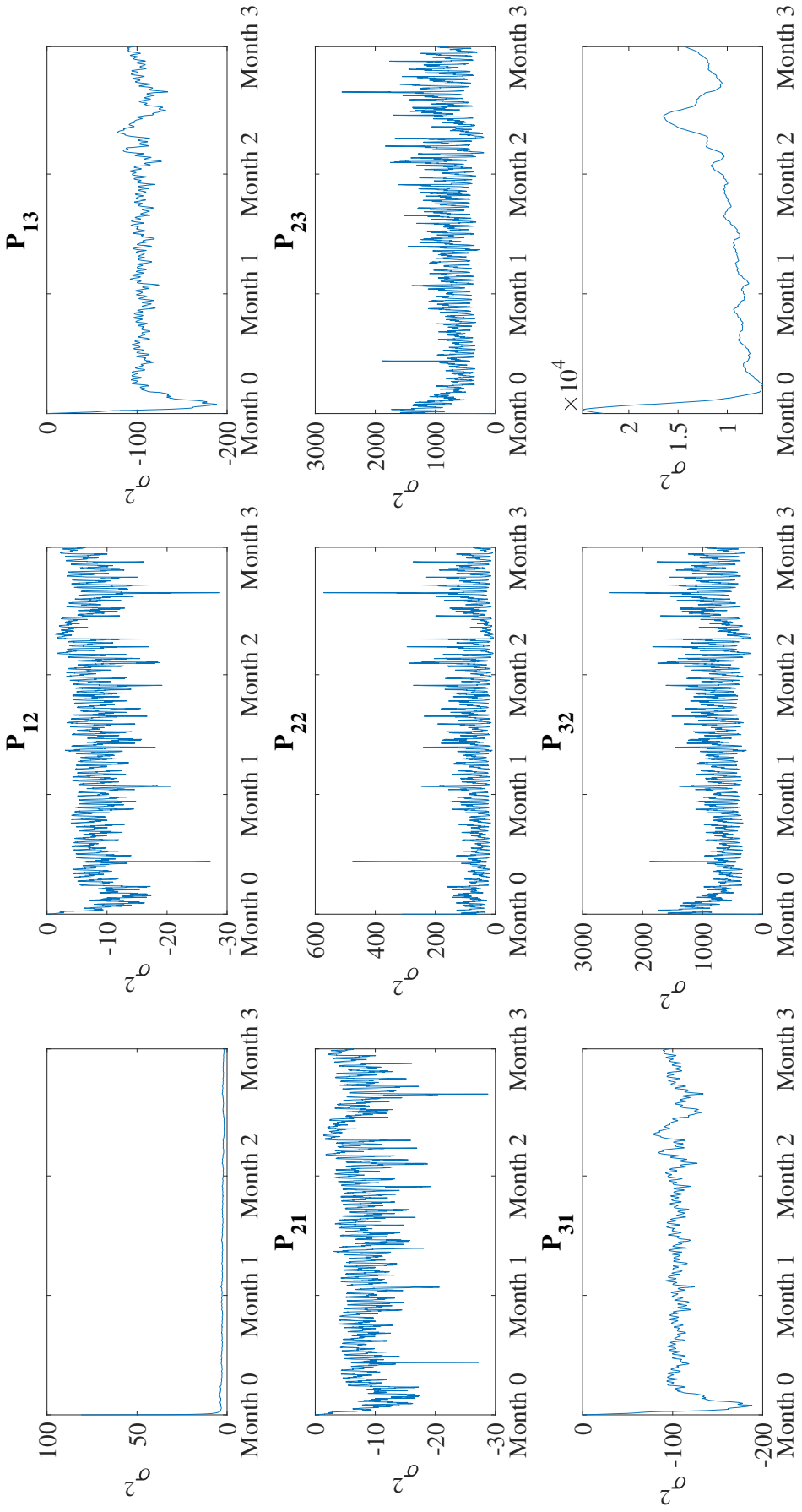

Figure 5.9. Covariance of the estimation-error of the augmented single-room GN model CEKF simulation with a sampling time of 60 s.

would be sufficient to estimate the quanta generation rate x_3 and thereby the number of quanta x_2. A measurement sampling rate of once per day, and not twice per day, is therefore used.

The CEKF performs well seeing that the estimated states rapidly converge to the measurements when using a measurement sampling time of 60 s. However, taking measurements every 60 s is unrealistic, but is used here to see what estimates can be obtained under ideal circumstances. A more realistic scenario, with a measurement rate of once per day, is discussed in the next section.

It is important to note that the artificial zero-mean Gaussian noise parameter, w_p, allows the EKF to better adjust the estimate of the quanta generation rate [10].

5.3.3 HEKF for the augmented single-room GN model

5.3.3.1 Simulation scenario and setup

The same model as in Section 5.3.2 is used here, but with a measurement time of 1 day (24 hours). The HEKF parameters are given in Tables 5.5 and 5.6. The same noise is added as in Section 5.3.2.

Table 5.6. HEKF parameters.

Simulation Time	Measurement Time	R	Q
60 s	1 day	4.86	$\begin{bmatrix} 0.1838 & 0 & 0 \\ 0 & 766.34 & 0 \\ 0 & 0 & 3456 \end{bmatrix}$

The simulation data, as shown in Figures 2.2 to 2.4, are the same as for the simulation in Section 5.3.2.

5.3.3.2 Simulation results

The model in (2.6) is simulated with a simulation step size of 60 s and a sampling (measurement) time of 1 day because the measurement data are not available at 60 s sampling intervals as assumed in

Section 5.3.2. The resulting simulations are shown in Figure 5.10 to Figure 5.13.

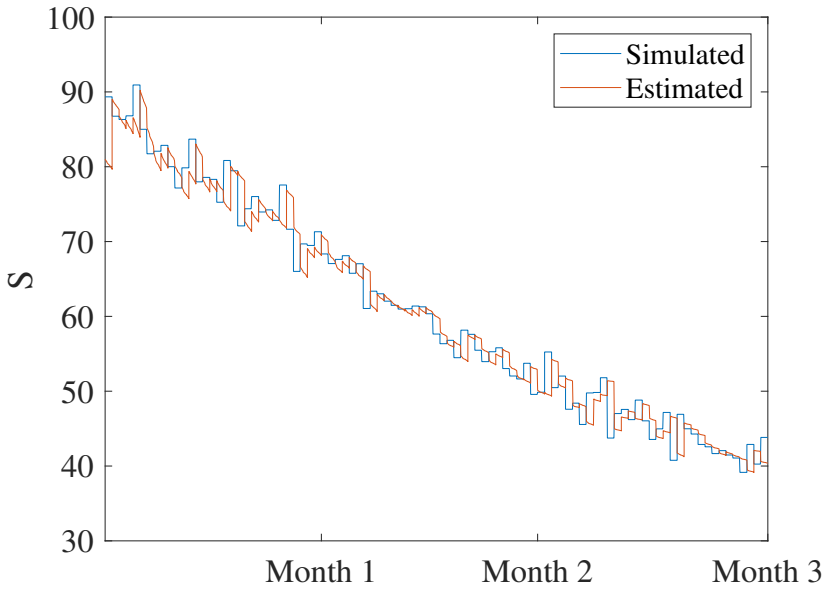

Figure 5.10. Number of susceptible animals of the augmented single-room GN model HEKF parameter estimation simulation with a sampling time of 1 day and simulation step size of 60 s. The simulated number of susceptible animals is shown in blue and the estimated number of susceptible animals is shown in orange.

From the Figures 5.10 to 5.13 it is can be seen that the HEKF quanta generation rate x_3 estimate converges using the same noise covariance matrices as used in Section 5.3.2, however the estimate is not very accurate, but remains within $0.5w_{x_1}$ after 40.031 days. The number of susceptible animals x_1 also reduces to 38 as it should. A large amount of deviation can be seen in the number of quanta in the room due to the discontinuities present in the measured state x_1.

The diagonal terms of figure 5.14 again show the variance of each of the states. The variance of the state x_1 decreases very quickly and remains low for the duration of the simulation, however some noise due to the discrete measurements can be seen. The variance for the x_2 state decreases from the initial value but remains large and increases throughout the remainder of the simulation. The variance of the x_3 state increases by a large amount for the remainder of the simulation.

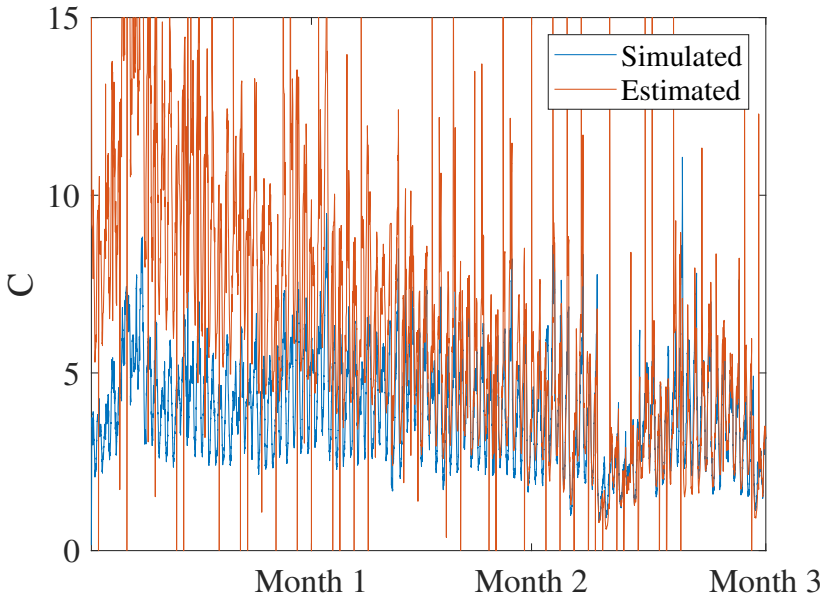

Figure 5.11. Number of quanta in the room of the augmented single-room GN model HEKF parameter estimation simulation with a measurement time of 1 day and simulation step size of 60 s. The simulated number of quanta in the room is shown in blue and the estimated number of quanta in the room is shown in orange.

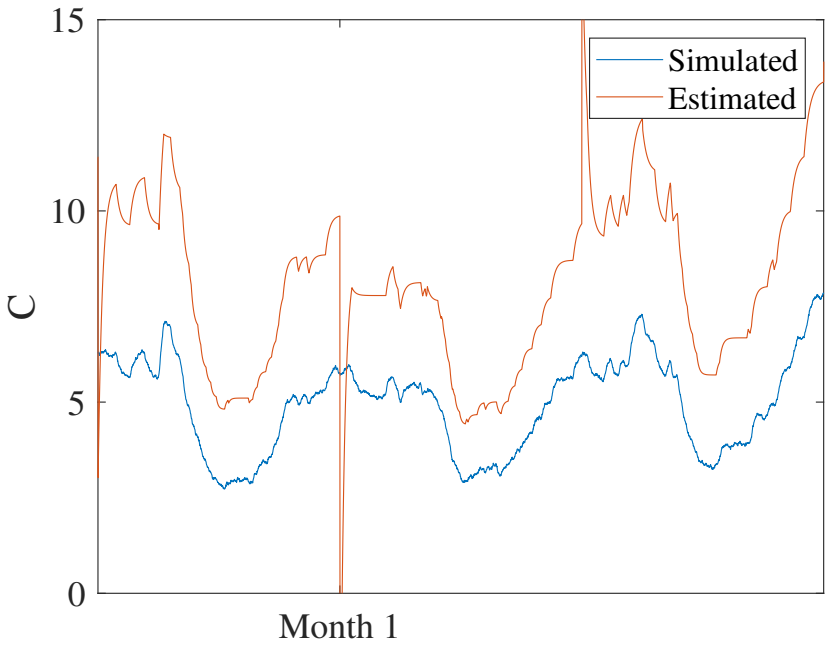

Figure 5.12. Time-zoomed number of quanta in the room of the augmented single-room GN model HEKF parameter estimation simulation with a measurement time of 1 day and simulation step size of 60 s. The simulated number of quanta in the room is shown in blue and the estimated number of quanta in the room is shown in orange. The period shown is 3 days.

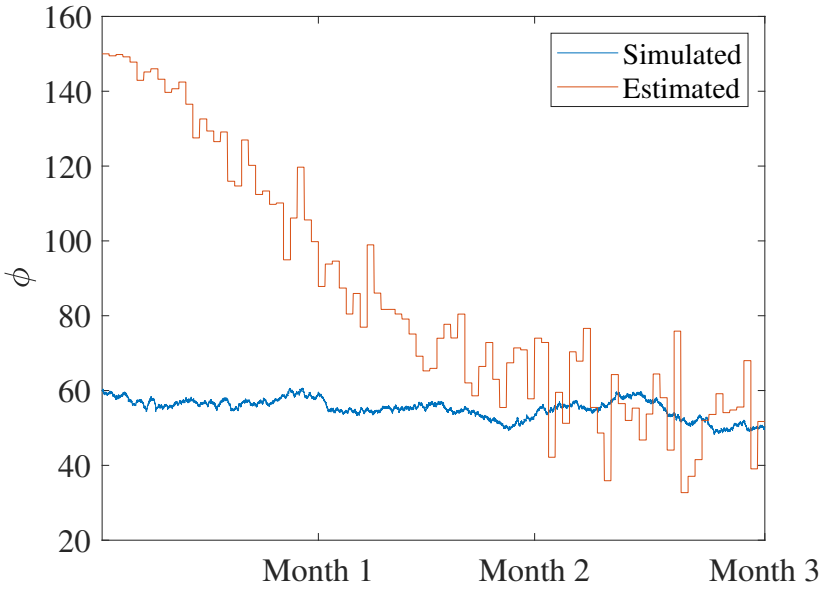

Figure 5.13. Quanta generation rate per infectious individual of the augmented single-room GN model HEKF parameter estimation with a measurement time of 1 day and simulation step size of 60 s. The simulated quanta generation rate per infectious individual is shown in blue and the estimated quanta generation rate per infectious individual is shown in orange.

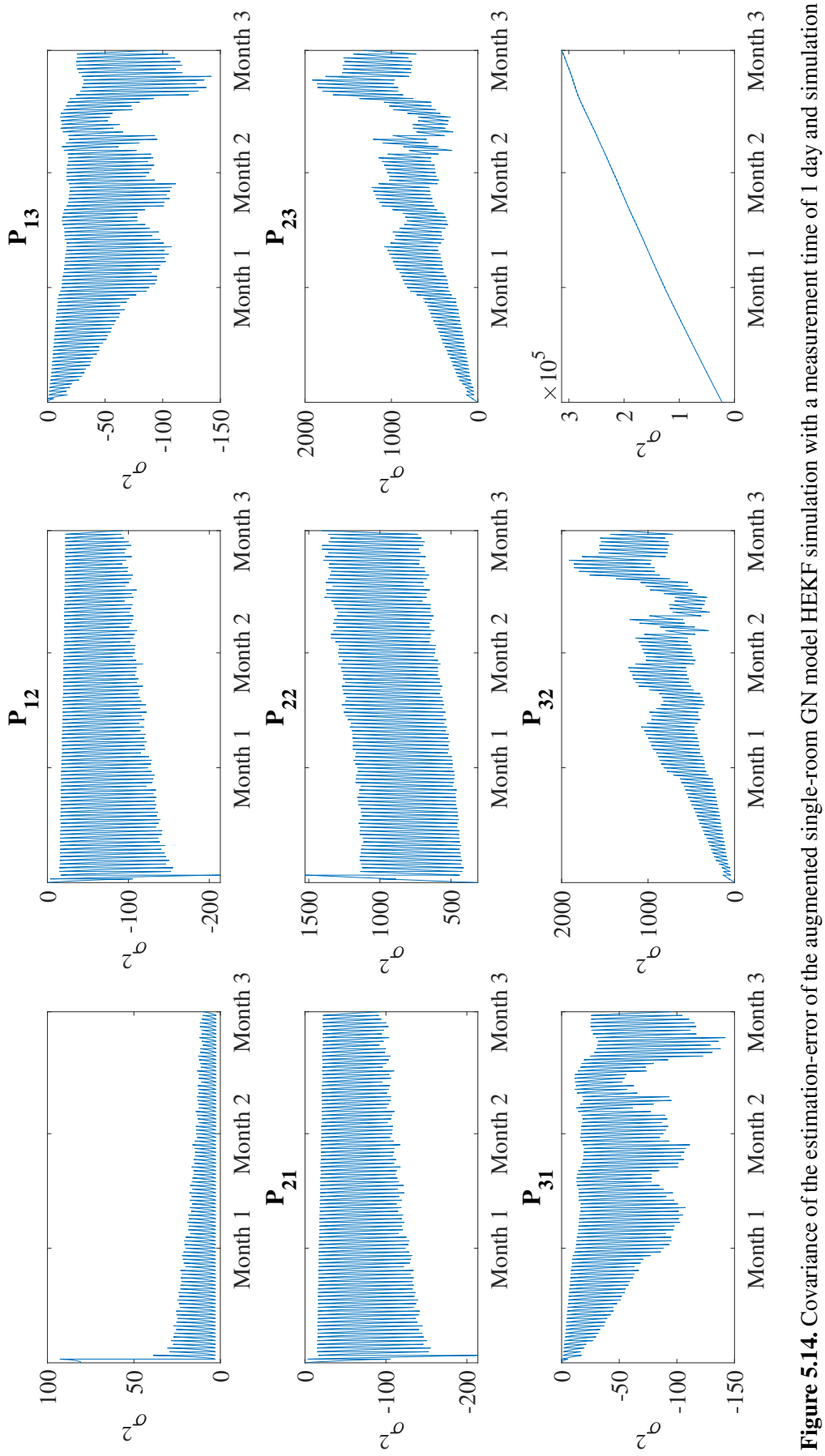

Figure 5.14. Covariance of the estimation-error of the augmented single-room GN model HEKF simulation with a measurement time of 1 day and simulation step size of 60 s.

5.4 TWO-ROOM GN MODEL

The model parameters were time-scaled to the sampling time used in the simulations in Sections 5.4.1, 5.4.2 and 5.4.3 and the simulation duration was 3 months.

5.4.1 CEKF for the standard two-room GN model

5.4.1.1 Simulation scenario and setup

The simulation sampling time for the standard two-room GN model is 60 s. The CEKF measurement updates are made using (5.6). Simulation data are used as in Section 2.5 (Figures 2.2 to 2.4 and Table 2.5). The measurement and process noise covariance matrices, R and Q, are given in Table 5.7.

Table 5.7. CEKF covariance matrix parameters.

R	Q
$\begin{bmatrix} 4.86 & 0 & 0 \\ 0 & 4.86 & 0 \\ 0 & 0 & 0.003375 \end{bmatrix}$	$\begin{bmatrix} 0.35 & 0 & 0 & 0 & 0 \\ 0 & 0.013 & 0 & 0 & 0 \\ 0 & 0 & 0.0015 & 0 & 0 \\ 0 & 0 & 0 & 22.603 & 0 \\ 0 & 0 & 0 & 0 & 0.6918 \end{bmatrix}$

The initial parameters for the standard two-room GN model are given in Table 2.5, and the initial CEKF parameters in Table 5.8. The initial number of susceptible animals are taken as $\hat{x}_1 = 81$ animals, the initial number of exposed individuals are taken as $\hat{x}_2 = 9$, the initial number of infected individuals are taken as $x_3 = 9$, the initial quanta in the ward is taken as $\hat{x}_4 = 17.14$ quanta and the initial quanta in the animal room as $\hat{x}_5 = 0.3333$ quanta.

5.4.1.2 Simulation results

Figures 5.15 to 5.21 show the results of the CEKF for the standard two-room model. The simulated number of susceptible animals, number of exposed animals and number of infected animals are shown

Table 5.8. CEKF initial parameters for the standard two-room GN model.

Parameter	Estimated Value
$\hat{x}_0$	$\begin{bmatrix} 81 \\ 9 \\ 9 \\ 17.14 \\ 0.3333 \end{bmatrix}$
P_0	$\begin{bmatrix} 81 & 0 & 0 & 0 & 0 \\ 0 & 81 & 0 & 0 & 0 \\ 0 & 0 & 81 & 0 & 0 \\ 0 & 0 & 0 & 302.76 & 0 \\ 0 & 0 & 0 & 0 & 0.1111 \end{bmatrix}$

in Figures 5.15, 5.16 and 5.17, respectively. The number of quanta in the ward and animal room for the standard two-room model are shown in Figures 5.18 to 5.21, respectively. The estimated number of susceptible animals converges quickly, like the standard single-room model CEKF, and has almost no error. The number of exposed and infected animals also converge after 6.25 days and 2.13 days, respectively.

The estimated number of quanta in the ward does not converge with the simulated number of quanta in the ward, as can be seen in Figure 5.18. The quanta state offset is also present in the number of quanta in the ward, as with the single-room model. A zoomed version of the number of quanta in the ward is shown in Figure 5.19. The estimated number of quanta in the animal room also does not converge, but deviates slightly more from the offset present in the ward. The number of quanta in the animal room is shown in Figure 5.20 and a zoomed version is shown in Figure 5.21.

The diagonal terms of figure 5.22 show the variance of each of the states. The variances of the states x_1, x_2 and x_3 decrease quickly and remain low for the duration of the simulation. The variances of the x_4 and x_5 states increase throughout the simulation.

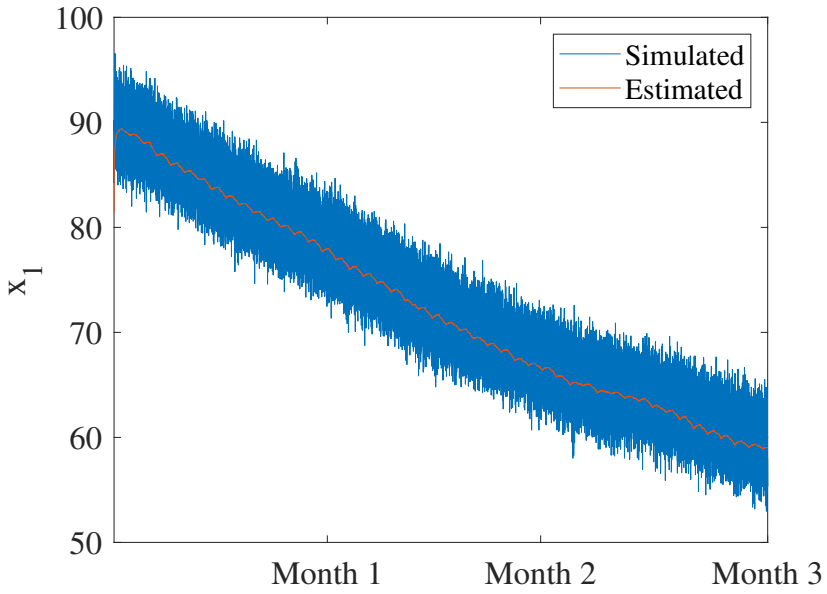

Figure 5.15. Number of susceptible animals of the standard two-room GN model estimation with a sampling time of 60 s. The simulated number of susceptible animals is shown in blue and the estimated number of susceptible animals is shown in orange.

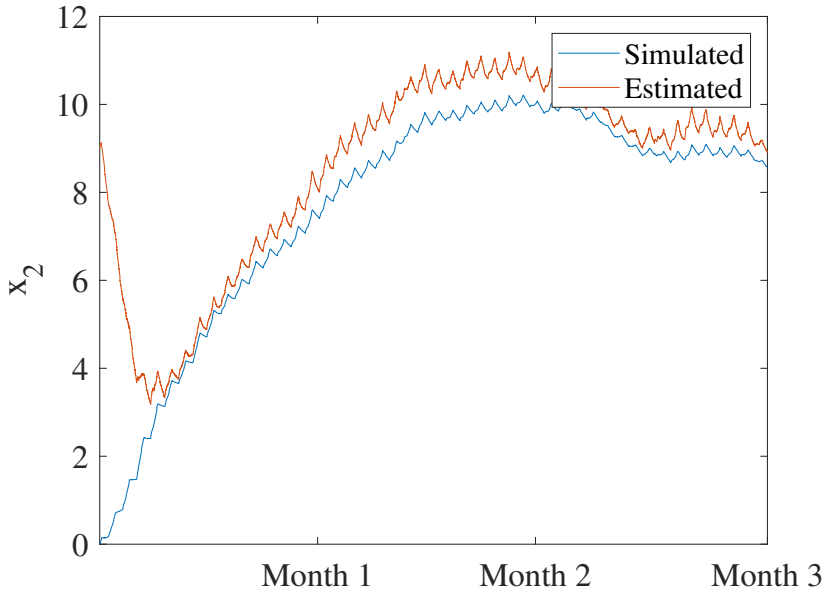

Figure 5.16. Number of exposed animals of the standard two-room GN model estimation with a sampling time of 60 s. The simulated quanta generation rate is shown in blue and the estimated quanta generation rate is shown in orange.

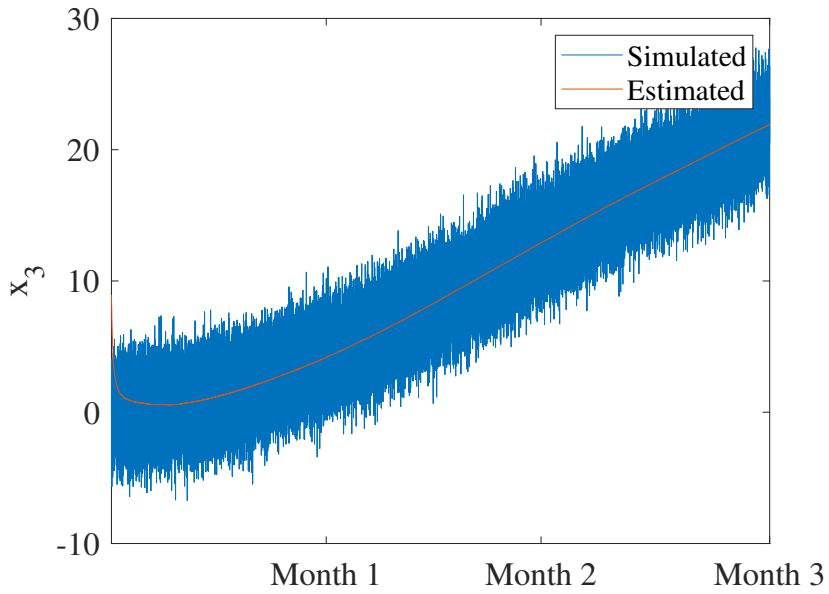

Figure 5.17. Number of infected animals of the standard two-room GN model estimation with a sampling time of 60 s. The simulated quanta generation rate is shown in blue and the estimated quanta generation rate is shown in orange.

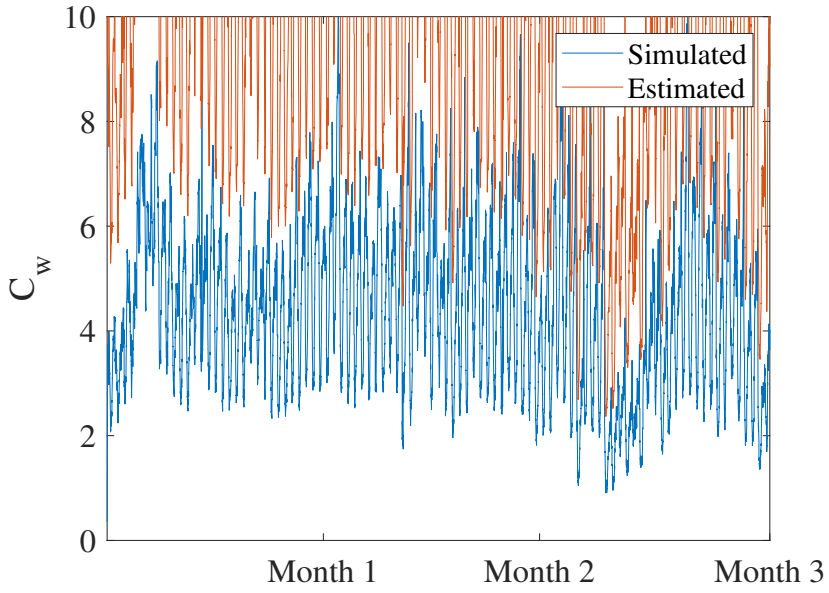

Figure 5.18. Number of quanta in the ward of the standard two-room GN model estimation with a sampling time of 60 s. The simulated number of quanta in the ward is shown in blue and the estimated number of quanta in the ward is shown in orange.

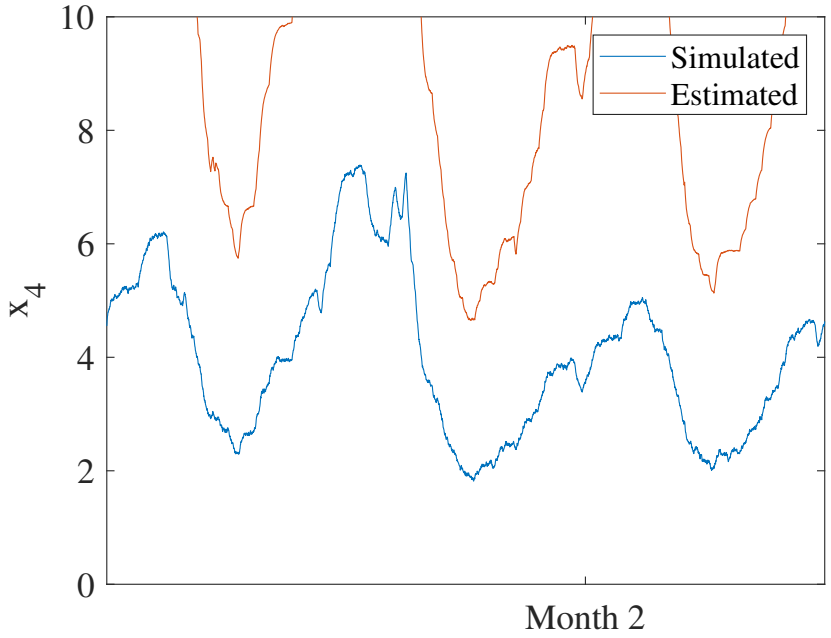

Figure 5.19. Time-zoomed number of quanta in the ward of the standard two-room GN model estimation with a sampling time of 60 s. The simulated number of quanta in the ward is shown in blue and the estimated number of quanta in the ward is shown in orange. The period shown is 3 days.

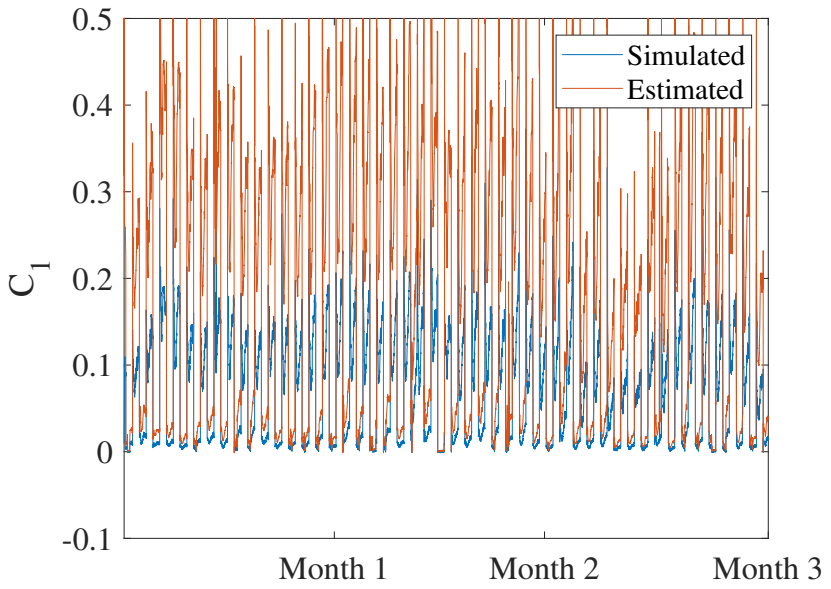

Figure 5.20. Number of quanta in the animal room of the standard two-room GN model estimation with a sampling time of 60 s. The simulated number of quanta in the animal room is shown in blue and the estimated number of quanta in the animal room is shown in orange.

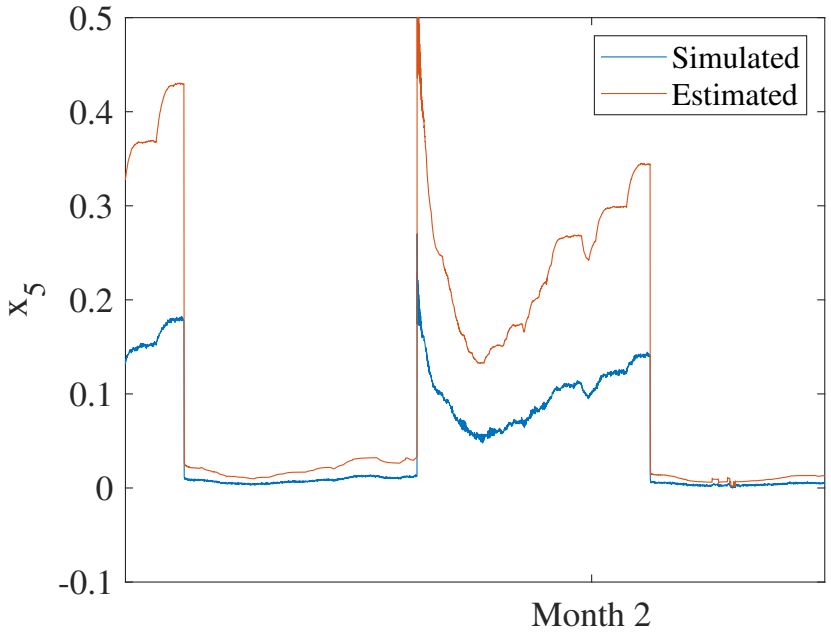

Figure 5.21. Time-zoomed number of quanta in the animal room of the standard two-room GN model estimation with a sampling time of 60 s. The simulated number of quanta in the animal room is shown in blue and the estimated number of quanta in the animal room is shown in orange. The period shown is 3 days.

5.4.2 CEKF for the simplified two-room GN model

5.4.2.1 Simulation scenario and setup

The simulation sampling time is again 60 *s* and the CEKF measurement updates are made using (5.6). Simulation data are used as in Section 5.3.2 (Figures 2.2 to 2.4 and Table 2.6). The measurement and process noise covariance matrices, R and Q, are given in Table 5.9.

Table 5.9. CEKF covariance matrix parameters for simplified two-room GN model.

R	Q
$\begin{bmatrix} 4.86 & 0 \\ 0 & 0.003375 \end{bmatrix}$	$\begin{bmatrix} 0.35 & 0 & 0 & 0 \\ 0 & 22.603 & 0 & 0 \\ 0 & 0 & 0.6918 & 0 \\ 0 & 0 & 0 & 48 \end{bmatrix}$

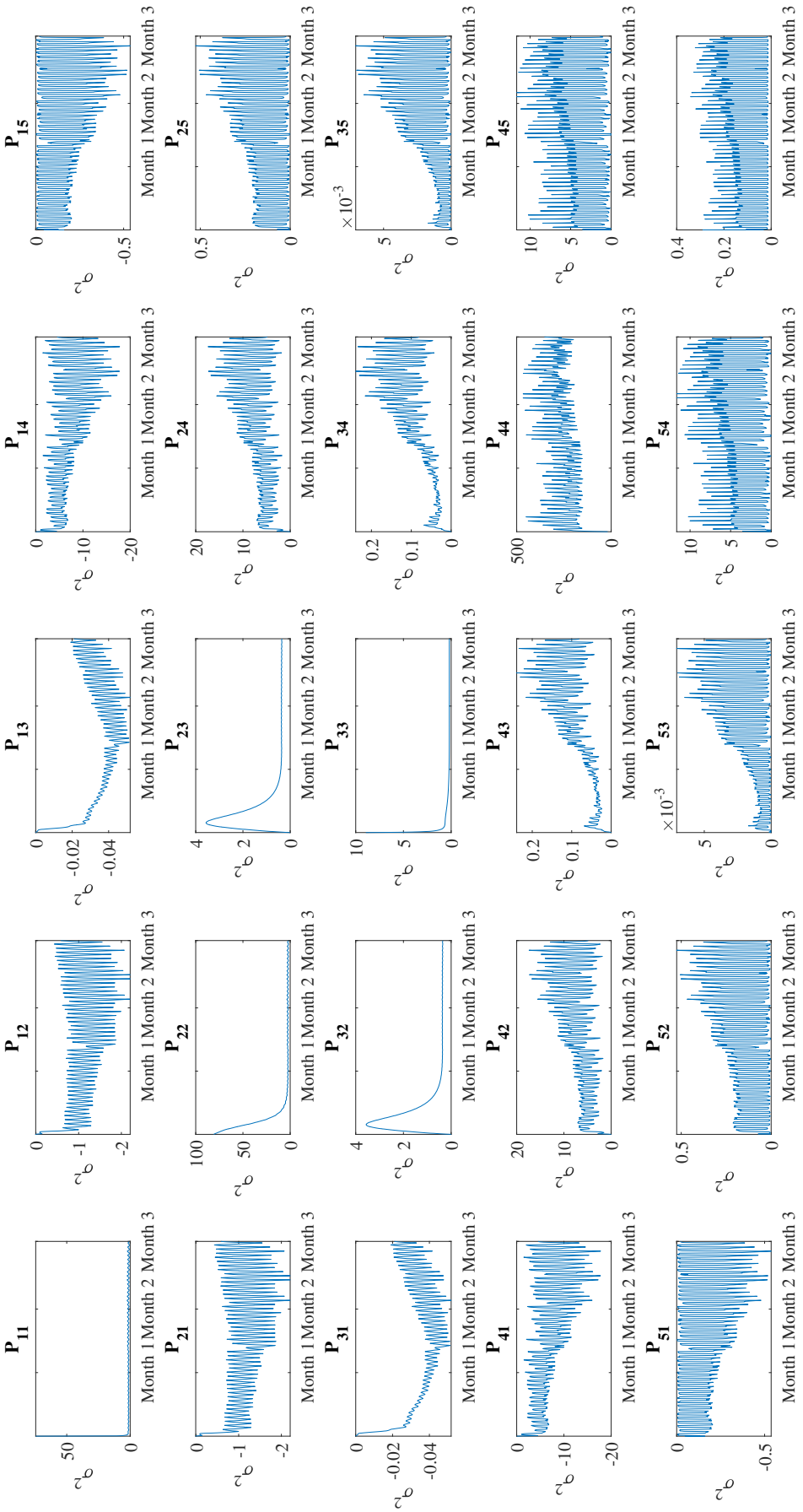

Figure 5.22. Covariance of the estimation-error of the standard two-room GN model CEKF simulation with a sampling time of 60 s.

The initial parameters for the simplified two-room GN model are given in Table 2.6, and the initial CEKF parameters in Table 5.10. The same noise is added as in Section 5.3.2.

Table 5.10. CEKF initial parameters for the simplified two-room GN model.

Parameter	Estimated Value
$\hat{x}_0$	$\begin{bmatrix} 81 \\ 17.14 \\ 0.3333 \\ 150 \end{bmatrix}$
P_0	$\begin{bmatrix} 81 & 0 & 0 & 0 \\ 0 & 302.76 & 0 & 0 \\ 0 & 0 & 0.1111 & 0 \\ 0 & 0 & 0 & 22500 \end{bmatrix}$

The initial number of susceptible animals are taken as $\hat{x}_1 = 81$ animals, the initial quanta in the ward is taken as $\hat{x}_4 = 17.14$ quanta, the initial quanta in the animal room as $\hat{x}_5 = 0.3333$ quanta and the initial quanta generation rate is taken as $\hat{x}_6 = 150$ quanta $\cdot$ d^{-1}.

5.4.2.2 Simulation results

The estimate of the number of susceptible animals x_1 converges to the correct number of susceptible animals after 16 days, as seen in Figure 5.23.

Figures 5.24 and 5.26 show that the initial estimates of the number of quanta in the ward x_4 and animal room x_5 converge quickly as with the number of susceptible animals x_1 estimate and converge to the simulated number of quanta in the ward and animal room in 16 days. The estimate of the number of quanta in the ward follows the simulated number of quanta accurately, resulting in an accurate estimate of the number of quanta in the animal room. Time-zoomed figures are shown in Figures 5.25 and 5.27. The quanta generation rate x_6 estimate also converges after 16 days as seen in Figure 5.28.

The diagonal terms of figure 5.29 show the variance of each of the states. The variances of the states x_1 and x_4 decrease quickly and remain low for the duration of the simulation. The variances of the x_3

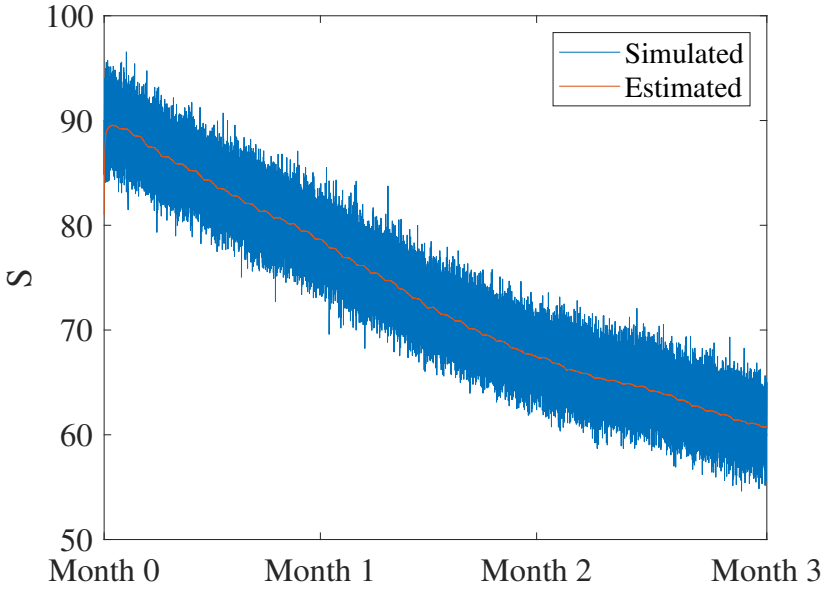

Figure 5.23. Number of susceptible animals of the simplified two-room GN model estimation with a sampling time of 60 s. The simulated number of susceptible animals is shown in blue and the estimated number of susceptible animals is shown in orange.

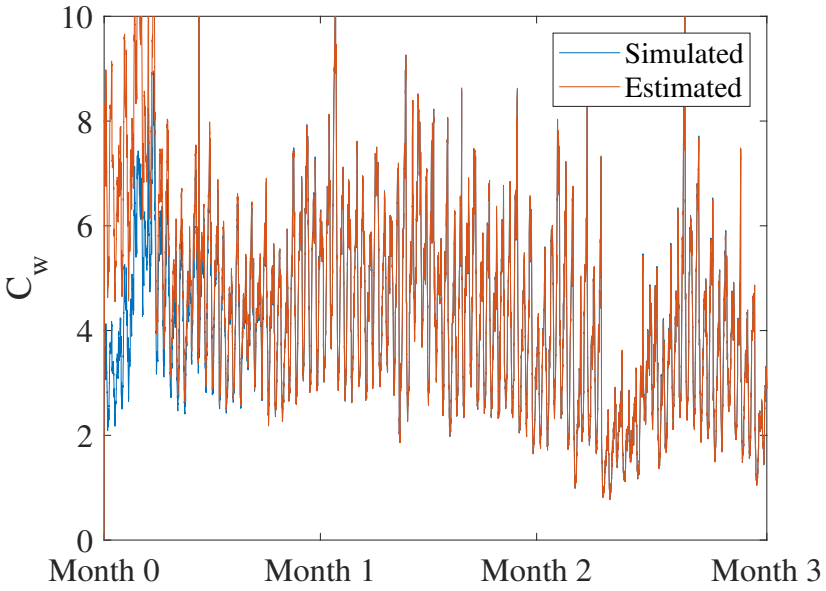

Figure 5.24. Number of quanta in the ward of the simplified two-room GN model estimation with a sampling time of 60 s. The simulated number of quanta in the ward is shown in blue and the estimated number of quanta in the ward is shown in orange.

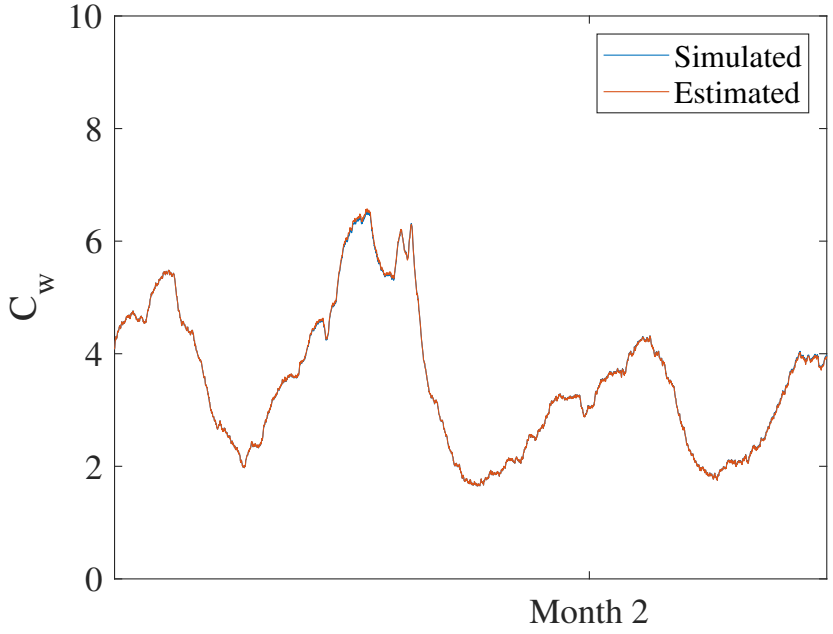

Figure 5.25. Time-zoomed number of quanta in the ward of the simplified two-room GN model estimation with a sampling time of 60 s. The simulated number of quanta in the ward is shown in blue and the estimated number of quanta in the ward is shown in orange. The period shown is 3 days.

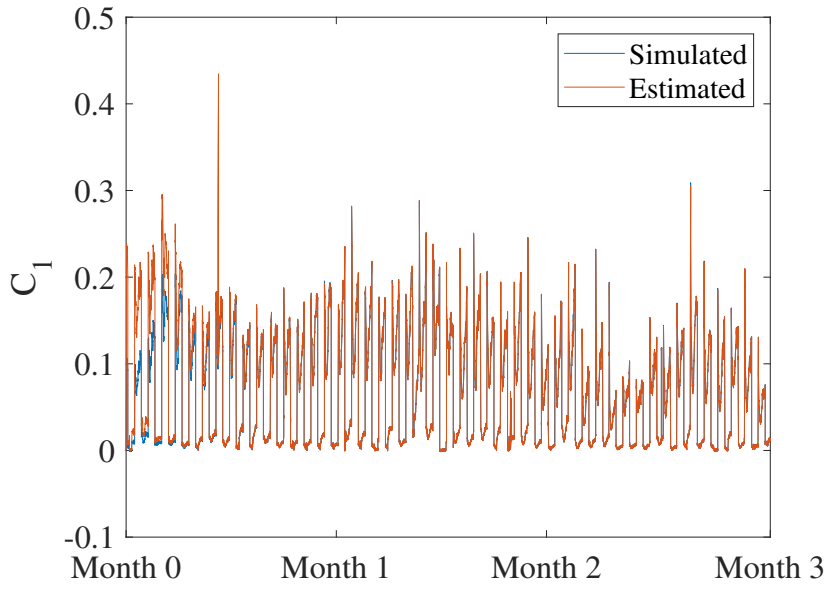

Figure 5.26. Number of quanta in the animal room of the simplified two-room GN model estimation with a sampling time of 60 s. The simulated number of quanta in the animal room is shown in blue and the estimated number of quanta in the animal room is shown in orange.

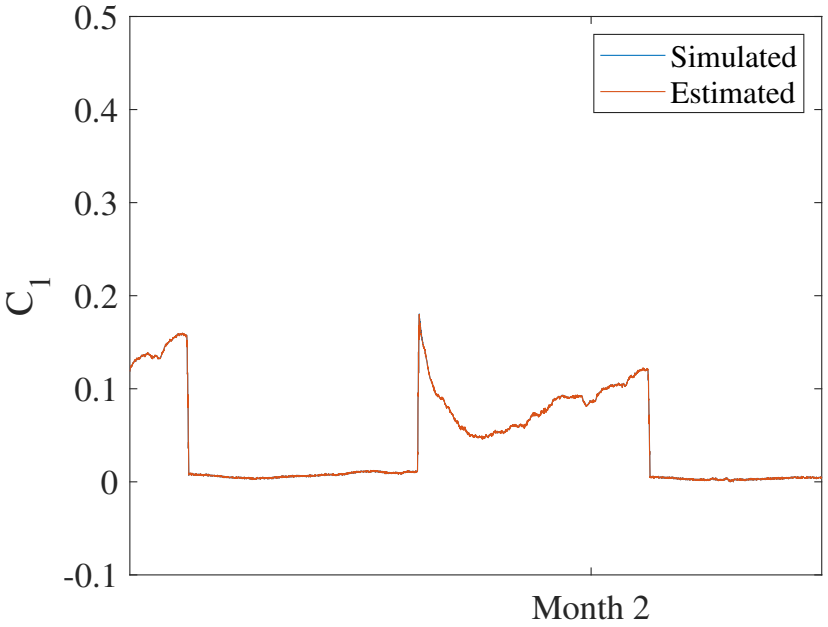

Figure 5.27. Time-zoomed number of quanta in the animal room of the simplified two-room GN model estimation with a sampling time of 60 s. The simulated number of quanta in the animal room is shown in blue and the estimated number of quanta in the animal room is shown in orange. The period shown is 3 days.

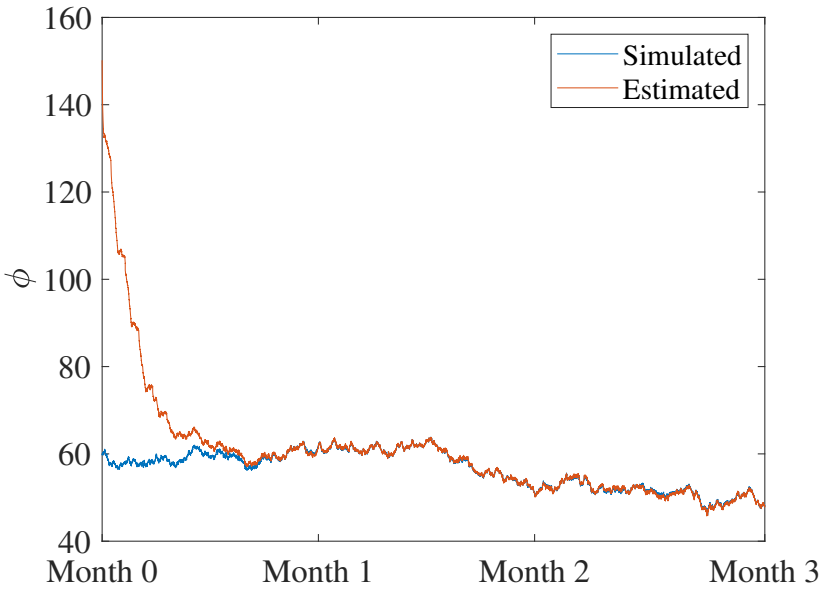

Figure 5.28. Quanta generation rate of the simplified two-room GN model estimation with a sampling time of 60 s. The simulated quanta generation rate is shown in blue and the estimated quanta generation rate is shown in orange.

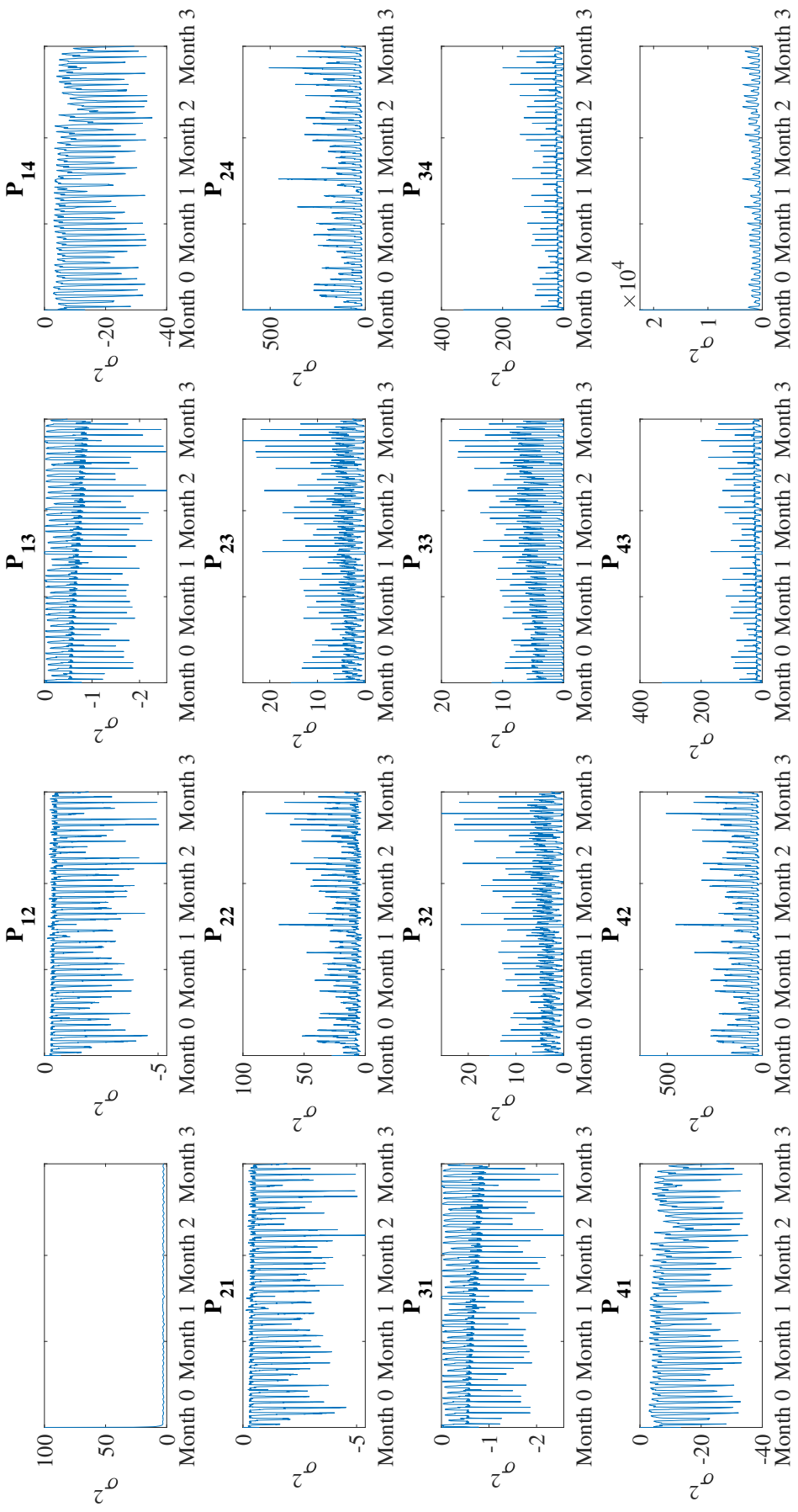

Figure 5.29. Covariance of the estimation-error of the simplified two-room GN model estimation with a sampling time of 60 s.

and x_4 states decrease from their initial value and remain lower than the initial value throughout the simulation.

5.4.3 HEKF for the simplified two-room GN model

5.4.3.1 Simulation scenario and setup

The same model as in Section 5.4.2 is used and the initial parameters are given in Tables 2.6, 5.10, and 5.11. The simulation data is the same as for the simulation in Section 5.4.2. The same noise is added as in Section 5.3.2.

Table 5.11. HEKF parameters.

Simulation Time	Measurement Time	R	Q
60 s	1 day	$\begin{bmatrix} 4.86 & 0 \\ 0 & 0.003375 \end{bmatrix}$	$\begin{bmatrix} 0.35 & 0 & 0 & 0 \\ 0 & 22.603 & 0 & 0 \\ 0 & 0 & 0.6918 & 0 \\ 0 & 0 & 0 & 48 \end{bmatrix}$

5.4.3.2 Simulation results

The model in (2.11) is simulated with a simulation step size of 60 s and a measurement time of 1 day, as in Section 5.3.3. Figure 5.30 to Figure 5.35 show the results.

Figure 5.30 shows that the number of susceptible animals x_1 are estimated fairly well. Figures 5.31 and 5.33 show that the filter does not estimate the correct quanta in the ward x_4 and animal room x_5. Time-zoomed figures are shown in Figures 5.32 and 5.34. The quanta generation rate x_6 estimate is shown in Figure 5.35, with the estimate converging to within $1w_{x_6}$ after 1 month. A large amount of deviation can be seen in the number of quanta in the rooms due to the discontinuities present in the measured state x_1.

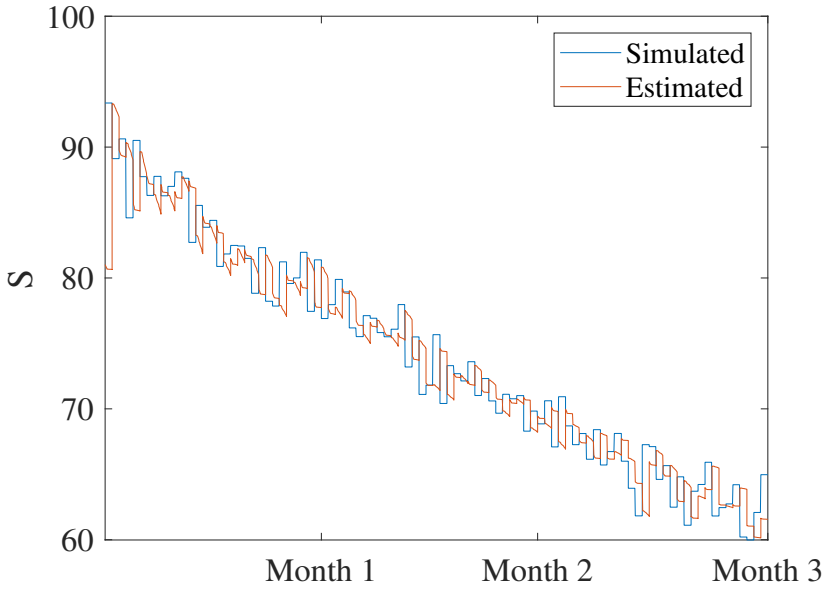

Figure 5.30. Number of susceptible animals of the simplified two-room GN model HEKF estimation simulation with a measurement time of 1 day and simulation step size of 60 s. The simulated number of susceptible animals is shown in blue and the estimated number of susceptible animals is shown in orange.

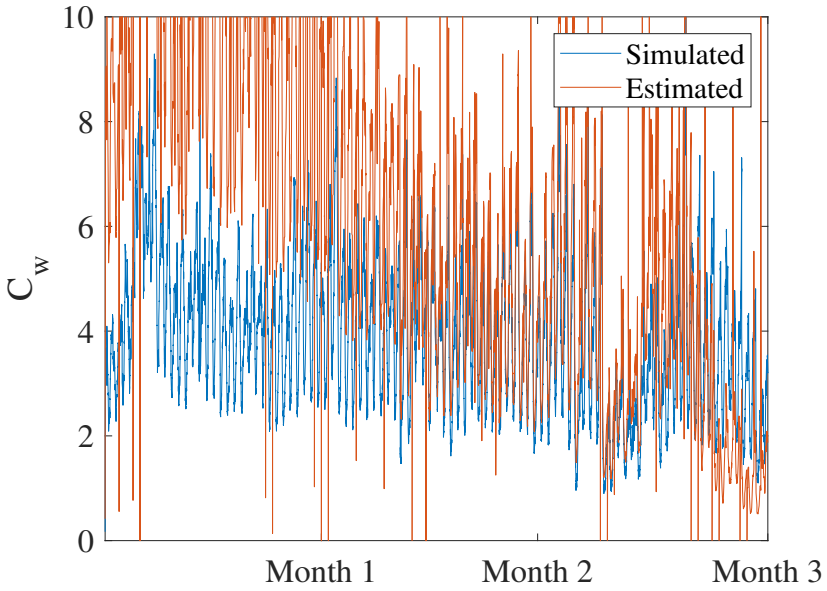

Figure 5.31. Number of quanta in the ward of the simplified two-room GN model HEKF estimation with a measurement time of 1 day and simulation step size of 60 s. The simulated quanta in the ward is shown in blue and the estimated quanta in the ward is shown in orange.

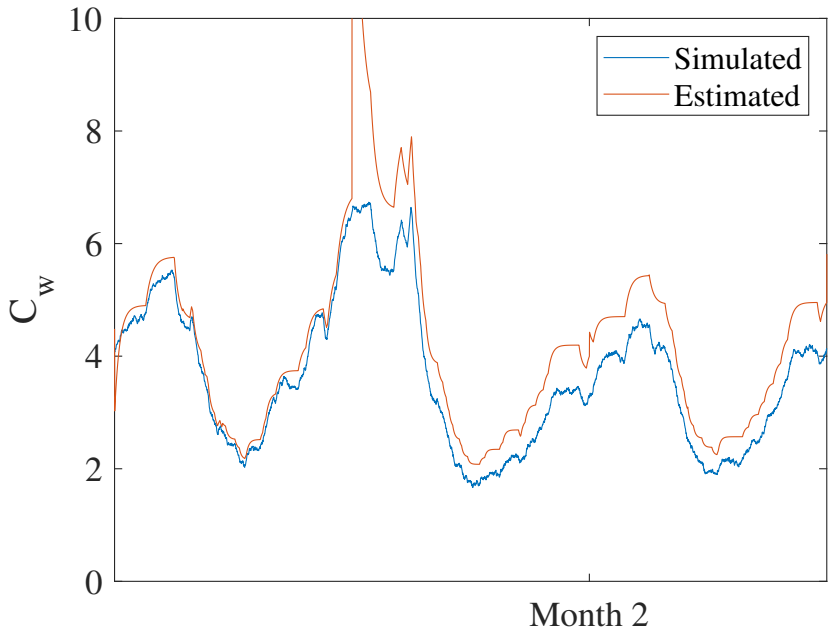

Figure 5.32. Time-zoomed number of quanta in the ward of the simplified two-room GN model HEKF estimation with a measurement time of 1 day and simulation step size of 60 s. The simulated quanta in the ward is shown in blue and the estimated quanta in the ward is shown in orange.

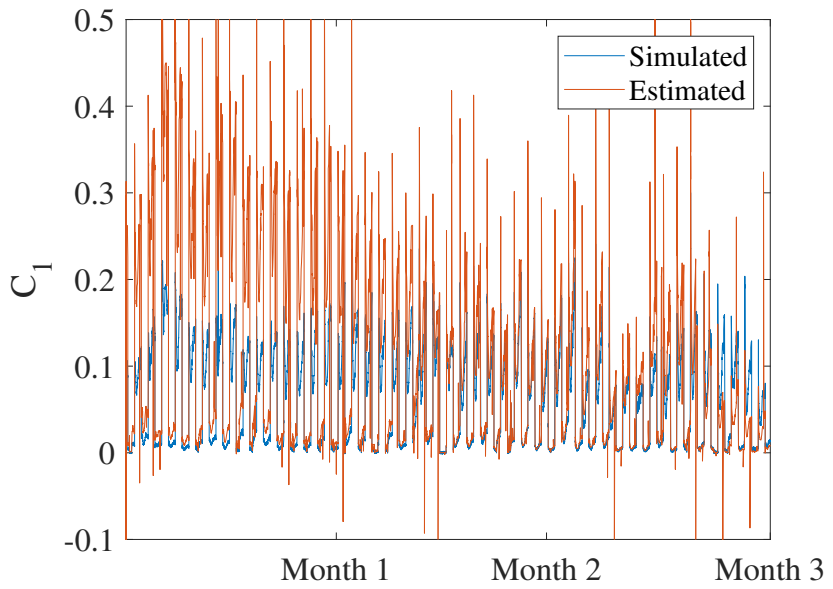

Figure 5.33. Number of quanta in the animal room of the simplified two-room GN model HEKF estimation simulation with a measurement time of 1 day and simulation step size of 60 s. The simulated number of quanta in the room is shown in blue and the estimated number of quanta in the room is shown in orange.

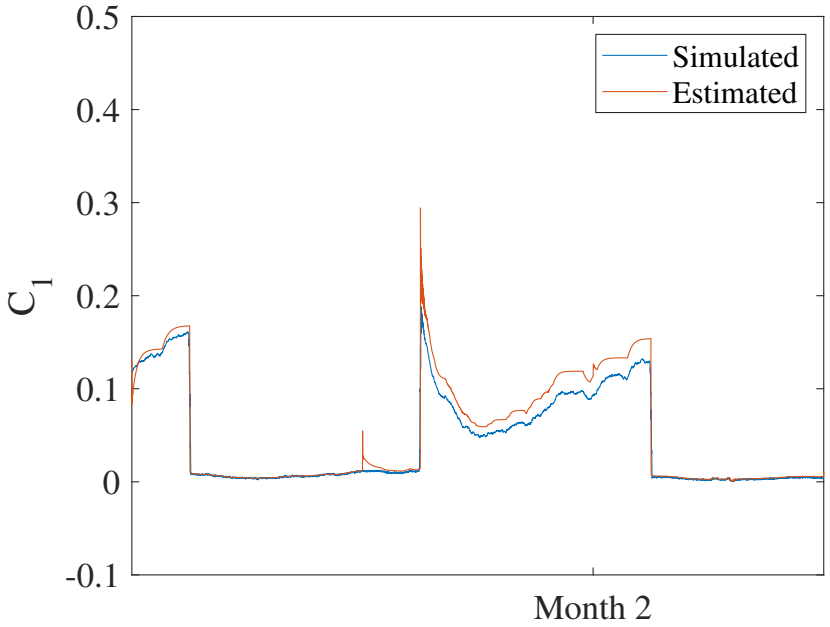

Figure 5.34. Time-zoomed number of quanta in the animal room of the simplified two-room GN model HEKF estimation simulation with a measurement time of 1 day and simulation step size of 60 s. The simulated number of quanta in the room is shown in blue and the estimated number of quanta in the room is shown in orange.

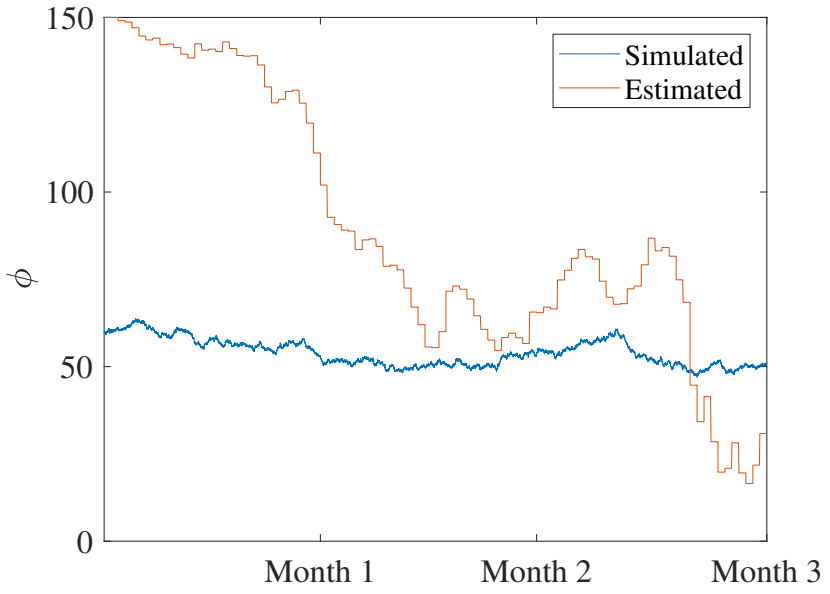

Figure 5.35. Quanta generation rate of the simplified two-room GN model HEKF estimation with a measurement time of 1 day and simulation step size of 60 s. The simulated quanta in the ward is shown in blue and the estimated quanta generation rate is shown in orange.

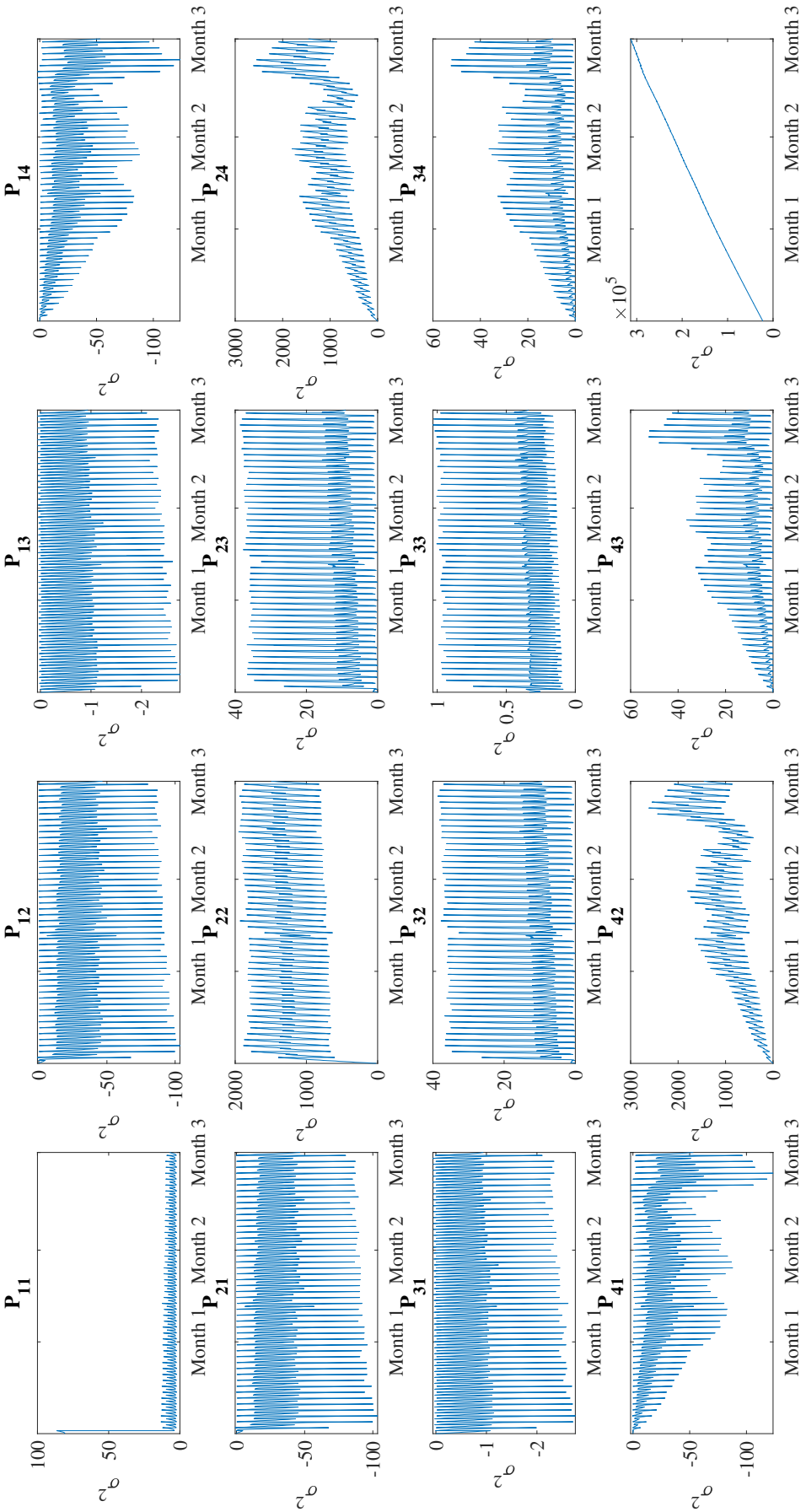

Figure 5.36. Covariance of the estimation-error of the simplified two-room GN model HEKF simulation with a measurement time of 1 day and simulation step size of 60 s and $P_{44} = 1$.

The diagonal terms of figure 5.36 show the variance of each of the states. The variances of the state x_1 decreases quickly and remains low for the duration of the simulation. The variances of the x_2 and x_3 states decrease from their initial value and remain lower than the initial value throughout the simulation. The variance of the x_3 state increases greatly throughout the simulation.

5.5 TESTING EXTREMES

The limits of the quanta generation rate parameter mismatch was tested in order to further determine the performance limits of the HEKF. The initial quanta generation rate parameter was set as in Table 5.12 for each of the simulations.

5.5.1 Simulation scenario and setup

A range of quanta generation rates were tested as in Table 5.12 [9]. The other simulation data remain the same as in Sections 5.3.3 and 5.4.3 for the single- and two-room models, respectively. Because of the large deviations for the quanta generation rates, the full range is taken for the calculation of the variance of the quanta generation rate $P_{0_{x_{3,6}}}$.

Table 5.12. Initial generation rate parameters and estimation-error covariance for single- and two-room GN models [9].

Description	Quanta per day	Single-room $P_{0_{x_{3,6}}}$
Average TB patient	30 quanta $\cdot$ d^{-1} [17]	92903
Office building outbreak	304.8 quanta $\cdot$ d^{-1} [17]	92903
Laryngeal case	1440 quanta $\cdot$ d^{-1} [17]	92903
Bronchoscopy-related outbreak	6000 quanta $\cdot$ d^{-1} [17]	92903
Bronchoscopy-related outbreak	8640 quanta $\cdot$ d^{-1} [8]	92903

5.5.2 Single-room GN model simulation results

Figures 5.37 to 5.41 show the results of the simplified two-room HEKF for the initial estimated quanta generation rates $\hat{x}_3$ in Table 5.12.

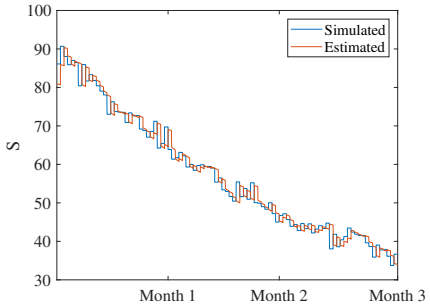

(a) Number of susceptible animals of the modified single-room GN model.

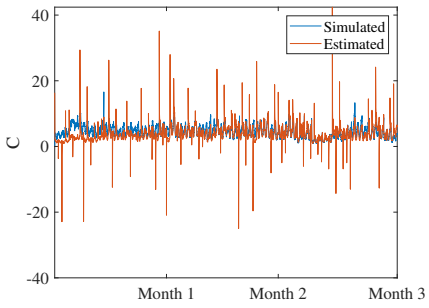

(b) Number of quanta in the room of the augmented single-room GN model.

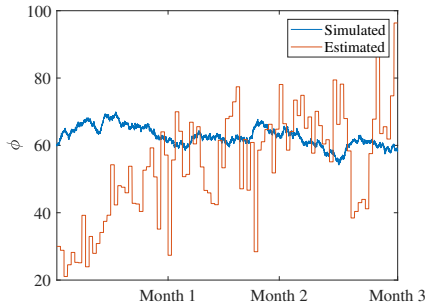

(c) Quanta generation rate per infectious individual of the augmented single-room GN model

Figure 5.37. Augmented single-room GN model HEKF simulation with a measurement time of 1 day, simulation step size of 60 s and a quanta generation rate of 30 quanta $\cdot$ d^{-1}. The measured data are shown in blue and the estimated data are shown in orange.

5.5.3 Two-room GN model simulation results

Figures 5.42 to 5.46 show the results of the simplified two-room HEKF for the initial estimated quanta generation rates $\hat{x}_6$ in Table 5.12. The generation rate estimate in Figure 5.42(d) can be seen to converge after 29 days, the same as for the HEKF in Section 5.4.3.

5.5.4 Discussion of extremes results

The results from Figures 5.37(a) to 5.41(c) showed that for initial generation rate parameters of 30 quanta$\cdot d^{-1}$ to 1440 quanta $\cdot$ d^{-1} for the augmented single-room GN model, the HEKF quanta

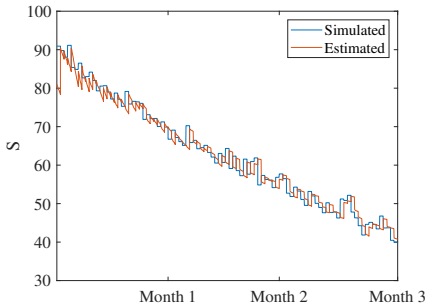

(a) Number of susceptible animals of the modified single-room GN model.

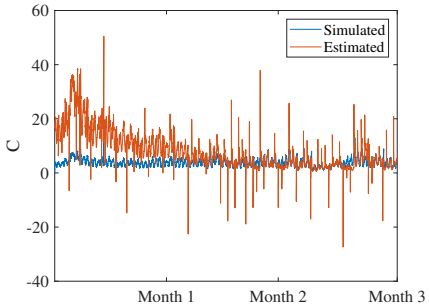

(b) Number of quanta in the room of the augmented single-room GN model.

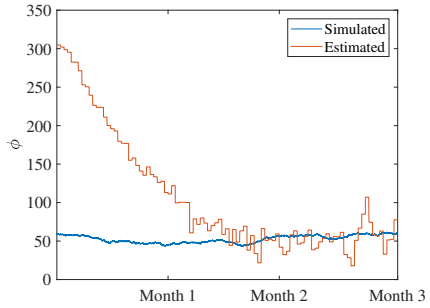

(c) Quanta generation rate per infectious individual of the augmented single-room GN model

Figure 5.38. Augmented single-room GN model HEKF simulation with a measurement time of 1 day, simulation step size of 60 s and a quanta generation rate of 304.8 quanta $\cdot$ d^{-1}. The measured data are shown in blue and the estimated data are shown in orange.

generation rate estimates converges in less than 2 months. For the remaining initial generation rate estimates in Table 5.12, the filter performance severely degrades.

From Figures 5.42(a) to 5.46 it can be seen that the same applies for initial generation rate parameters of 30 quanta$\cdot d^{-1}$ to 304.8 quanta $\cdot$ d^{-1} for the simplified two-room GN model, the HEKF converges in less than 40 days for any of the initial generation rate estimates in Table 5.12.

The HEKF quanta generation rate therefore converges to within $w_{x_{3,6}}$ for quanta generation rates given in Table 5.12 that are up to 24 times larger for the single-room GN model and 5 times larger for the two-room GN model.

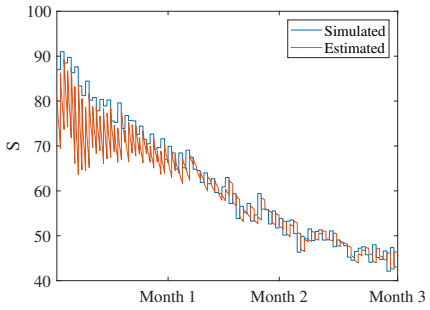

(a) Number of susceptible animals of the modified single-room GN model.

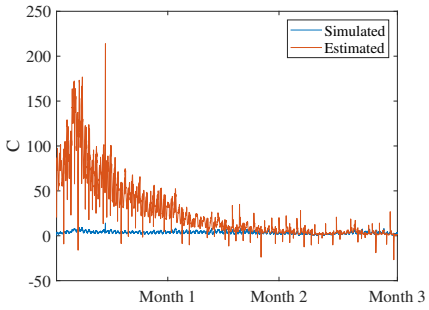

(b) Number of quanta in the room of the augmented single-room GN model.

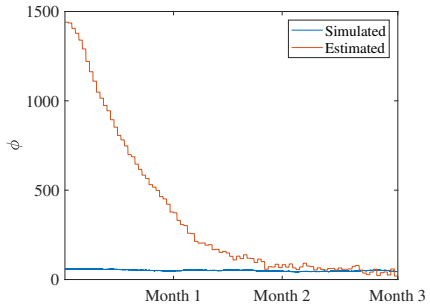

(c) Quanta generation rate per infectious individual of the augmented single-room GN model

Figure 5.39. Augmented single-room GN model HEKF simulation with a measurement time of 1 day, simulation step size of 60 s and a quanta generation rate of 1440 quanta $\cdot$ d^{-1}. The measured data are shown in blue and the estimated data are shown in orange.

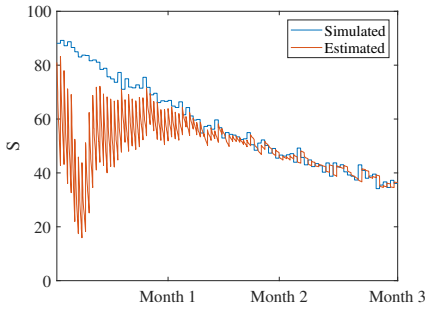

(a) Number of susceptible animals of the modified single-room GN model.

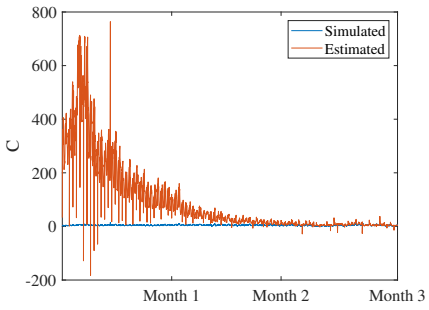

(b) Number of quanta in the room of the augmented single-room GN model.

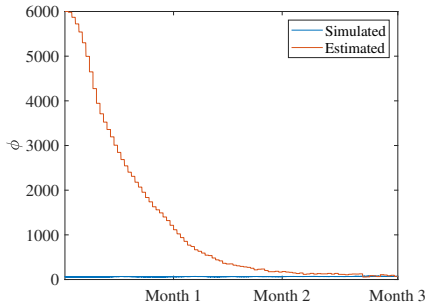

(c) Quanta generation rate per infectious individual of the augmented single-room GN model

Figure 5.40. Augmented single-room GN model HEKF simulation with a measurement time of 1 day, simulation step size of 60 s and a quanta generation rate of 6000 quanta $\cdot$ d^{-1}. The measured data are shown in blue and the estimated data are shown in orange.

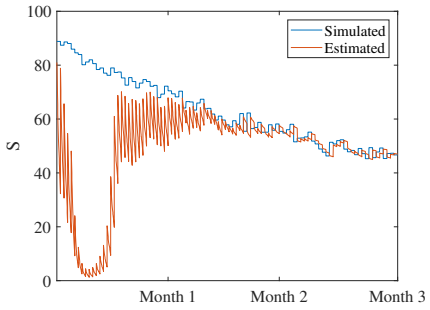

(a) Number of susceptible animals of the modified single-room GN model.

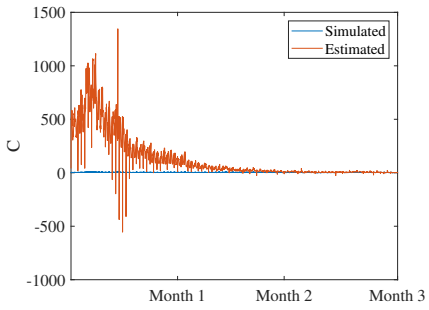

(b) Number of quanta in the room of the augmented single-room GN model.

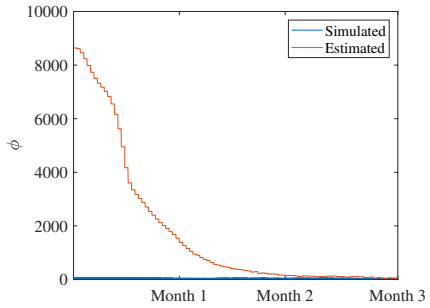

(c) Quanta generation rate per infectious individual of the augmented single-room GN model

Figure 5.41. Augmented single-room GN model HEKF simulation with a measurement time of 1 day, simulation step size of 60 s and a quanta generation rate of 8640 quanta $\cdot$ d^{-1}. The measured data are shown in blue and the estimated data are shown in orange.

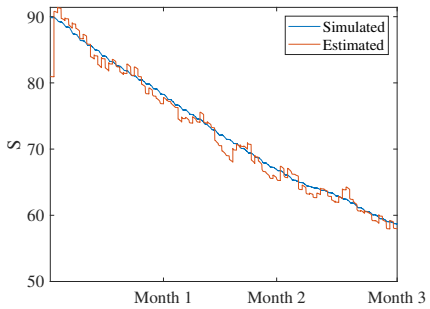

(a) Number of susceptible animals of the modified two-room GN model.

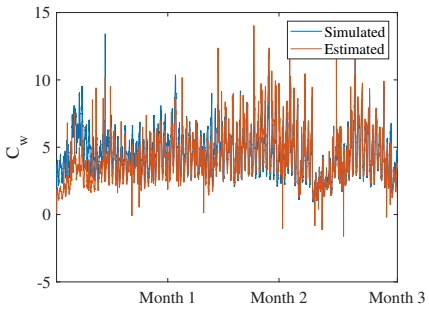

(b) Number of quanta in the ward of the simplified two-room GN model.

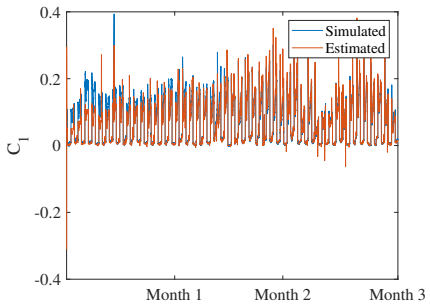

(c) Number of quanta in the animal room of the simplified two-room GN model.

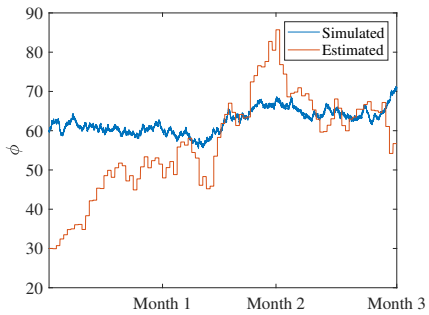

(d) Quanta generation rate per infectious individual of the simplified two-room GN model

Figure 5.42. Simplified two-room GN model HEKF simulation with a measurement time of 1 day, simulation step size of 60 s and a quanta generation rate of 30 quanta $\cdot$ d^{-1}. The measured data are shown in blue and the estimated data are shown in orange.

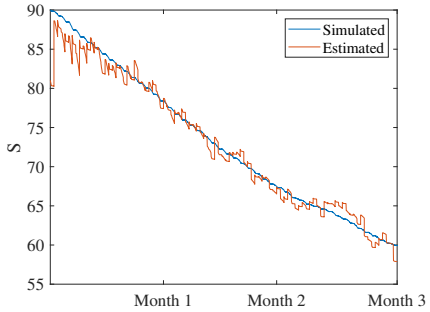

(a) Number of susceptible animals of the modified two-room GN model.

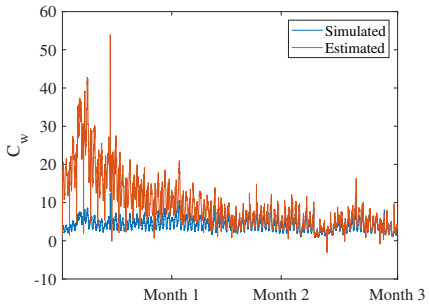

(b) Number of quanta in the ward of the simplified two-room GN model.

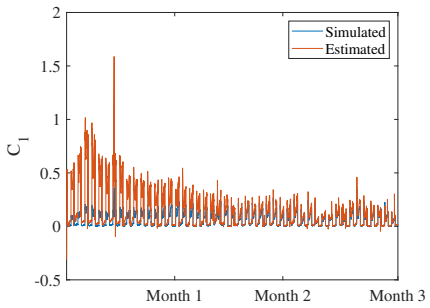

(c) Number of quanta in the animal room of the simplified two-room GN model.

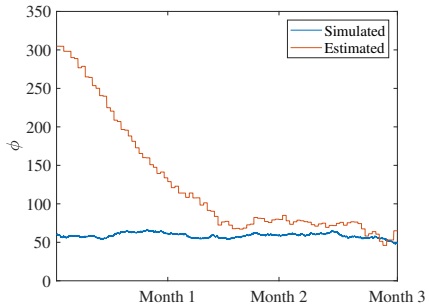

(d) Quanta generation rate per infectious individual of the simplified two-room GN model

Figure 5.43. Simplified two-room GN model HEKF simulation with a measurement time of 1 day, simulation step size of 60 s and a quanta generation rate of 304.8 quanta $\cdot$ d^{-1}. The measured data are shown in blue and the estimated data are shown in orange.

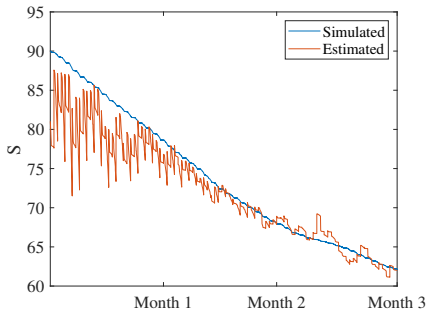

(a) Number of susceptible animals of the modified two-room GN model.

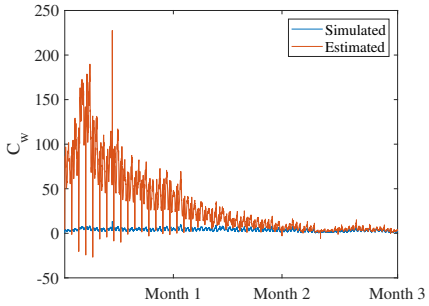

(b) Number of quanta in the ward of the simplified two-room GN model.

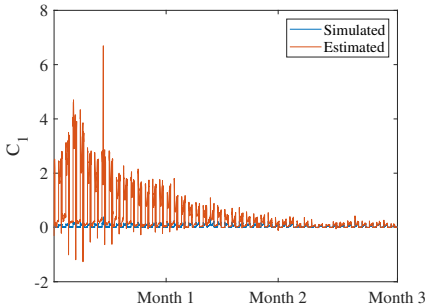

(c) Number of quanta in the animal room of the simplified two-room GN model.

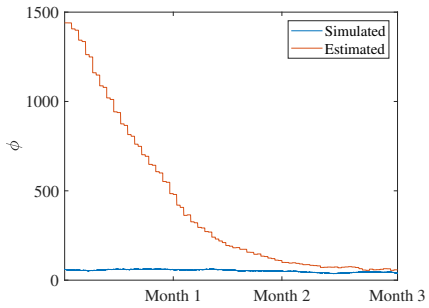

(d) Quanta generation rate per infectious individual of the simplified two-room GN model

Figure 5.44. Simplified two-room GN model HEKF simulation with a measurement time of 1 day, simulation step size of 60 s and a quanta generation rate of 1440 quanta $\cdot$ d^{-1}. The measured data are shown in blue and the estimated data are shown in orange.

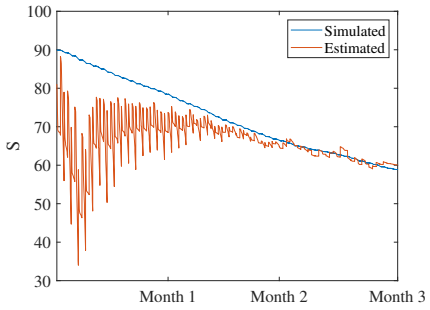

(a) Number of susceptible animals of the modified two-room GN model.

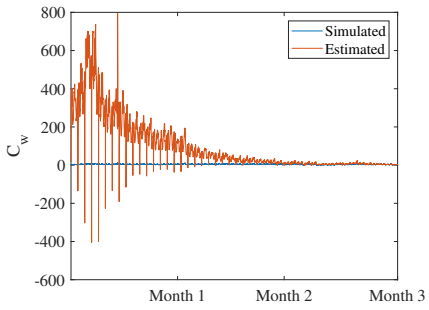

(b) Number of quanta in the ward of the simplified two-room GN model.

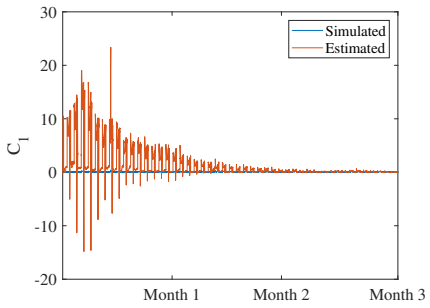

(c) Number of quanta in the animal room of the simplified two-room GN model.

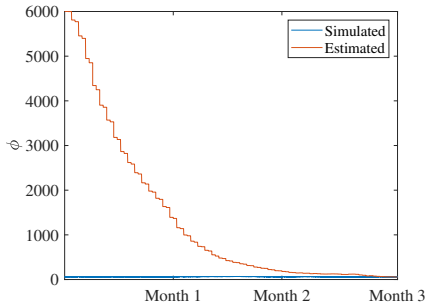

(d) Quanta generation rate per infectious individual of the simplified two-room GN model

Figure 5.45. Simplified two-room GN model HEKF simulation with a measurement time of 1 day, simulation step size of 60 s and a quanta generation rate of 6000 quanta $\cdot$ d^{-1}. The measured data are shown in blue and the estimated data are shown in orange.

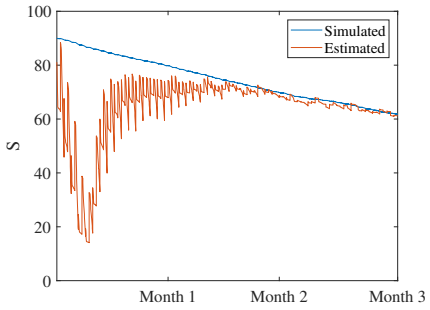

(a) Number of susceptible animals of the modified two-room GN model.

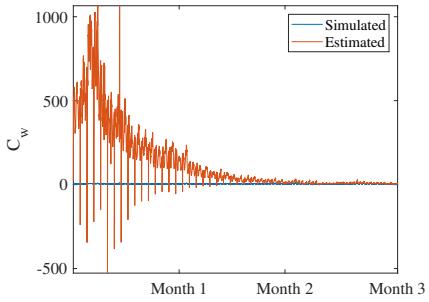

(b) Number of quanta in the ward of the simplified two-room GN model.

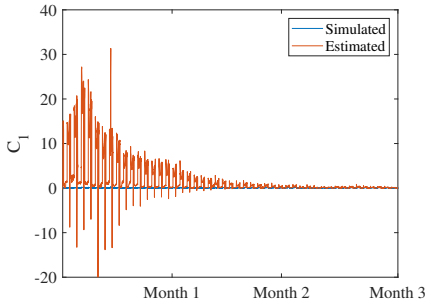

(c) Number of quanta in the animal room of the simplified two-room GN model.

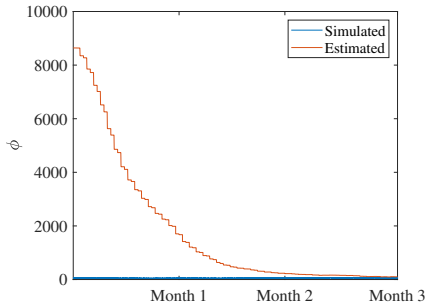

(d) Quanta generation rate per infectious individual of the simplified two-room GN model

Figure 5.46. Simplified two-room GN model HEKF simulation with a measurement time of 1 day, simulation step size of 60 s and a quanta generation rate of 8640 quanta $\cdot$ d^{-1}. The measured data are shown in blue and the estimated data are shown in orange.

5.6 SUMMARY OF RESULTS

Table 5.13 shows a summary of the results and a normalised root mean square error (NRMSE) of each of the simulations for the number of quanta in the ward and animal room. These are normalised since the two models will have different levels of quanta and are compared directly. The NRMSE is calculated as:

$$NRMSE = \frac{\sqrt{\sum \frac{(y-\hat{y})^T \cdot (y-\hat{y})}{N}}}{max(y)}. \tag{5.11}$$

The analysis is performed using the data after the estimate has reached steady-state because of the large deviation of the estimate at the start of the simulation. The NRMSE is calculated for the error between the estimated and simulated quanta after 1 month because this is close to the longest settling time of the models with 10% mismatch, which is 29 days. The NRMSEs of the standard single-room and two-room GN models are also given in Table 5.13.

NRMSEs of the augmented single-room and simplified two-room GN models where the initial estimation-error covariance estimates (P_{33} for the augmented GN model and P_{44} for the simplified two-room GN model) are increased to 100 are shown below the initial results and the NRMSEs of the varied generation rate estimates are shown in the third section of the table.

Table 5.13. Root mean square error of the simulated and estimated number of quanta in the ward and animal room.

Model	Estimator	Covariance	Initial generation rate estimate	Simulation step size	Measurement time	Time before estimate converges	NRMSE of Quanta in ward after 30 days	NRMSE of Quanta in animal room after 30 days
Standard SR model	CEKF	22500	150	60 s	60 s	-	0.52736	-
Augmented SR model	CEKF	22500	150	60 s	60 s	4 d	0.017927	-
Augmented SR model	HEKF	22500	150	60 s	86400 s	40 d	0.19391	-
Standard TR model	CEKF	22500	150	60 s	60 s	-	0.524115	0.264879
Simplified TR model	CEKF	22500	150	60 s	60 s	16 d	0.001247	0.001610
Simplified TR model	HEKF	22500	150	60 s	86400 s	29 d	0.197057	0.127613
Augmented SR model	HEKF	92903	30	60 s	86400 s	29 d	0.138239	-
Augmented SR model	HEKF	92903	304.8	60 s	86400 s	37 d	0.207078.	-
Augmented SR model	HEKF	92903	1440	60 s	86400 s	56 d	0.842612	-
Augmented SR model	HEKF	92903	6000	60 s	86400 s	85 d	1.917687	-
Augmented SR model	HEKF	92903	8640	60 s	86400 s	93 d	3.945932	-
Simplified TR model	HEKF	92903	30	60 s	86400 s	10 d	0.049026	0.031235
Simplified TR model	HEKF	92903	304.8	60 s	86400 s	40 d	0.199792	0.129669
Simplified TR model	HEKF	92903	1440	60 s	86400 s	63 d	1.293609	0.797211
Simplified TR model	HEKF	92903	6000	60 s	86400 s	84 d	2.990538	1.944071
Simplified TR model	HEKF	92903	8640	60 s	86400 s	90 d	3.471771	2.269840

CHAPTER 6 DISCUSSION

6.1 DISCUSSION

6.1.1 Single-room GN models

The GN model is in state-space format which allows for simulation with non-zero initial conditions, the use of nonsteady-state parameters (such as the ventilation rate), and the design of state estimators. The state-space format also allows one to easily add additional states to the model, such as the quanta generation rate per infectious individual.

The single-room GN model, as opposed to the two-room GN model, has fewer states but the same number of measurements. Fewer states make state estimation easier as it implies fewer parameters that are susceptible to noise and unknown disturbances. The single-room GN model describes the infection of susceptible entities by infectious entities who occupy the same room. This is often the case in hospital settings, but it does not account for the ventilation of infectious droplets to other rooms.

The model assumes that the susceptible animals are immediately infected upon exposure to the droplet nuclei and therefore incorporates the incubation period of the disease into the quanta parameter. The other assumptions made are that the air in the room is well mixed, the infectious entities are equally infectious, the susceptible animals are equally susceptible and that they have the same pulmonary ventilation rate. The quanta parameter now essentially contains the uncertainty of each of the assumptions made, the measurement noise, and unknown disturbances.

The single-room GN model was augmented with the quanta generation rate as an additional state and a sensitivity and identifiability analysis was performed on the model. The sensitivity to deviation is the

same for both models regarding the quanta generation rate parameter, pulmonary ventilation rate of the susceptible animals and ward ventilation rate.

The algebraic identifiability analysis indicates that the single-room model is identifiable. However, with only the measurement of the susceptibles available, it is only possible to solve for the combined unmeasured parameters θ_1. This means that the effect of the different parameters (like the pulmonary ventilation rate p and quanta generation rate ϕ) are indistinguishable from each other. This means that only one of the parameters that make up the combined unmeasured parameters θ may be unknown in order to solve for that parameter. Any deviation in the actual value of the variables, that are set as fixed and derived from literature, will result in a compensating deviation of the variable that is solved for. As an example, if ϕ is chosen to be solved for, and all the other parameters in θ are chosen from literature, but the actual value of p, which is a value from literature, is 10% greater for this group of guinea pigs, then the solution of ϕ will be 10% less than the actual value of ϕ for this group. This implies the variable that is solved for has significant uncertainty.

The observability analysis showed that the single-room GN model is observable. It should also be noted that if the number of susceptible animals reduce to 0, the rank of the observability matrix reduces to 1 and the model becomes unobservable. The determinant of the observability codistribution matrix must be non-zero in order for the system to be observable.

Results from the CEKF, for which a measurement time of 60 s is used, are quite favourable. An NRMSE of the quanta in the ward of 0.017927 was obtained. This is 29.4 times less than when using the standard single-room GN model (for which the quanta in the ward estimate could not converge), also using a measurement time of 60 s. The HEKF, for which a measurement time of 1 day is used, resulted in an NRMSE of 0.19391 which is 2.72 times greater than the standard single-room GN model. The convergence time for the CEKF and HEKF were 3.9 and 40 days, respectively.

Figures 5.37 to 5.41 show the results obtained when the quanta generation rate parameter is varied between 0.5, 5, 2 4, 100 and 144 times the simulated quanta generation rate of 60 quanta $\cdot$ d^{-1} for the modified single-room model. These generation rates were used from literature to determine the extremes for which the HEKF can estimate the generation rate. The varied generation rate mismatch HEKFs do not perform as well as the CEKF. The filter can, for a deviation of up to 24 times greater, estimate the quanta in the ward with NRMSEs less than that of the standard single-room GN model,

but a large amount of deviation in the estimate is present. The variances of the states for the CEKF simulations decrease and remain lower than the initial values. The variances for the x_2 and x_3 states increase however for the HEKF simulation, indicating poor performance.

The quanta generation rate and thereby the number of quanta in the ward can therefore be accurately estimated using the augmented GN model CEKF, but performance is degraded for the the HEKF. The CEKF results can be used to better determine the number of quanta present in a ward and are less susceptible to measurement noise and unknown disturbances than when determining the number of quanta and generation rates when using for example methods such as a Nelder-Mead search algorithm.

The estimators for the augmented single-room GN model require measurements of the ventilation rate out of the ward, the pulmonary ventilation rate of the susceptible individuals (measured or estimated), the total room volume, measurements of the number of susceptible individual and the time between each measurement. Most of these measurements only have to be made once or can be obtained from sensors.

6.1.2 Two-room GN models

The two-room GN model adds the incubation period and the transmission of the disease between two-rooms through ventilation. The model is able to simulate the transmission of the disease as it spreads from one room to another, assuming that the ventilated air is not sterilised and the ventilation rates between the rooms are measured. The model can also be expanded to more than two-rooms, making it possible to model disease transmission throughout a building.

The number of quanta ϕ in the two-rooms and the incubation period α of the disease cannot be measured and the uncertainty of the model lies in these three parameters. The same assumptions are made as for the single-room GN models, with the added assumption that the incubation period of the disease is the same for each individual. The uncertainty that is contained in these assumptions are spread across the number of quanta in the ward and number of quanta in the adjacent rooms.

The simplified two-room GN model removed the incubation period, added the quanta generation rate

as a state, and assumed that once an animal has been exposed to the disease it shows signs of infection. This assumption however causes the estimate of the number of quanta to be less than it actually is because there might be more animals who have not tested positive but have been exposed, meaning the quanta would be greater if those animals are included in the measurements.

Although the sensitivity of the simplified two-room GN model is less than that of the augmented single-room GN model regarding the quanta generation rate, pulmonary ventilation rate and ward ventilation rate parameters, the two-room model also showed sensitivity to deviation of the animal room ventilation rate, increasing the uncertainty of the model. Like the augmented single-room GN model, the simplified two-room GN model is identifiable and any deviation in the variables will result in a compensating deviation of the variable that is solved for. This means that the variables are indistinguishable from one another, as with the augmented single-room GN model.

For the two-room GN augmented model, a measurement of the change in number of susceptible animals in addition to the number of susceptible animals is required to make the two-room GN model observable. A problem arises if the air flow into the animal room becomes zero. When the air flow into the animal room becomes zero, the rank of the observability codistribution matrix becomes 2 and the model becomes unobservable.

The CEKF (measurement time 60 s) and HEKF (measurement time 1 day) estimates of the quanta in the ward and animal rooms converge after 16 and 29 days respectively. The NRMSEs of the quanta in the ward and the quanta in the animal rooms for the CEKF are 420.3 and 164 times smaller, respectively, than for the standard two-room GN model. The HEKF NRMSEs for the quanta in the ward and animal rooms are 2.66 and 2.07 times smaller respectively than for the standard two-room GN model.

Figures 5.42 to 5.46 show the results obtained when the quanta generation rate parameter is varied between 0.5, 5, 24, 100 and 144 times the actual quanta generation rate of 60 quanta $\cdot$ d^{-1} for the modified two-room model. Only the NRMSEs of the mismatched HEKFs with deviations of up to 5 times greater are less than that of the standard two-room GN model. The variances of the states for the CEKF simulations decrease and remain lower than the initial values, and the simplified two-roon GN model CEKF performs well. The variances for the quanta and quanta generation rate states increase again for the HEKF simulation, indicating poor performance.

The number of quanta in the two rooms and the quanta generation rate can therefore be estimated reasonably well. This model requires the same measurements as the single-room GN model in addition to the added ventilation rate and volume of the animal room.

CHAPTER 7 CONCLUSION

A reduction in the transmission of TB is essential to reduce new cases and thereby reduce the number of deaths from TB in the future. Towards this end, two TB risk of transmission models in literature were investigated [8, 19]. Both models rely on a quanta generation rate that cannot be directly measured, as a measurement of infectiousness. If this quanta generation rate can be estimated using nonlinear state estimators, a feedback control system can potentially be used to reduce the transmission of TB by controlling room ventilation rates and, where applicable, also use ultraviolet germicidal irradiation (UVGI) to prevent transmission [12, 46, 47, 48].

Simulating the sensitivity of each model to deviation in parameters showed that the two models are practically the same and in the case of the two-room model, an increased uncertainty arises from the additional room. The algebraic identifiability indicates that both the models are identifiable. Only (3.4) can be solved for indicating that the effect of the different parameters (like the pulmonary ventilation rate p and quanta generation rate ϕ) are indistinguishable from each other. This means that only one of the parameters that make up the combined unmeasured parameters θ may be unknown in order to solve for that parameter. This implies the variable that is solved for has significant uncertainty.

The standard Gammaitoni and Nucci (GN) model was adapted into an augmented single-room GN model, and a two-room GN model from literature was adapted into a simplified two-room GN model. Both modified models were shown to be observable, which means that it is theoretically possible to estimate the quanta state in these models given the available measurements.

Kalman filters were used to estimate the quanta state. First, a continuous-time extended Kalman filter (CEKF) was used for both adapted models using a simulation and measurement time of 60 s. Accurate

quanta state estimates were achieved in both cases. Taking measurements every 60 s is however unrealistic, but was used to see what estimates can be obtained under ideal circumstances.

A more realistic scenario, with a measurement rate of once per day, was used next. For these estimates, a hybrid extended Kalman filter (HEKF) was required as it is able to deal with simulations where the time between model output measurements is greater than the time between measurements of other model parameters. The quanta state for both the augmented single-room and simplified two-room GN models was estimated reasonably well.

Real-time measurement of the number of quanta in a room is not possible since the parameter contains uncertainty related to an individual's immune response [6] and TST measurements can take up to 72 hours to indicate infection [4]. The measurement of the concentration infectious particles in the air is possible using bioaerosol particle sensors [49, 50, 51]. Pairing the infectious particle concentration measurement with a modified dose-response model, more accurate estimates of the risk of transmission can be made [52, 53].

The measurements would only be able to identify the concentration of bio-aerosols of a specific size, 1-5 μ m [6, 33, 54, 55], and not the exact composition thereof [49]. The estimates could therefore be further improved using filters. The effects of control measures could then also be investigated in real-time.

The efficacy of UV control measures and the placement thereof relative to the ventilation in- and outlets should also be taken into account [56, 57]. Zonal models can be used to model the interaction between these control measures.

REFERENCES

[1] World Health Organization, "Tuberculosis," www.who.int/topics/tuberculosis/en/, accessed 2016/03/28.

[2] ——, *Global tuberculosis report 2015*, 20th ed. World Health Organization, 2015.

[3] ——, *Global tuberculosis report 2019*. World Health Organization, 2019.

[4] R. R. Küsel, I. K. Craig, and A. C. Stoltz, "Modeling the Airborne Infection Risk of Tuberculosis for a Research Facility in eMalahleni, South Africa," *Risk Analysis*, vol. 39, no. 3, pp. 630–646, 2019.

[5] W. F. Wells, *Airborne Contagion and Air Hygiene. An Ecological Study of Droplet Infections.* Cambridge: Harvard University Press, 1955.

[6] E. A. Nardell, "Wells revisited: infectious particles vs. quanta of Mycobacterium tuberculosis infection - don't get them confused," *Mycobacterial Diseases*, vol. 6, pp. 5–7, 2016.

[7] T. A. Yates, P. Y. Khan, G. M. Knight, J. G. Taylor, T. D. McHugh, M. Lipman, R. G. White, T. Cohen, F. G. Cobelens, R. Wood *et al.*, "The transmission of mycobacterium tuberculosis in high burden settings," *The Lancet Infectious Diseases*, vol. 16, no. 2, pp. 227–238, 2016.

[8] L. Gammaitoni and M. C. Nucci, "Using a mathematical model to evaluate the efficacy of TB control measures," *Emerging Infectious Diseases*, vol. 3, pp. 335–342, 1997.

[9] C. B. Beggs, C. J. Noakes, P. A. Sleigh, L. A. Fletcher, and K. Siddiqi, "The transmission of tuberculosis in confined spaces: An analytical review of alternative epidemiological models," *International Journal of Tuberculosis and Lung Disease*, vol. 7, pp. 1015–1026, 2003.

[10] D. J. Simon, *Optimal State Estimation*. Hoboken: John Wiley & Sons, 2006.

[11] E. Riley, G. Murphy, and R. Riley, "Airborne spread of measles in a suburban elementary school," *American Journal of Epidemiology*, vol. 107, no. 5, pp. 421–432, 1978.

[12] Y. Li, J. Tang, C. Noakes, and M. J. Hodgson, "Engineering control of respiratory infection and low-energy design of healthcare facilities," *Science and Technology for the Built Environment*, vol. 21, no. 1, pp. 25–34, 2015.

[13] J. Taylor, T. Yates, M. Mthethwa, F. Tanser, I. Abubakar, and H. Altamirano, "Measuring ventilation and modelling M. tuberculosis transmission in indoor congregate settings, rural KwaZulu-Natal," *The International Journal of Tuberculosis and Lung Disease*, vol. 20, no. 9, pp. 1155–1161, 2016.

[14] S. Rudnick and D. Milton, "Risk of indoor airborne infection transmission estimated from carbon dioxide concentration," *Indoor Air*, vol. 13, no. 3, pp. 237–245, 2003.

[15] C. J. Noakes, C. B. Beggs, P. A. Sleigh, and K. G. Kerr, "Modelling the transmission of airborne infections in enclosed spaces," *Epidemiology and Infection*, vol. 134, no. 5, pp. 1082–1091, 2006.

[16] C. J. Noakes and P. A. Sleigh, "Mathematical models for assessing the role of airflow on the risk of airborne infection in hospital wards," *Journal of the Royal Society Interface*, vol. 6, no. 6, pp. S791–S800, 2009.

[17] E. A. Nardell, J. Keegan, S. A. Cheney, and S. Etkind, "Airborne infection: Theoretical limits of protection achievable by building ventilation," *American Review of Respiratory Disease*, vol. 144, pp. 302–306, 1991.

[18] M. Mphaphlele, A. S. Dharmadhikari, P. A. Jensen, S. N. Rudnick, T. H. V. Reenen, M. A. Pagano, W. Leuschner, T. A. Sears, S. P. Milonova, M. V. D. Walt, A. C. Stoltz, K. Weyer, and E. A. Nardell, "Institutional tuberculosis transmission: Controlled trial of upper room ultraviolet air disinfection: A basis for new dosing guidelines," *American Journal of Respiratory and Critical Care Medicine*, vol. 192, pp. 477–484, 2015.

[19] D. Strydom, R. R. Küsel, and I. K. Craig, "When is it appropriate to model transmission of tuberculosis using a dose response model?" *IFAC-PapersOnLine*, vol. 50, no. 2, pp. 31–36, 2017.

[20] A. S. Dharmadhikari and E. A. Nardell, "What animal models teach humans about tuberculosis," *American Journal of Respiratory Cell and Molecular Biology*, vol. 39, no. 5, pp. 503–508, 2008.

[21] C. Noakes and P. Sleigh, "Applying the Wells-Riley equation to the risk of airborne infection in hospital environments: The importance of stochastic and proximity effects," *Indoor Air 2008 : The 11th International Conference on Indoor Air Quality and Climate*, 2008.

[22] C. Beggs, C. Noakes, P. Sleigh, L. Fletcher, and K. Kerr, "Methodology for determining the susceptibility of airborne microorganisms to irradiation by an upper-room UVGI system," *Journal of Aerosol Science*, vol. 37, no. 7, pp. 885–902, 2006.

[23] M. Nicas, "Estimating exposure intensity in an imperfectly mixed room," *American Industrial Hygiene Association Journal*, vol. 57, no. 6, pp. 542–550, 1996.

[24] N. S. Nise, *Control Systems Engineering*, 6th ed. Hoboken: John Wiley & Sons, 2011.

[25] N. L. Risser, D. W. Belcher, J. B. Bushyhead, and B. M. Sullivan, "The accuracy of tuberculin skin tests: self-assessment by adult outpatients," *Public Health Reports*, vol. 100, no. 4, p. 439, 1985.

[26] E. A. Nardell, "Air sampling for tuberculosisâĂŤhomage to the lowly guinea pig," *Chest*, vol. 116, no. 4, pp. 1143–1144, 1999.

[27] D. Goletti, A. Sanduzzi, and G. Delogu, "Performance of the tuberculin skin test and interferon-γ release assays: an update on the accuracy, cutoff stratification, and new potential immune-based approaches," *The Journal of Rheumatology Supplement*, vol. 91, pp. 24–31, 2014.

[28] G. H. Mazurek, S. E. Weis, P. K. Moonan, C. L. Daley, J. Bernardo, A. A. Lardizabal, R. R. Reves, S. R. Toney, L. J. Daniels, and P. A. LoBue, "Prospective comparison of the tuberculin skin test and 2 whole-blood interferon-γ release assays in persons with suspected tuberculosis," *Clinical infectious diseases*, vol. 45, no. 7, pp. 837–845, 2007.

[29] S. Clark, Y. Hall, and A. Williams, "Animal models of tuberculosis: Guinea pigs," *Cold Spring Harbor perspectives in medicine*, vol. 5, no. 5, p. a018572, 2015.

[30] R. L. Riley, W. F. Wells, C. C. Mills, W. Nyka, and R. L. McLean, "Air hygiene in tuberculosis: Quantitative studies of infectivity and control in a pilot ward: A cooperative study between the veterans administration, the johns hopkins university school of hygiene and public health, and the maryland tuberculosis association," *American Review of Tuberculosis and Pulmonary Diseases*, vol. 75, no. 3, pp. 420–431, 1957.

[31] R. Riley, C. Mills, F. O'Grady, L. Sultan, F. Wittstadt, and D. Shivpuri, "Infectiousness of air from a tuberculosis ward: ultraviolet irradiation of infected air: comparative infectiousness of different patients," *American Review of Respiratory Disease*, vol. 85, no. 4, pp. 511–525, 1962.

[32] R. L. Riley, C. Mills, W. Nyka, N. Weinstock, P. Storey, L. Sultan, M. Riley, W. Wells *et al.*, "Aerial dissemination of pulmonary tuberculosis. a two-year study of contagion in a tuberculosis ward." *American Journal of Hygiene*, vol. 70, no. 2, pp. 185–96, 1959.

[33] C. M. Issarow, N. Mulder, and R. Wood, "Modelling the risk of airborne infectious disease using exhaled air," *Journal of Theoretical Biology*, vol. 372, pp. 100 – 106, 2015.

[34] X. Xia and C. H. Moog, "Identifiability of nonlinear systems with application to HIV/AIDS models," *Transactions on Automatic Control*, vol. 48, pp. 330–336, 2003.

[35] R. Hermann and A. Krener, "Nonlinear controllability and observability," *IEEE Transactions on Automatic Control*, vol. 22, no. 5, pp. 728–740, 1977.

[36] S. Sastry, *Nonlinear systems: analysis, stability, and control*. Springer Science & Business Media, 2013, vol. 10.

[37] J. Valappil and C. Georgakis, "Systematic estimation of state noise statistics for extended Kalman filters," *AIChE Journal*, vol. 46, no. 2, pp. 585–601, 2000.

[38] V. Bavdekar, A. Deshpande, and S. Patwardhan, "Identification of process and measurement noise covariance for state and parameter estimation using extended Kalman filter," *Journal of Process Control*, vol. 21, no. 4, pp. 585–601, 2011.

[39] R. E. Kalman, "A new approach to linear filtering and prediction problems," *Journal of Basic Engineering*, vol. 82, no. 1, pp. 35–45, 1960.

[40] R. Schneider and C. Georgakis, "How to not make the extended Kalman filter fail," *Industrial & Engineering Chemistry Research*, vol. 52, no. 9, pp. 3354–3362, 2013.

[41] L. E. Olivier and I. K. Craig, "Development and application of a model-plant mismatch expression for linear time-invariant systems," *Journal of Process Control*, vol. 32, pp. 77–86, 2015.

[42] P. Narula, V. Piratla, A. Bansal, S. Azad, and P. Lio, "Parameter estimation of tuberculosis transmission model using ensemble Kalman filter across Indian states and union territories," *Infection, Disease & Health*, vol. 21, no. 4, pp. 184–191, 2016.

[43] A. Labuschagne, A. van der Merwe, N. van Rensburg, and L. Zietsman, *An Introduction to Numerical Analysis*. Pretoria: Hatfield Press, 2013.

[44] B. J. Odelson, M. R. Rajamani, and J. B. Rawlings, "A new autocovariance least-squares method for estimating noise covariances," *Automatica*, vol. 42, no. 2, pp. 303 – 308, 2006.

[45] B. P. Lathi, *Linear systems and signals*. New York: Oxford University Press, 2010.

[46] C. Beggs, K. Kerr, J. Donnelly, P. Sleigh, D. Mara, and G. Cairns, "The resurgence of tuberculosis in the tropics. An engineering approach to the control of Mycobacterium tuberculosis and other airborne pathogens: a UK hospital based pilot study," *Transactions of The Royal Society of Tropical Medicine and Hygiene*, vol. 94, no. 2, pp. 141–146, 2000.

[47] C. Beggs and P. Sleigh, "A quantitative method for evaluating the germicidal effect of upper room UV fields," *Journal of Aerosol Science*, vol. 33, no. 12, pp. 1681 – 1699, 2002.

[48] Y. Li, G. M. Leung, J. Tang, X. Yang, C. Chao, J. Z. Lin, J. Lu, P. V. Nielsen, J. Niu, H. Qian *et al.*, "Role of ventilation in airborne transmission of infectious agents in the built environment-a multidisciplinary systematic review." *Indoor Air*, vol. 17, no. 1, pp. 2–18, 2007.

[49] B. Ghosh, H. Lal, and A. Srivastava, "Review of bioaerosols in indoor environment with special reference to sampling, analysis and control mechanisms," *Environment International*, vol. 85, pp. 254–272, 2015.

[50] S. Bhangar, J. Huffman, and W. Nazaroff, "Size-resolved fluorescent biological aerosol particle concentrations and occupant emissions in a university classroom," *Indoor Air*, vol. 24, no. 6, pp. 604–617, 2014.

[51] H. J. Tobias, M. P. Schafer, M. Pitesky, D. P. Fergenson, J. Horn, M. Frank, and E. E. Gard, "Bioaerosol mass spectrometry for rapid detection of individual airborne Mycobacterium tuberculosis H37Ra particles," *Applied and Environmental Microbiology*, vol. 71, no. 10, pp. 6086–6095, 2005.

[52] G. N. Sze To and C. Y. Chao, "Review and comparison between the Wells-Riley and dose-response approaches to risk assessment of infectious respiratory diseases," *Indoor Air*, vol. 20, no. 1, pp. 2–16, 2010.

[53] E. A. Nardell, "Catching droplet nuclei: toward a better understanding of tuberculosis transmission," *American Journal of Respiratory and Critical Care Medicine*, vol. 169, no. 5, pp. 553–554, 2004.

[54] L. Liu, J. Wei, Y. Li, and A. Ooi, "Evaporation and dispersion of respiratory droplets from coughing," *Indoor Air*, vol. 27, no. 1, pp. 179–190, 2017.

[55] S. Yang, G. W. Lee, C. Chen, C. Wu, and K. Yu, "The size and concentration of droplets generated by coughing in human subjects," *Journal of Aerosol Medicine*, vol. 20, no. 4, pp. 484–494, 2007.

[56] M. Sung and S. Kato, "Estimating the germicidal effect of upper-room UVGI system on exhaled air of patients based on ventilation efficiency," *Building and Environment*, vol. 46, no. 11, pp. 2326–2332, 2011.

[57] C. J. Noakes, M. A. I. Khan, and C. A. Gilkeson, "Modeling infection risk and energy use of upper-room ultraviolet germicidal irradiation systems in multi-room environments," *Science and Technology for the Built Environment*, vol. 21, no. 1, pp. 99–111, 2015.

[58] M. Nicas, "An analytical framework for relating dose, risk, and incidence: An application to occupational tuberculosis infection," *Risk Analysis*, vol. 16, pp. 527–538, 1996.

ADDENDUM A DOSE RESPONSE MODEL

A dose response model is given in (A.1). A dose-response (DR) model based on the Wells-Riley model makes use of infectious dose data to determine the probability of infection, where the dose is the number of pathogen required to infect a certain amount of the population. A 50% infectious dose is therefore the dose of pathogen required to infect half of the exposed population [52, 58].

$$\frac{dS}{dt} = -\frac{p}{V}CS\frac{dC}{dt} = -\frac{F}{V}C + IG\zeta \tag{A.1}$$

where G is the number of airborne TB bacilli released per infector per unit of time and ζ is the fraction of infectious particles deposited in the alveolar region [58], then the infectious particles are measured in infectious doses. The GN model uses quanta as a measurement of infectivity and the dose response model uses infectious dose as a measurement for this purpose. Otherwise the two models are the same.

The DR model has the benefit of taking the immune status and susceptibility of an individual into account, via the β parameter. This term is separate from the generation of infectious dose parameter whereas in the GN model, the generation and susceptibility is one term. It is of great importance that a realistic level of exposure in susceptible individuals is determined when using DR models.

A.1 SENSITIVITY ANALYSIS

The figures in this section show the comparison of the sensitivity to deviation of the model parameters for the standard GN model compared to the dose response model. Figure A.1 shows a deviation of a single patient instead of a 10% deviation, seeing that there cannot be a 10% increase in the number of

patients. Figure A.2 shows the effect of a 10% deviation of the quanta and infectious dose generation rates. Figure A.3 shows the effect of a 10% deviation of the fraction of infectious particles deposited in the alveolar region. The sensitivity to a deviation of the pulmonary ventilation rate is shown in Figure A.4. The effect of a 10% deviation of the ward extraction ventilation rate is shown in Figure A.5.

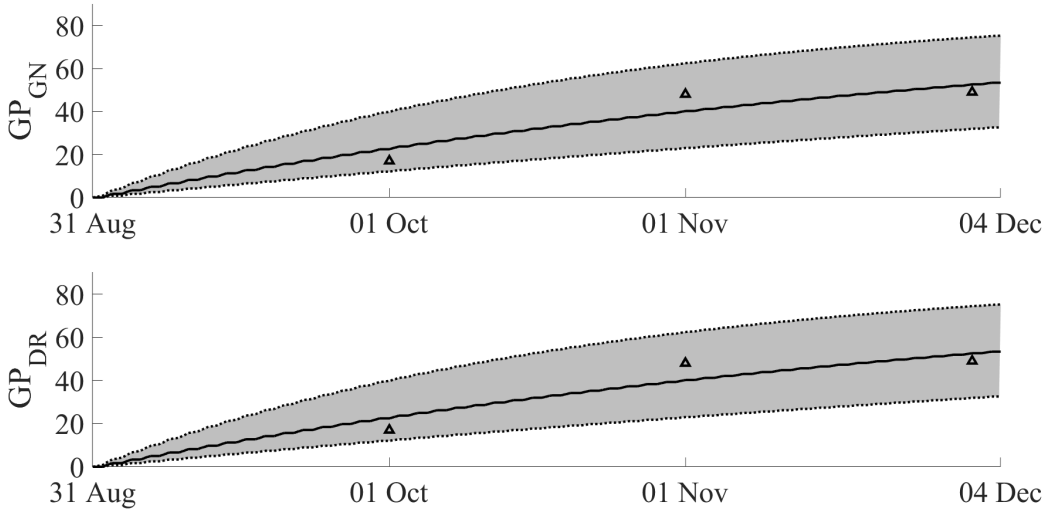

Figure A.1. Sensitivity to deviation of the number of infectors for the dose-response and the GN models.

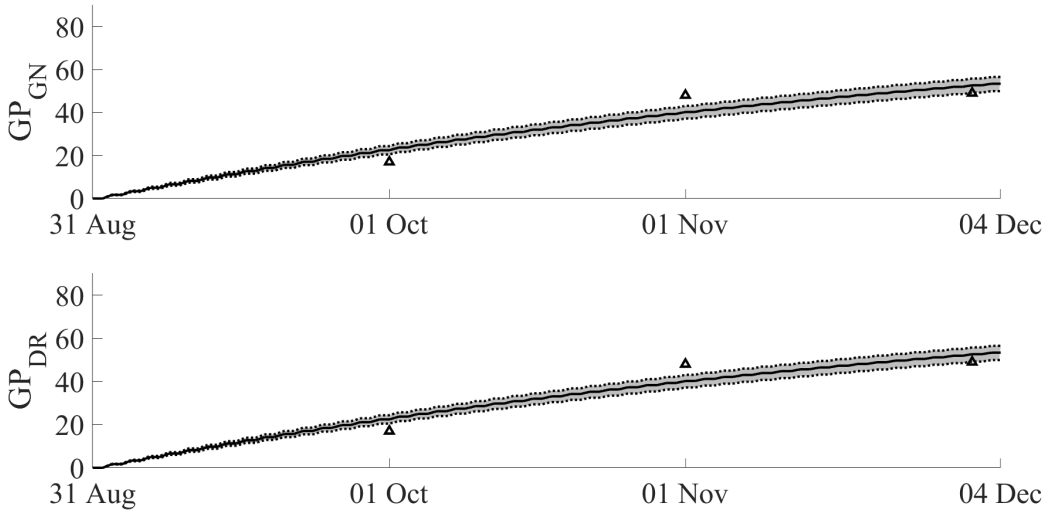

Figure A.2. Sensitivity to deviation of the quanta and infectious dose generation rates for the GN and dose-response models.

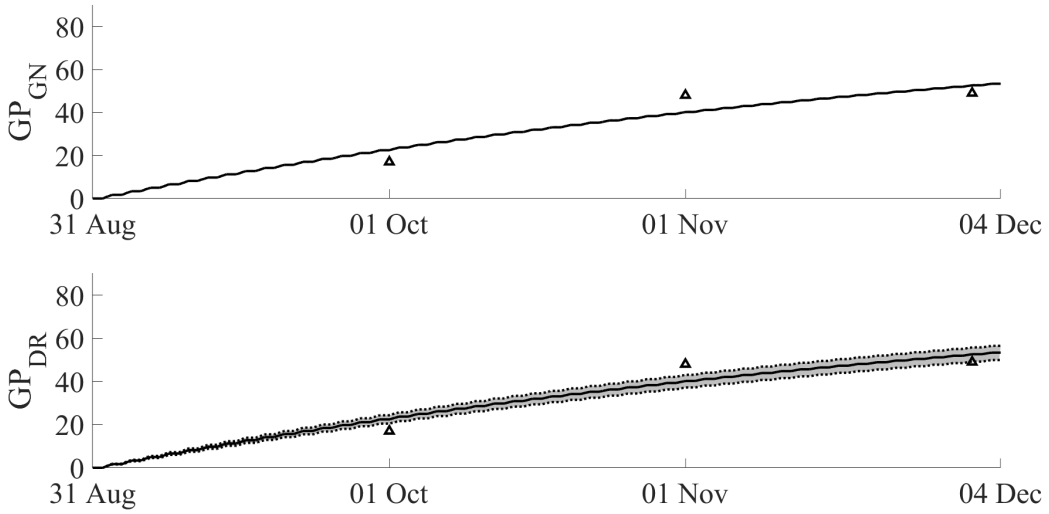

Figure A.3. Sensitivity to deviation of the beta parameter for the dose-response model.

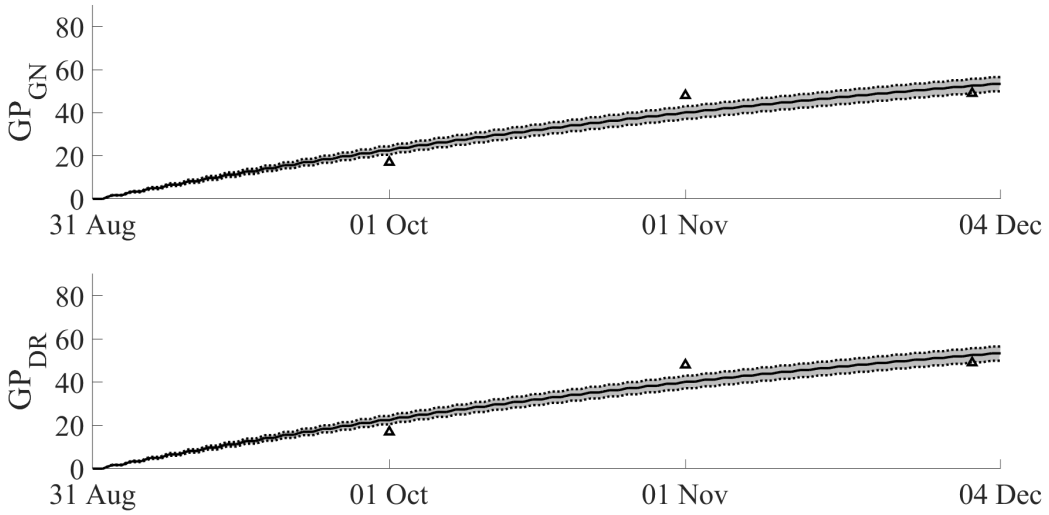

Figure A.4. Sensitivity to deviation of the pulmonary ventilation rate for the dose-response and GN models.

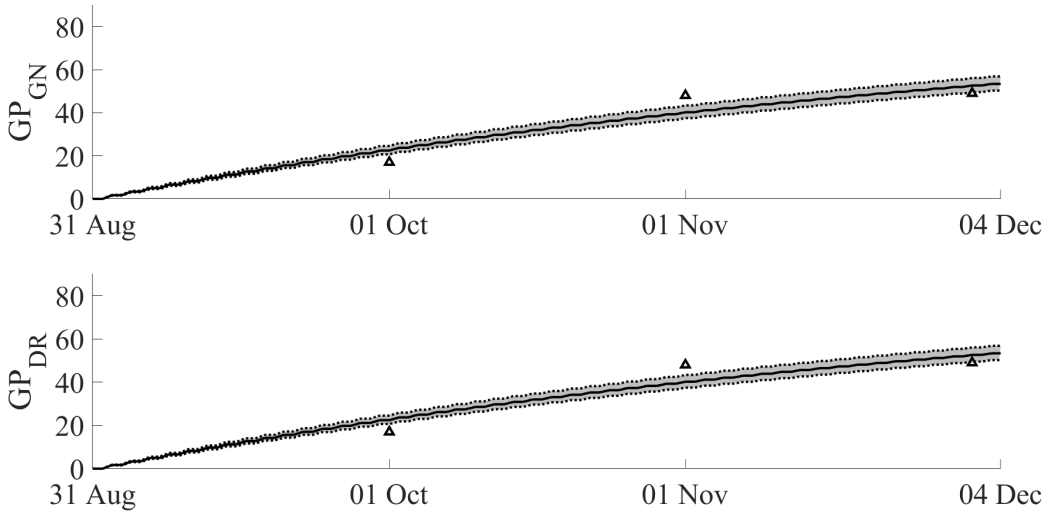

Figure A.5. Sensitivity to deviation of the ward ventilation rate for the dose-response and GN models.

A.2 IDENTIFIABILITY ANALYSIS

Assuming that a method is available to measure the number of infectious particles, the measured variables become:

$$\begin{aligned} y_1(t) &= S(t) \\ y_2(t) &= C(t). \end{aligned} \tag{A.2}$$

The model in (A.1) can be expressed in terms of these measured variables:

$$\begin{aligned} \dot{y_1} &= -\frac{p}{V} y_1 y_2 \\ \dot{y_2} &= -N y_2 + \gamma. \end{aligned} \tag{A.3}$$

To solve this algebraically, let

$$\begin{aligned} \theta_{G1} &= -\frac{p}{V} \\ \theta_{G2} &= -N \\ \theta_{G3} &= \gamma, \end{aligned} \tag{A.4}$$

which gives:

$$\begin{aligned} \dot{y_1} &= \theta_{G1} y_1 y_2 \\ \dot{y_2} &= \theta_{G2} y_2 + \theta_{G3}. \end{aligned} \tag{A.5}$$

Equation A.5 was used to determine the identifiability of θ_{G1}.

$$\begin{aligned} \begin{bmatrix} y_1 y_2 \end{bmatrix} \begin{bmatrix} \theta_{G1} \end{bmatrix} &= \begin{bmatrix} \dot{y_1} \end{bmatrix} \\ rank \begin{bmatrix} y_1 y_2 \end{bmatrix} &= 1 \end{aligned} \tag{A.6}$$

This is the same as the length of the vector containing the unknown θ_{G1}, meaning that this unknown can be estimated from these measurements. As with the GN model identifiability, two measurements of y_1 and one measurement of y_2 is required.

Taking equation A.5, the identifiability of θ_{G2} and θ_{G3} can be determined:

$$\begin{bmatrix} y_2 & 1 \\ \dot{y}_2 & 0 \end{bmatrix} \begin{bmatrix} \theta_{G2} \\ \theta_{G3} \end{bmatrix} = \begin{bmatrix} \dot{y}_2 \\ \ddot{y}_2 \end{bmatrix}$$
$$rank \begin{bmatrix} y_2 & 1 \\ \dot{y}_2 & 0 \end{bmatrix} = 2. \tag{A.7}$$

This is the same as the length of the vector containing the unknowns θ_{G2} and θ_{G3}, meaning that these unknowns can also be estimated from these measurements. However, in order to estimate these parameters, at least two measurements of y_1 and three measurements of y_2 are needed. This shows that three parameters are identifiable for the case where both the number of susceptibles and number of particles can be measured.

A.3 DOSE RESPONSE MODEL DISCUSSION

The measurement of infectious TB particles would be required to justify using infectious doses when modelling the risk of transmission of tuberculosis. The dose response model can be useful for simulation studies without such a measurement, but there is little benefit in using the more complex dose response model unless the number of infectious TB particles can be measured. This is because the uncertainties associated with the additional dose response model parameters are otherwise lumped into the parameter representing the generation of infectious particles, as with the GN model [19].